THE BELL SYSTEM
TECHNICAL JOURNAL

VOLUME XXXVIII SEPTEMBER 1959 NUMBER 5

Studies in Tropospheric Propagation Beyond the Horizon*

By A. B. CRAWFORD, D. C. HOGG and W. H. KUMMER

(Manuscript received April 17, 1959)

This paper describes an extended series of experiments in beyond-the-horizon propagation on a 171-mile overland path using 460 and 4110 mc. The following aspects of the propagation were investigated: the effect of antenna size on signal level and fading characteristics, wavelength dependence, seasonal and diurnal effects, a new form of diversity reception, the bandwidth capability of the medium. Many of the experiments were directed toward a better understanding of the mechanism of propagation.

TABLE OF CONTENTS

* This work was supported in part by Contract AF18(600)-572 with the U. S. Air Force, Air Research and Development Command.

I. INTRODUCTION

There has been a tremendous increase in interest in tropospheric propagation beyond the horizon since Bullington[1] first suggested its useful properties in 1950. Early studies at Bell Telephone Laboratories and elsewhere[2] led to the design and installation of large-scale military and commercial systems. To a great extent, the design of these systems was based on limited data, since time did not permit the implementation of long-term research programs specifically designed to study the mechanism of the propagation. Hand-in-hand with the interest in the systems themselves, several theories were proposed to explain the propagation. These can be classified into three general types: scattering by atmospheric turbulence (Booker-Gordon),[3] mode propagation (Carroll-Ring)[4] and reflection from atmospheric layers (Friis, Crawford and Hogg).[5]

This paper describes the results of a series of experiments conducted on a 171-mile overland path between Pharsalia, New York, and Crawford Hill, New Jersey, during the period from May 1955 to September 1958.

At the time these experiments were planned, some of the characteristics of beyond-the-horizon propagation were known, but other important properties had not been investigated thoroughly. Some of the aims of our experiment were: to study the effect of antenna size on signal level and fading characteristics; to determine the wavelength dependence of the propagation; to look for seasonal and diurnal effects; to investigate a new form of diversity reception which combines the outputs of twin-feed horns horizontally or vertically disposed at the focal point of a single paraboloid; to study the bandwidth capability of

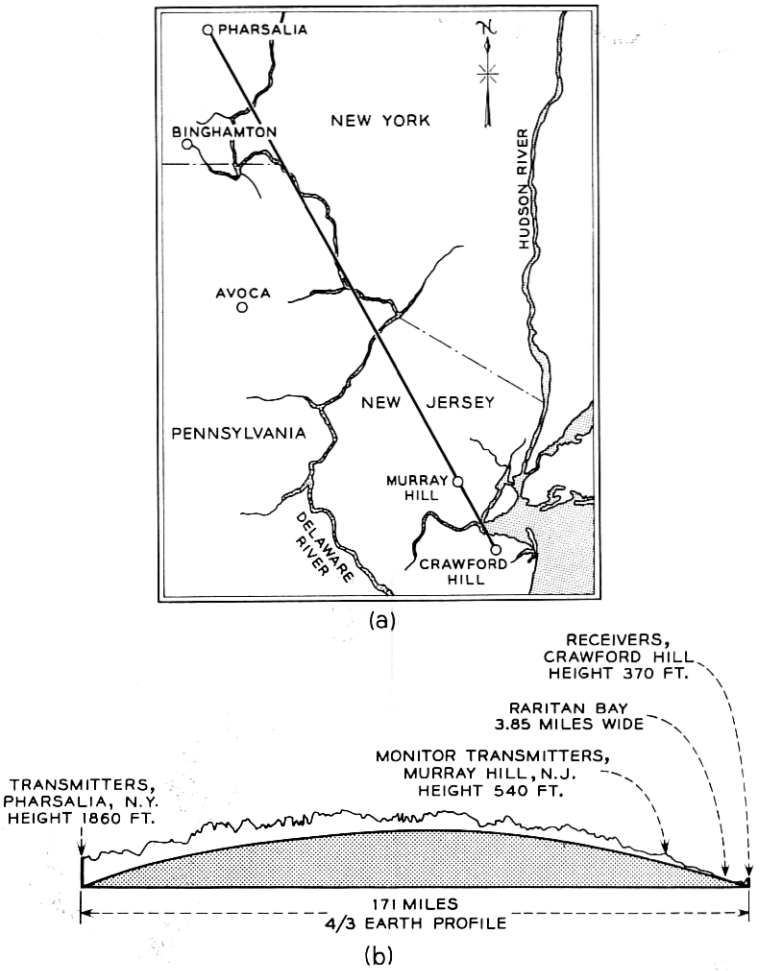

Fig. 1 — Propagation path.

the propagation; to learn as much as possible about the mechanism involved.

Previous experience in the short-wave and microwave fields had shown that a valuable research tool for studying propagation mechanisms is a narrow beam receiving antenna capable of being scanned through the incoming wave fronts. For the present experiment, a solid-surface aluminum paraboloid, 60 feet in diameter,* was constructed on

* This antenna was designed by H. T. Friis.[6]

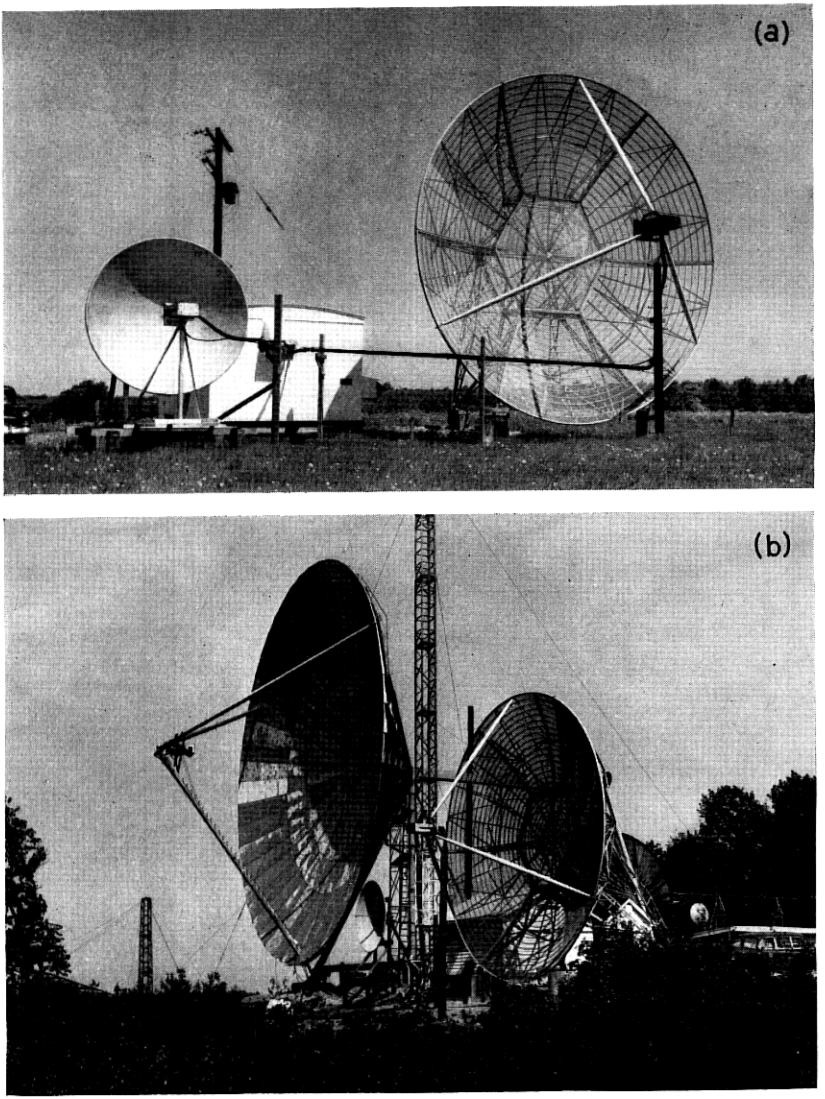

Fig. 2 — Terminal sites: (a) transmitter; (b) receiver.

Crawford Hill. Means were provided for scanning the antenna through an angle of approximately three degrees in azimuth and elevation at a rate of about four scans per minute.

The map in Fig. 1(a) shows the location of the transmission path for the experiment. The immediate foregrounds of the transmitting and

receiving sites are unobstructed, as shown in the profile map. This particular path was chosen to pass over the Murray Hill Laboratory, thereby providing a line-of-sight path with good clearance above ground between the Crawford Hill and Murray Hill locations [Fig. 1(b)]. The Murray Hill tower therefore was an excellent location for a monitor transmitter to be used in measuring the performance of the receiving antennas and to serve as a reference point for the angle of arrival measurements.

To investigate the effect of antenna size, two transmitting antennas, 10 feet and 28 feet in diameter, and three receiving antennas, 8 feet, 28 feet and 60 feet in diameter, were available (see Fig. 2). To study the propagation at two widely separated wavelengths, low-power transmitters designed for unattended operation at 4110 mc and 460 mc were installed at the Pharsalia site. Composite-feed horns consisting of a small 4110-mc horn within a 460-mc horn were available to permit operation at either of the two frequencies. Table I lists the frequencies, transmitter power, antenna gains and other data relating to the experiment.

In discussing the experimental results, comparisons are made with the theory of reflections from atmospheric layers.[5] This theory is based on the simple assumption that propagation beyond the horizon is due to reflections from a large number of randomly disposed layers in the volume of the atmosphere common to the beams of the transmitting and receiving antennas. The reflecting layers are formed by relatively steep gradients in the dielectric constant of the atmosphere; these gradients have been observed by refractometer measurements. While no claim is made that this theory is unique in explaining beyond-the-horizon propagation, it has been found to be in good agreement with experimental data.

References to some of the published work in the field are given in the paper but no attempt has been made to present a complete list of references. Ref. 2 contains many papers on the subject and references to many others. Refs. 8 and 9 give a list of references up to 1958.

The remainder of this paper is divided into seven sections, as follows:

Section II describes the design of the experiment and discusses the transmitting and receiving-recording apparatus.

Section III is concerned with the median received power and its dependence on antenna size and wavelength. It was found that, over a one-year period, the median signal level at 4110 mc received with the 60-foot antenna exceeded that received with the 8-foot antenna by only 6 db, compared with the difference of 17 db in the gains of the antennas. Comparing transmission at 460 mc and 4110 mc in a scaled experiment,

TABLE I — PARAMETERS FOR THE 171-MILE EXPERIMENTAL CIRCUIT

Frequency, mc	Transmitter Power	Free Space Path Loss, db	Antennas						Free Space Received Power		Estimated Beyond-the-Horizon Loss, db†	Estimated Received Power, dbm
			Transmitting			Receiving						
			Diameter, feet	Gain, db	Line loss, db	Diameter, feet	Gain, db	Line loss, db	Antenna Sizes, feet	Power, dbm*		
4110	20–30 watts 43 dbm	153.5	10	38.5	0.33	8	37.0	0.32	10–8	−36	73	−109
			28	47.5	0.44	28	47.5	0.47				
						60	54.5	1.6	28–60	−10.5		—
460	500–700 watts 57 dbm	134.5	10	20.5	0.79	8	—	—	10–28	−28.5	73	−101.5
			28	30.5	1.35	28	30.5	1.29				
						60	37.0	2.15	28–60	−13.5		—

* Including antenna line loss.
† From Ref. 7, Fig. 4.

it was found that, on the average, the median received power was proportional to the wavelength, as predicted by the theory.

Section IV gives the results of scanning or beam-swinging experiments using the 60-foot antenna at 4110 mc. The angular distribution of the received energy varied from day to day; it was found to be directly related to the ratio of the median power received on the 60-foot and 8-foot antennas. On the average, the apparent half-power beamwidth of the 60-foot antenna was about 1.0°, compared with the free space value of 0.3°.

Section V is a study of instantaneous fading rates. It is shown that the fading rate (at 4110 mc) is related to the size of the antennas and to the velocity of horizontal drift winds normal to the propagation path in the common volume of the antenna beams. In a scaled experiment, the ratio of the fading rates at 460 mc and 4110 mc was found to be significantly greater than the ratio of the frequencies.

Section VI discusses the twin-feed diversity experiments. At 4110 mc this type of diversity proved to be effective for both horizontally and vertically disposed feed horns. At 460 mc the diversity was effective at all times only for vertically placed feeds; with horizontal feed disposition, the effectiveness was a function of the rate of fading.

Section VII is a theoretical and experimental study of the characteristics of the short-term fading of the received signals; in particular, the number of one-way signal crossings and average duration of fade at a given signal level are treated for a single channel and for multichannel diversity systems.

Section VIII describes the results of frequency-sweep experiments intended to yield information on the bandwidth capability of the propagation. The transmission in a band of 15 mc centered at 4110 mc was characterized by the selective fading typical of multipath propagation. The bandwidth, defined as the frequency spacing of nulls in the transmission band, was about 5 mc on the average and was sensibly independent of antenna size, rate of fading and median signal level.

II. DESIGN OF THE EXPERIMENT

The experiments to be described have been carried out at Holmdel on beyond-the-horizon propagation using an experimental circuit of 171 miles between Pharsalia, New York, and Crawford Hill, New Jersey (Figs. 1 and 2). There are no obstructions in the transmitting and receiving foregrounds. The foreground profile at the receiving location is shown in Fig. 3.

The design of equipment for experiments in this type of propagation

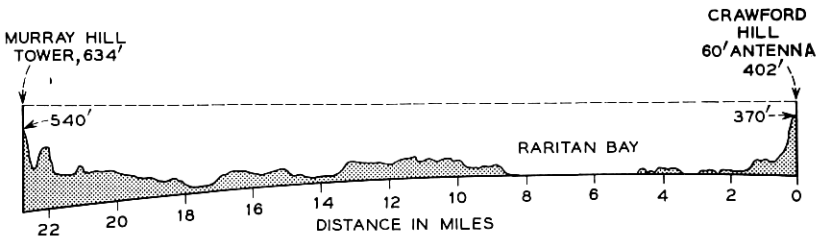

Fig. 3 — Foreground path profile at receiving end.

is dictated by the transmission path selected as well as by the experiments to be performed. Since propagation conditions vary considerably from hour to hour as well as from week to week and month to month, a particular experiment may run from several months to a year, with continuous recording of data being taken for several days each week. Several different equipment setups may be used in any one week. These are then repeated in succeeding weeks.

Equipment reliability and gain stability are important design considerations if a large amount of experimental data is to be obtained with minimum personnel. Flexibility of equipment setups and automatic data-taking also reduce the manpower needed and increase the time available for recording.

For our experiment, the transmitting equipment was designed for unattended operation with bimonthly maintenance periods; the receiving equipment was calibrated every four days.

2.1 *Receiver Design*

The receiver design is determined by the power available at the transmitter, the path loss and the antennas employed.

Table I summarizes the parameters used in this particular propagation path. The estimated beyond-the-horizon loss of 73 db was taken from Bullington[7] and gave the best estimate available at the beginning of our project. The signal will vary about 15 db around this value because of seasonal changes in transmission. From Table I it is seen that the average median level of received power will be -109 dbm at 4 kmc; during the worst period it will drop to -124 dbm.

It is known that the instantaneous signal is usually Rayleigh-distributed; it will drop 10 db below the median for 6.7 per cent of the time, 20 db below the median for 0.7 per cent of the time and 30 db below for 0.07 per cent of the time. The lowest expected signal level for 0.07 per cent of the time for the worst period would be -124 dbm $-$ 30 db $=$ -154 dbm.

TABLE II — REQUIRED RECEIVER BANDWIDTHS FOR VARIOUS SIGNAL-TO-NOISE RATIOS

Bandwidth, kc	Signal-to-Noise Ratio, db, for $P_R = -109$ dbm
150	1
25	9
6	15

Assuming an over-all noise figure of 12 db and a median received power of −109 dbm, we can calculate the bandwidth needed for various signal-to-noise ratios. The results are shown in Table II. Thus, from the table it is apparent that a 6-kc bandwidth is needed at low signal levels, since the median signal level can drop to −124 dbm. For that level, the signal-to-noise ratio would be 15 db + (−124 dbm + 109 dbm) = 0 db. The use of the 6-kc bandwidth means that the transmitter and receiver frequencies must be controlled to better than one part in 10^6.

The description of the equipment follows; the receivers will be discussed first, then the transmitters and finally the recording equipment.

2.2 *Receivers and Transmitters*

Two receivers are used; each has two RF heads, one for 4 kmc and one for 460 mc, with both feeding into the same IF portion of the receiver. Hence two channels of a single frequency or two different frequencies can be recorded simultaneously. The 4-kmc receiver will be discussed first; it is to be understood that the only difference between it and the 460 mc receiver is in the RF section and first beating oscillator.

In the 4-kmc receiver the RF signal is mixed with the first beating oscillator in a balanced converter. A matched pair of 1N23C and 1N23CR crystals are used, the IF cable to the first amplifier being adjusted for the best noise figure. The converter noise figure is 9 to 11 db, depending on the crystals selected.

To achieve the narrow bandwidths required, we used the conventional technique of quadruple detection. The details are indicated on Fig. 4. The gain of each IF stage (66 mc, 1.8 mc bandwidth; 3 mc, 150 kc bandwidth; 150 kc, 25 or 6 kc bandwidth) is adjusted so that its gain is equal to the signal-to-noise ratio improvement when that IF is added in the receiver. In other words, a broadband detector at the output of any of the IF stages will read the same amount of noise when the RF converter is connected to a matched load.

The 66-mc amplifier* has five stages with a grounded-grid WE417A input stage. The gain of the amplifier is 95 db, for low-level input. Automatic gain control is applied to two stages to increase the dynamic range from 28 db to 60 db. Compression is applied only to the 66 mc amplifier and is controlled by the output of the last detector; this means that the relative db calibration at the last detector is the same for any IF bandwidth selected, assuming that the other IF amplifiers are linear. Additional loss must be inserted at the RF end if the signal is high and the narrowest IF bandwidth is used.

Succeeding IF amplifiers are linear over the intended range of operation. The automatic gain control amplifier is a high-level 40-db linear amplifier with a low output impedance (5000 ohms); it is linear up to 0.7 volt input. Hence the dc output after the detector is at a high level (-100 volts for -71 dbm input to the receiver using the 25-kc bandwidth) and at low impedance. A portion of this output voltage is used as the AGC voltage, which is fed back to the 66-mc IF. Gain stability problems are considerably reduced by not using any dc amplification in the receiver.

Frequency stability is achieved by using crystal-controlled beating oscillators. The one with the most critical stability problem is the first beating oscillator, which consists of a modified Western Electric microwave generator.

The gain stability of the over-all system is ± 1 db for about one-half week; this is using the 50-db range on the receiver and the 6-kc bandwidth. The frequency stability for that same period is $\pm 1\frac{1}{2}$ kc. The frequency deviation is recorded on a recorder with a 0–10 kc scale.

The 460-mc receiver consists of a WE416B triode as an RF amplifier, a crystal-controlled beating oscillator and two IF stages. The IF output is connected through an IF attenuator to the rest of the receiver, as shown in Fig. 4.

There are two cw transmitters used in these propagation tests. Both are crystal-controlled and designed for unattended operation by remote control. The control circuits incorporate time sequence, with air pressure and safety interlocking devices. The transmitters will be described with the aid of Fig. 5.

The power output of the 4-kmc transmitter is obtained from a Sperry SAC41 three-stage klystron amplifier. The RF output is 20–30 watts with a drive of 50 mw.

As stated in the last section, the frequency stability of the transmitter must be better than $\pm 1\frac{1}{2}$ kc (four parts in 10^7), when the narrowest IF

* Designed by W. C. Jakes, Jr., of the Holmdel laboratory of Bell Telephone Laboratories.

amplifier of the receiver is used. To achieve this, the driver for the klystron amplifier is a modified TD-2 Western Electric microwave generator. The modifications include increased temperature stability of the crystal oscillator by the use of specially cut crystals and a different crystal oven. The complete generator is also temperature-controlled.

An Esterline-Angus recorder monitors the power delivered to the antenna. Calibrated RF attenuators, directional couplers and power meter are used to calibrate the E-A recorder.

The 460-mc transmitter uses a crystal-controlled oscillator with frequency multiplication and amplifying stages to obtain the required 500 watts output. The component parts of this transmitter are: Motorola Type TA110 15-watt crystal-controlled exciter; Radio Engineering Labs transmitter output amplifier and power amplifier.

Since the frequency is about one-tenth that of the 4 kmc transmitter,

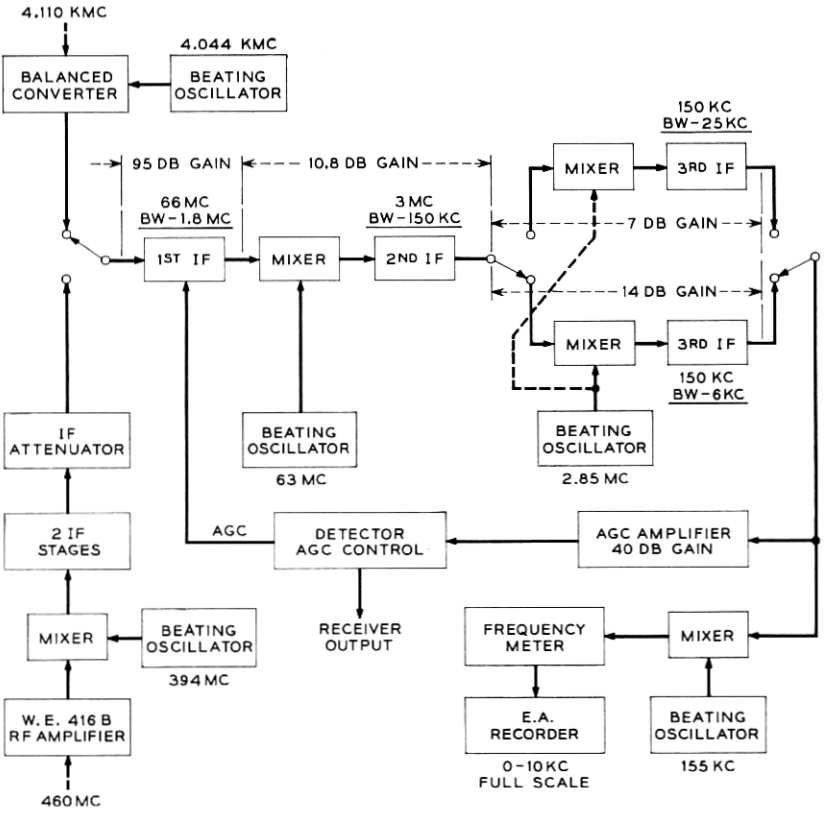

Fig. 4 — 460-mc and 4-kmc cw receivers.

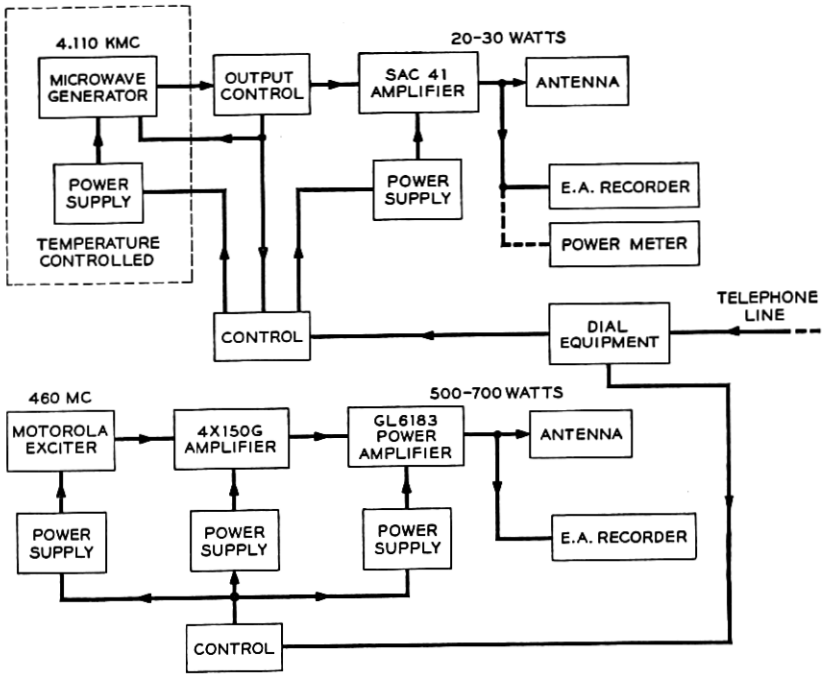

Fig. 5 — 460-mc and 4-kmc cw transmitters.

the frequency stability need only be one-tenth as good when measured on a percentage basis. However, the stability of the transmitter is only $\pm 2\frac{1}{2}$ kc. Since the transmitter power output is higher at 460 mc than at 4110 mc, the 6-kc receiver bandwidth is not required, and the stability of $\pm 2\frac{1}{2}$ kc is satisfactory when the 25-kc bandwidth is used.

2.3 *Recording Apparatus*

In propagation studies it is desirable to record the data so that the maximum information can be obtained without having to convert the original data into other presentations. Hence the presentation of the data depends on what use is to be made of them. Our program has consisted of the following analyses: statistical distribution of median signal levels and short-term fading for a long period, say a year (operation 60 hours a week); angle of arrival studies; diversity studies; and frequency sweep experiments.

Fig. 6 shows the setup for recording median signal levels with periodic sampling of the short-term fading. The output of the receiver is con-

nected to a Sanborn two-channel recorder. This recorder has a time constant (t.c.) of 0.015 second and has a recording speed of from 0.5 to 50 mm per second. The receiver output is also connected to a Doelcam dc amplifier which drives the Esterline-Angus (E-A) recorder through a 0 to 25 second t.c. circuit. The dc amplifier has a frequency response from 0 to 42 cps and is stable to 1 per cent full scale on a long-term basis. The Sanborn recorder is energized to take a sample of short-term fading every half-hour for an interval adjustable from one-half to five minutes. A marker pen on the E-A recorder is also energized during that period.

The recording setups for the angle of arrival, diversity and frequency-sweep experiments will be discussed in the sections where the experiments are described.

2.4 *Calibration Procedure*

The calibration procedure of the receivers consists of several steps. First, the RF input of the receiver is terminated in a matched load. Then each IF amplifier is adjusted to have the same noise output as the 66-mc IF amplifier of that receiver. This is done by means of a broadband crystal detector whose frequency response is constant within $\pm\frac{1}{4}$ db from 100 kc to 70 mc. The high-level 150-kc amplifier and high-level detector are adjusted to give -100 volts dc out with 0.7 volt ac in.

The matched load is removed from the input of the receiver and is replaced by a 4-kmc RF signal generator. This RF signal generator uses a microwave generator similar to the one used at the transmitter. Its output, monitored by a microwave power meter, is fed to the receiver input through calibrated directional couplers and RF attenuators. For an RF signal of -71 dbm (25 kc IF bandwidth), the AGC control is

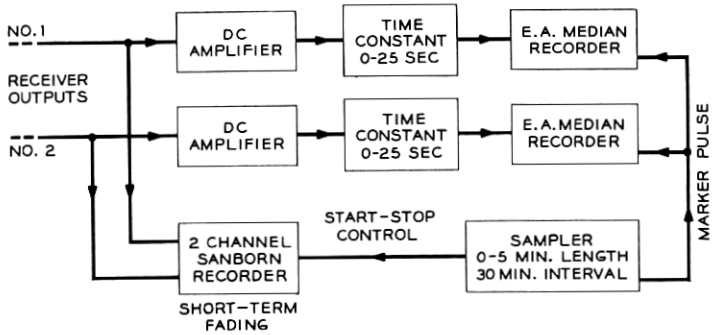

Fig. 6 — Recording setups for measuring median signal levels with periodic sampling of short-term fading.

adjusted to give −100 volts dc output. A calibration curve in steps of 5 db is taken; this completes the calibration.

To calibrate at 460 mc, a Hewlett-Packard Type 608A signal generator is used. This unit has a built-in power meter and calibrated attenuator.

III. MEDIAN RECEIVED POWER

In this section we shall discuss the median signal levels received on a tropospheric beyond-the-horizon system. In the first part our discussion will be limited to one frequency of transmission, 4 kmc; here we receive simultaneously on two antennas with different aperture areas. One of the interesting aspects of this type of propagation is that the power received by an antenna does not increase linearly with an increase in aperture area. The effect has been called "aperture-to-medium coupling loss" and "loss in antenna gain." The phenomenon has not been noticed at the lower frequencies primarily because it does not become appreciable until the aperture is of the order of a hundred wavelengths for a path of two hundred miles or so. Antennas of this aperture are physically realizable at present only in the microwave region.

In the second part of this section a scaled experiment to determine the wavelength dependence in this type of transmission is described; it is performed using simultaneous operation at two radio frequencies, 460 mc and 4 kmc, using almost equal antenna beamwidths. The antenna beamwidths are broad enough to make the "loss in gain" negligible; hence the atmosphere is the controlling factor in the transmission.

3.1 *Dependence on Antenna Size at 4 kmc*

In this study the received signal level was recorded for about 60 hours each weekend; the period of the experiment was from January 1956 to January 1957. The 4-kmc transmitter was used with the 10-foot antenna. Fig. 7 shows the common volume subtended by the antenna beams and the elevations involved. The results of this study show that the ratio of the median signal levels received by the 60-foot antenna and the 8-foot antenna are usually much smaller than would be expected on the basis of the antenna gains. The ratio of the gains of these two antennas is 17 db at 4 kmc. The ratio of the power levels received by the two antennas varies considerably from day to day and in some instances from hour to hour; on a yearly basis it is 5.7 db.

A strong seasonal dependence, as reported by Bean and Meany[10] and Bullington, has also been observed. The data indicate that the received signal level is approximately 15 db higher in summer than in winter.

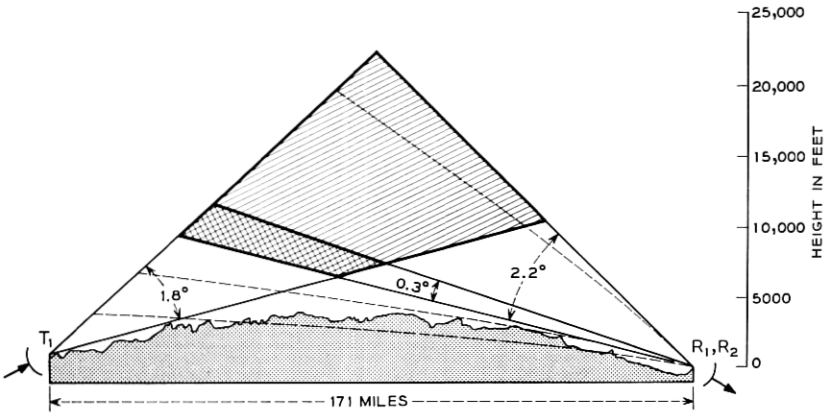

Fig. 7 — Common volumes in elevation plane for the 4-kmc circuit. The half-power beamwidths are shown for the 10-foot transmitting antenna (T_1) and the 60-foot (R_1) and 8-foot (R_2) receiving antennas. The dotted lines show the bending of the beams of the receiving antennas during unusual weather conditions at the receiving end (see Section 4.2).

This dependence is shown to be closely related to the refractive index of the atmosphere derived from data taken at ground level near the center of the path.

The fading range of the 15-minute medians is obtained for each weekend's recording. The fading range is taken as the ratio of the power levels at the 10 per cent and 90 per cent points of the distribution curve. The fading range of the 15-minute medians averaged over the year is 13 db for the signal on the 60-foot antenna and 9 db for the signal received on the 8-foot antenna.

3.1.1 *Method of Data Analysis — Samples of Recordings*

The received signal levels were recorded on Esterline-Angus recorders using a time constant of 25 seconds. The 15-minute medians were then tabulated and reduced to a percentage-of-time basis. The resultant distribution of these medians for the particular weekend period was plotted in percentage of time versus dbm on arithmetic probability paper. By this method the median received power level is established at the 50 per cent of time point for the given weekend. We will now discuss some samples of weekend recordings.

Fig. 8 shows a segment of the weekend recording for May 25–28, 1956. This record is typical of the field strengths encountered during the year. In this case the distributions for both antennas are fairly linear and

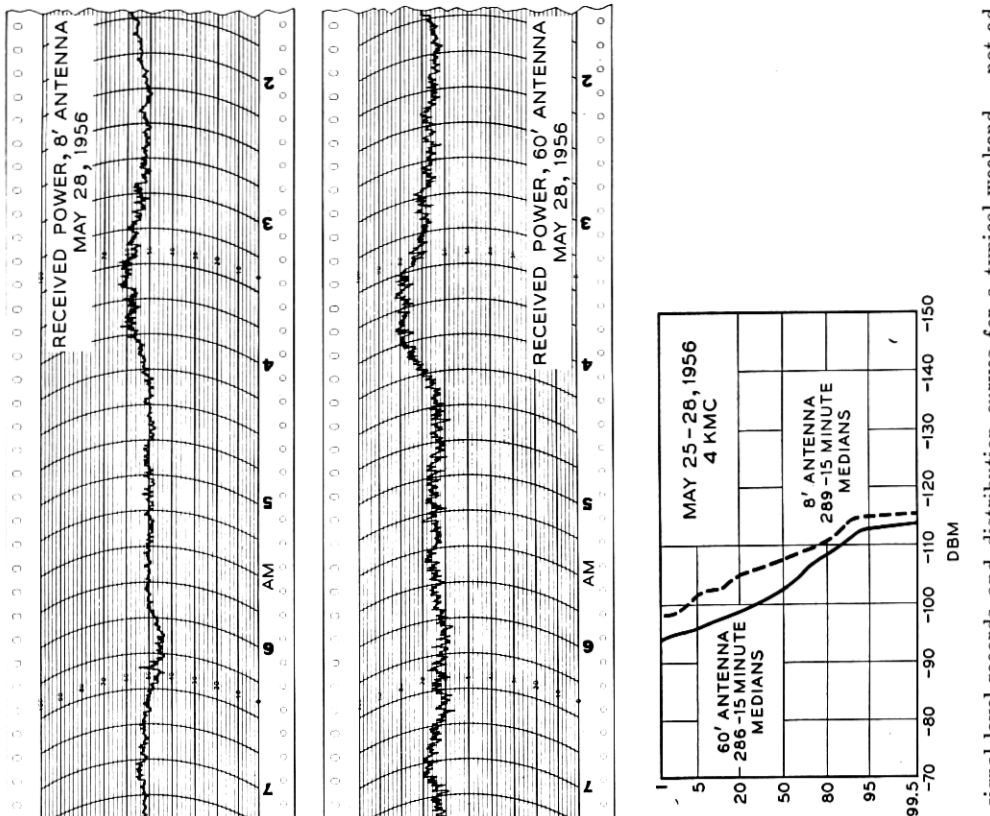

Fig. 8 — Segments of median signal level records and distribution curves for a typical weekend — not adjusted for antenna line losses (see Table I). The full scale on the records is -75 dbm. The 10 foot transmitting

indicate that the received power is distributed randomly when plotted in percentage of time versus decibels. The difference between the 50 per cent points of the two distributions is about 5.0 db, as indicated by the circles marked on the curves. When adjusted for antenna line losses, this difference becomes 6.3 db.

During the weekend of October 21–24, 1955, the difference in the medians of the two antenna was about 8.5 db, as shown in Fig. 9 (9.8 db when adjusted). Some of these distributions were far from linear, since there often was a departure from linearity in the curve at the higher signal level and low percentage-of-time regions. This condition was observed several times during the year; it is believed to be due to large stratified layers in the atmosphere.

The weekend of March 23–26, 1956, gave us our lowest medians of the year. A segment of the record is shown in Fig. 10. In this case the medians for the two antennas are almost equal; this is often found when the received power level is low.*

3.1.2 *Distribution of Weekend Medians for One Year*

The median signal levels of each weekend are plotted for the year from January 8, 1956, to January 13, 1957, in Fig. 11. The points represent the average power available at the output of the antenna feed horns. It may be seen from this curve that small ratios of the power received by the two antennas are most prevalent during the winter months.

In Fig. 12, the weekend (60-hour) medians of Fig. 11 have been plotted on a percentage-of-time basis for the year. The median values of these curves establish the performance of the antennas on a yearly basis. From the ratio of these medians we find that the power output of the 60-foot antenna is 5.7 db above that of the 8-foot antenna.

The median power output of the 8-foot antenna (on a yearly basis) was -109 dbm. Since the power received under free-space conditions for the 8-foot antenna would be -36 dbm, the transmission loss, relative to free space, was 73 db at 4110 mc for this 171-mile path.

3.1.3 *Comparison with Theory*

In the theory of reflection by layers, the transmission loss in radio propagation beyond the horizon for equal size transmitting and receiv-

* The numerous spikes in the record are reflections from aircraft flying through the path. These reflections are much more evident on the record obtained from the 8-foot antenna, since the 8-foot antenna gives a greater common volume than the 60-foot antenna (see Fig. 7).

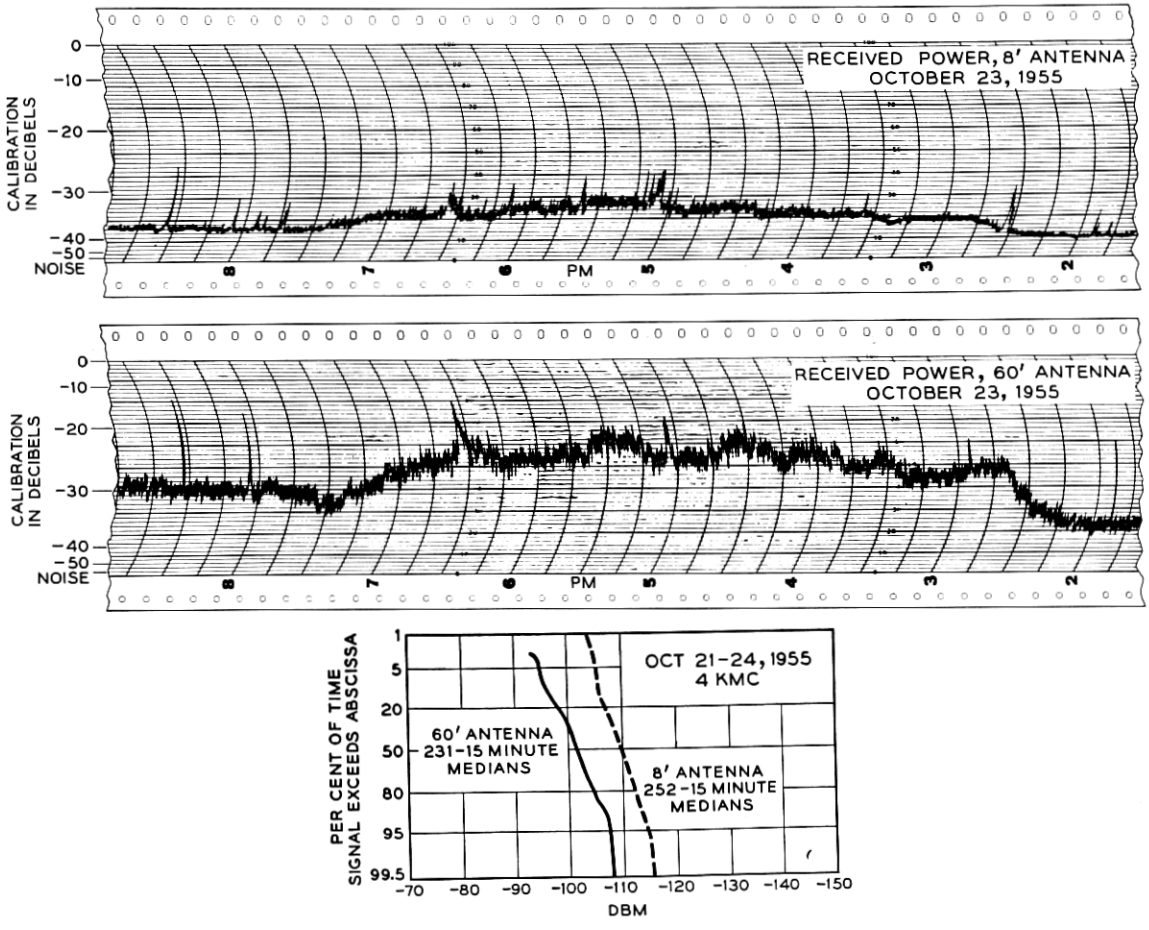

Fig. 9 — Segments of median signal level records and distribution curves for a high median signal weekend.

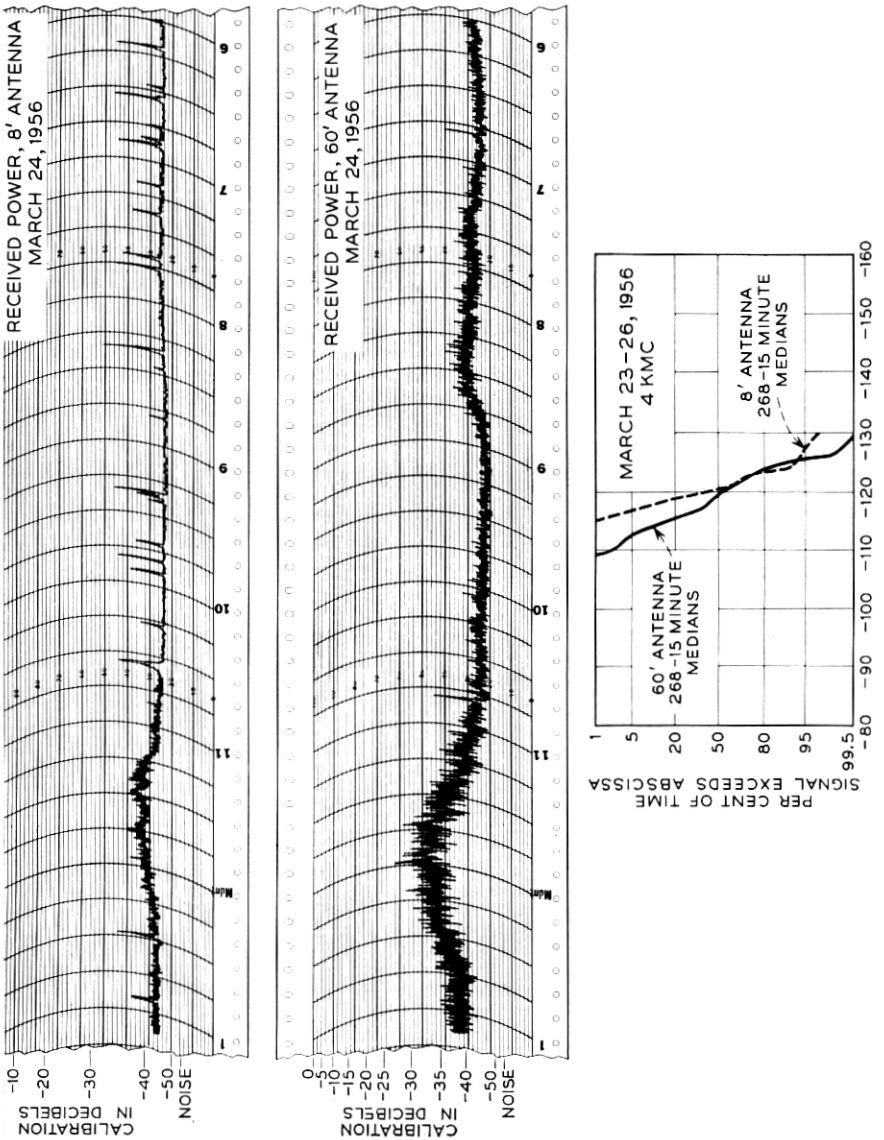

Fig. 10 — Segments of median signal level records and distribution curves for a low median signal weekend. The full scale on the records is −76 dbm.

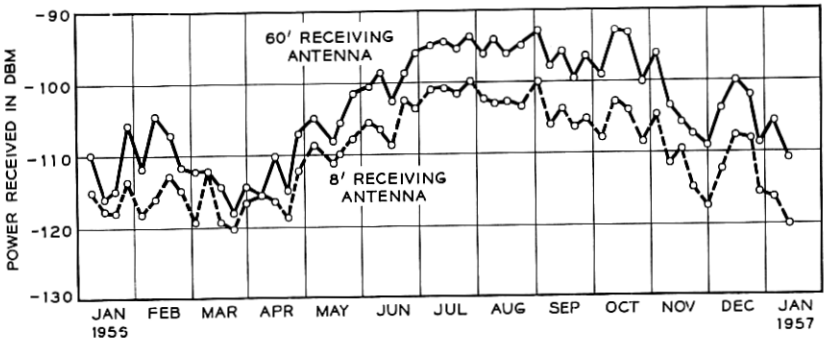

Fig. 11 — Weekend medians (60 hours) for one year of power received at 4110 mc. The 10-foot transmitting antenna was used with a power input of 43 dbm. Received power adjusted for antenna line losses. Period: January 1956 through January 1957.

ing antennas is given by three factors, as shown below in (1). The first term in brackets represents the power that would be received in free space, the second term involves the characteristics of the atmosphere, and the third term is a correction factor for narrow beam antennas:

$$P_R = \left[\frac{P_T\lambda^2}{4a^2\alpha^2}\right]\left[\frac{4M\lambda}{3\theta^4}\right]\left[\frac{\frac{\alpha}{\theta} f\left(\frac{\alpha}{\theta}\right)}{2+\frac{\alpha}{\theta}}\right], \tag{1}$$

where

P_R and P_T are the powers received and transmitted,
α, for actual antennas, may be taken as the half-power beamwidth,
θ is the angle between the lower edge of the idealized antenna pattern and a straight line joining the terminals and
$2a$ is the distance between the terminals.

These parameters are shown in Fig. 13 (Ref. 5, p. 636). Also,
λ is the wavelength,
M is a factor which includes the average size, number and strength of layers in the atmosphere, and

$$f\left(\frac{\alpha}{\theta}\right) = 1 + \frac{1}{\left(1+\frac{\alpha}{\theta}\right)^4} - \frac{1}{8}\left(\frac{2+\frac{\alpha}{\theta}}{1+\frac{\alpha}{\theta}}\right)^4. \tag{2}$$

We now compare the power received by the 60-foot and 8-foot antennas

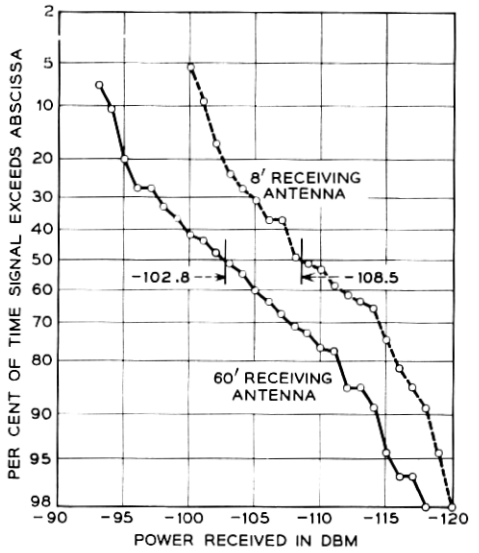

Fig. 12 — Yearly distribution of 60-hour weekend medians of power received at 4110 mc.

at 4 kmc using the theory. Since unequal beamwidths are involved, a generalization of (1) is necessary. (This is carried out in the Appendix.) The result is

$$\frac{P_{R_2}}{P_{R_1}} = \frac{\alpha_{R_1}{}^2(\alpha_T + 2\theta)\left[f\left(\frac{\alpha_T}{\theta}\right) + f\left(\frac{\alpha_{R_2}}{\theta}\right) - \left(\frac{\theta}{\theta + \alpha_{R_2}}\right)^4 f\left(\frac{\alpha_T - \alpha_{R_2}}{\theta + \alpha_{R_2}}\right)\right]}{\alpha_{R_2}\alpha_T(\alpha_{R_2} + 2\theta)\left[f\left(\frac{\alpha_T}{\theta}\right) + f\left(\frac{\alpha_{R_1}}{\theta}\right) - \left(\frac{\theta}{\theta + \alpha_T}\right)^4 f\left(\frac{\alpha_{R_1} - \alpha_T}{\theta + \alpha_T}\right)\right]}. \quad (3)$$

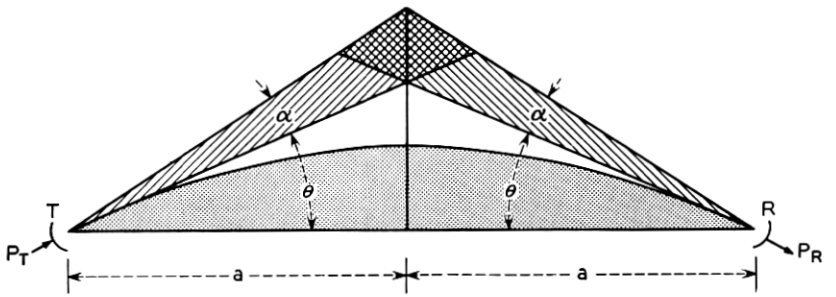

Fig. 13 — Parameters in a beyond-the-horizon circuit.

Substituting the appropriate parameters for this circuit, $\theta = 0.9°$ (4/3 earth), $\alpha_T = 1.8°$ (10-foot antenna), $\alpha_{R_1} = 2.2°$ (8-foot antenna), $\alpha_{R_2} = 0.33°$ (60-foot antenna), we get

$$\frac{P_{R_2}}{P_{R_1}} = 6.5 \text{ (8.1 db)}.$$

This compares favorably with our measurements of 5.7 db. This measured value is somewhat smaller than one might expect purely from the "loss in gain" of the 60-foot antenna, since it also includes the effects of local bending at the receiving site, as discussed in Section 4.2.

3.1.4 *Relationship between Propagation Data and Meteorological Conditions*

It is apparent from Fig. 11 that the received power has a strong seasonal dependence, being as much as 15 db higher in summer than in winter. In Fig. 14 the weekend values have been averaged over the month and replotted along with the average monthly temperature. The temperature, relative humidity and atmospheric pressure at ground level

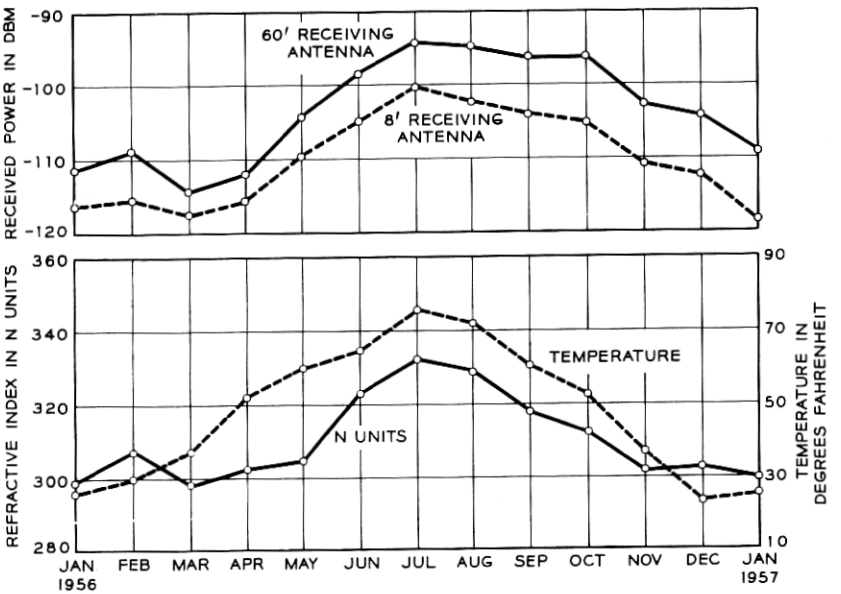

Fig. 14 — Monthly medians of received power at 4110 mc compared with surface temperature and refractive index from weather station at Avoca, Pa.

were obtained from the weather station at Avoca, Pennsylvania, which is near the middle of the propagation path. From these data the refractive index at the ground level was calculated and is also shown in Fig. 14. The formula[10] used for calculating the refractive index is:

$$N = (n - 1) \times 10^6 = \frac{77.6}{T}\left(p + \frac{4810\, e_s\, RH}{T}\right), \tag{4}$$

where

N = refractive index in "N" units,
n = refractive index of the atmosphere,
p = atmospheric pressure in millibars,
T = temperature in degrees Kelvin,
e_s = saturation vapor pressure in millibars for the temperature, T, and
RH = relative humidity.

The correlation between the received power level and the refractive index is believed to be due in part to the bending of the radio waves, as discussed in the theory (Ref. 5, p. 640). Thus, in the summer season when the refractive index is highest, more bending occurs and therefore the received power is higher.

3.2 *Wavelength Dependence*

This section describes a study in which measurements were made simultaneously at two widely separated wavelengths to investigate the wavelength dependence. The half-power beamwidths of the antennas are fairly broad at both frequencies, the vertical and horizontal beamwidths along with antenna sizes being shown in Fig. 15. While the beamwidths of the antennas used for the two wavelengths are not exactly equal, there is supporting evidence from our other experiments that the beams in all cases are sufficiently broad to insure that atmospheric effects are controlling over the effects of antenna size.

The method of analysis was the same as that for the experiment described in the previous section.

3.2.1 *Received Power at 460 and 4110 mc*

Fig. 16 shows the median power levels for both the 460-mc and 4110-mc signals. While the data are for a 21-month period (from April 1956 through December 1957) the data are plotted as a yearly period; the data from April through December 1956 were combined with data for

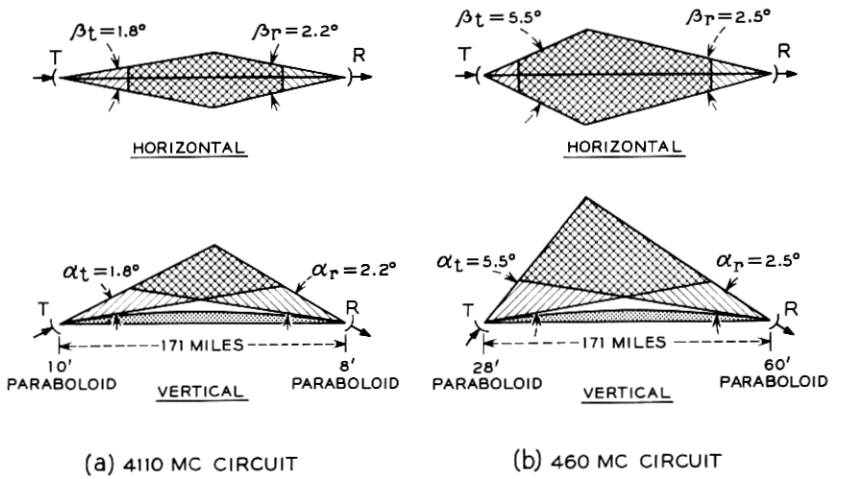

Fig. 15 — Antenna beamwidths and common volumes for wavelength dependence study: (a) 4110 mc; (b) 460 mc.

the corresponding month in 1957 and plotted as one month. The available data for the months of January through April 1957 were sparse. A seasonal variation in the received level similar to that noted in the previous section is evident in Fig. 16.

The weekend (60-hour) medians of received power were normalized to the power that would be received under free-space conditions for both wavelengths and cumulative distributions were made. These data are shown in Fig. 17. The median beyond-the-horizon transmission loss is 61.5 db at 460 mc and 69.8 db at 4110 mc. The long-term median received power relative to free-space transmission is 8.3 db greater at 460 mc than at 4110 mc.

3.2.2 *Variations in Wavelength Dependence — Comparison with Theory*

The wavelength dependence was found to vary considerably from day to day. In order to determine the variability of the wavelength dependence, the weekly median beyond-the-horizon transmission loss in excess of the free-space loss at 460 and 4110 mc was expressed as a ratio. A cumulative distribution curve of these ratios is shown in Fig. 18.* The ratio, T_{460}/T_{4110}, is the relative transmission coefficient at 460 and 4110 mc. It should be emphasized that, since the antenna beams used

* Bolgiano[11] has found a similar wavelength dependence using Lincoln Laboratory data.

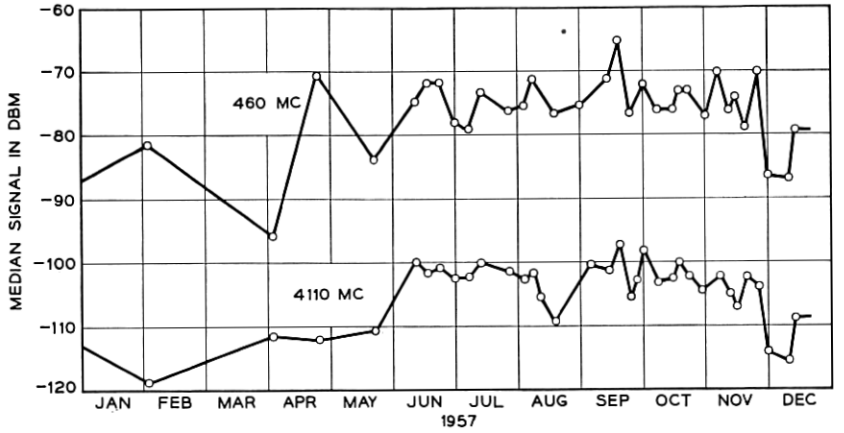

Fig. 16. — Median received signal levels for one year at 460 and 4110 mc. At 460 mc the 28-foot transmitting antenna was used with a power input of 57 dbm, signals were received on the 60-foot antenna. At 4110 mc, the 10-foot transmitting antenna was used with a power input of 43 dbm, signals were received on the 8-foot antenna. The data have not been adjusted for antenna line losses (see Table I). Period: April 1956 through December 1957.

were large, it is believed that this distribution is a true representation of the effect of the atmosphere on the propagation at the two widely

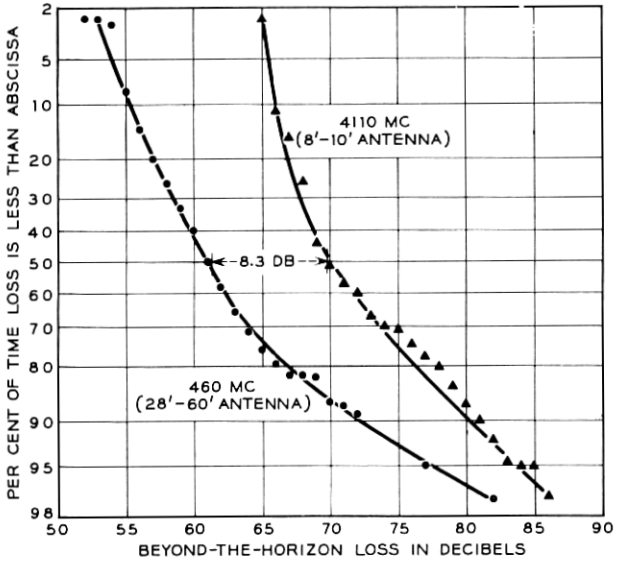

Fig. 17 — Distribution of the beyond-the-horizon transmission loss in excess of the free-space loss at 460 and 4110 mc. Period: April 1956 through December 1957.

separated wavelengths. Since the distributions were obtained using the 60-hour weekend medians instead of the 15-minute medians, an abrupt change of slope occurs in the extreme values.

With the aid of Fig. 18 we see that the median value of the relative transmission loss is 8.3 db. At the 95 per cent point on the distribution the 460-mc signal is about 19 db greater than the 4110-mc signal. At the 2 per cent point the received signal levels at both frequencies are about equal (all relative to free space).

Wavelength dependence has also been considered in the theory. In the last section we were concerned with the antenna sizes at one frequency; here we keep the beamwidths constant and vary the frequency. Using (1) one obtains

$$\frac{P_{R_1}/P_{R_2}\text{ (beyond horizon)}}{P_{R_1}/P_{R_2}\text{ (free space)}} = \left(\frac{\lambda_1}{\lambda_2}\right)^1,$$

when we have intermediate size layers (Case 3) (see Ref. 5, p. 637, Equation 17). For large layers (Case 1) this ratio becomes

$$\frac{P_{R_1}/P_{R_2}\text{ (beyond horizon)}}{P_{R_1}/P_{R_2}\text{ (free space)}} = \left(\frac{\lambda_1}{\lambda_2}\right)^2,$$

while for small layers (Case 2) we have

$$\frac{P_{R_1}/P_{R_2}\text{ (beyond horizon)}}{P_{R_1}/P_{R_2}\text{ (free space)}} = \left(\frac{\lambda_1}{\lambda_2}\right)^0.$$

For large layers in the atmosphere (Case 1), the wavelength dependence is 19.0 db for the frequencies used; if layers in the atmosphere are small (Case 2) the wavelength dependence is 0 db. For intermediate size layers (Case 3) we get 9.5 db, which compares favorably with the measured value of 8.3 db.

IV. CHARACTERISTICS OF THE SIGNALS RECEIVED ON A LARGE APERTURE ANTENNA

In order to learn more about the mechanism of the propagation, an experiment was carried out using the scanning feature of the 60-foot paraboloid antenna.[6] The experiment was designed to investigate the variation in received power as the beam of the antenna was scanned in azimuth and elevation. A further aim was to look for relationships between the scanning data and the median signal levels received simultaneously on the 60-foot antenna and on the 8-foot comparison antenna. A discussion of the aiming of narrow-beam antennas as it is affected by

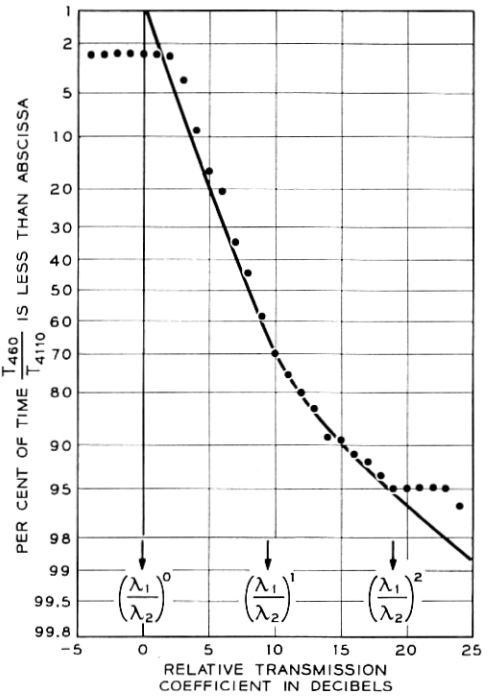

Fig. 18 — Disitrbution of the wavelength dependence of the relative transmission coefficient at 460 and 4110 mc. Period: April 1956 through December 1957.

foreground terrain and local atmospheric conditions concludes the section.

4.1 *Beam Swinging Experiment*

In this experiment the 10-foot transmitting antenna and the 4-kmc transmitter are used; Fig. 19 shows the setup at the receiving end. A dc voltage which is proportional to the angle of rotation of the 60-foot antenna is derived from potentiometers and fed to the X-axis of an oscillograph. The signal from the receiver is placed on the Y-axis and is recorded by using a Polaroid camera attached to the oscillograph. The total scan is 2.8° in azimuth and 3.0° in elevation. The period of a single scan is 15 seconds. Since the period of the short-term fading can be an order of magnitude smaller than the scan period, an integration method is used to average out the time variation of the received signal.*

* A rapid beam-swinging experiment has recently been performed by Waterman.[12]

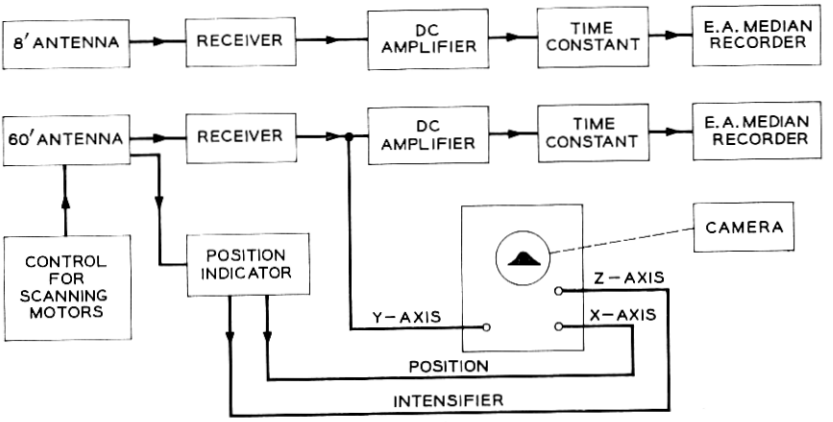

Fig. 19 — Recording setup for beam-swinging experiment.

This is accomplished by superposing 12 scans on a single photographic exposure. During this interval the type of fading as well as the median signal level remain fairly constant.

The median signal levels received simultaneously on the 60-foot antenna and on an 8-foot comparison antenna are recorded on Esterline-Angus recorders; the time constant of the recorder circuits is 25 seconds. The 60-foot antenna is aimed for maximum signal for recording the median level.

4.1.1 *Examples of Beam-Broadening*

Figs. 20 and 21 show sample scans taken with the 60-foot antenna at 4.11 kmc; these were chosen to illustrate interesting characteristics of the received signal. The angles, δ_{10} and γ_{10}, represent the width of the patterns in degrees at the 10-db points for horizontal and vertical scans respectively; they are obtained by drawing an envelope through the maxima of the photographed signal and measuring the width of the envelope at points 10 db below the maximum signal level. The zero on the angle scale represents the same antenna orientation for all the pictures; it is otherwise arbitrary.

Fig. 20(a) shows azimuth and elevation scans on the line-of-sight Murray Hill-Crawford Hill path. It will be noted that there is some asymmetry in the patterns of Fig. 20(a); this is because the feed horn used was one of an assembly of horns used for other experiments. Thus, the gain and beamwidth were not optimum.

Fig. 20(b) shows a rather unusual transmission phenomenon. It is

characterized by a very high median received signal level (about 35 db higher than that usually observed) and by very slow fading (on the order of one fade per minute). At this time the free-space beamwidth and gain of the large antenna were realized. These observations point to the existence of a large stratified layer in the region common to the beams of the transmitting and receiving antennas.

Fig. 20(c) has a pattern width slightly broader than the free-space

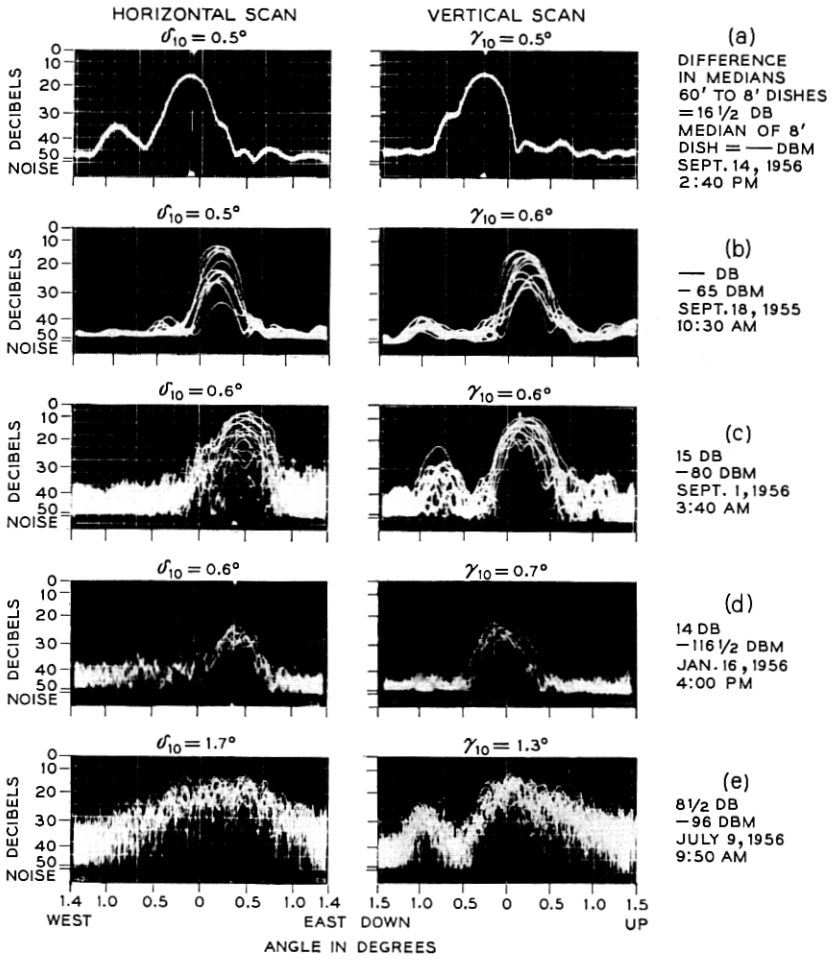

Fig. 20 — Sample scans of signals received on the 60-foot antenna at 4110 mc. The zero on the angle scale represents the same antenna orientation for all pictures; it is otherwise arbitrary.

beamwidth, but it is characterized by more rapid fading than in Fig. 20(b). Fig. 20(d) shows that it is possible to have very little beam-broadening (near free-space characteristic) for low median signal levels.

Fig. 20(e) is an example of the average beam-broadening observed on this circuit. Two features of the vertical scan are worth noting: the linear decrease in received power (in db) as the angle of elevation of the antenna is increased from 0° to 1.5° is typical; the lobe near 1° down is due to reflection from the foreground of the receiving site and will be discussed in more detail later.

Fig. 21(a) shows a very broad pattern; the received power is essentially independent of the azimuth setting of the antenna. We believe that this condition is due to numerous reflecting layers of small dimension in the atmosphere.

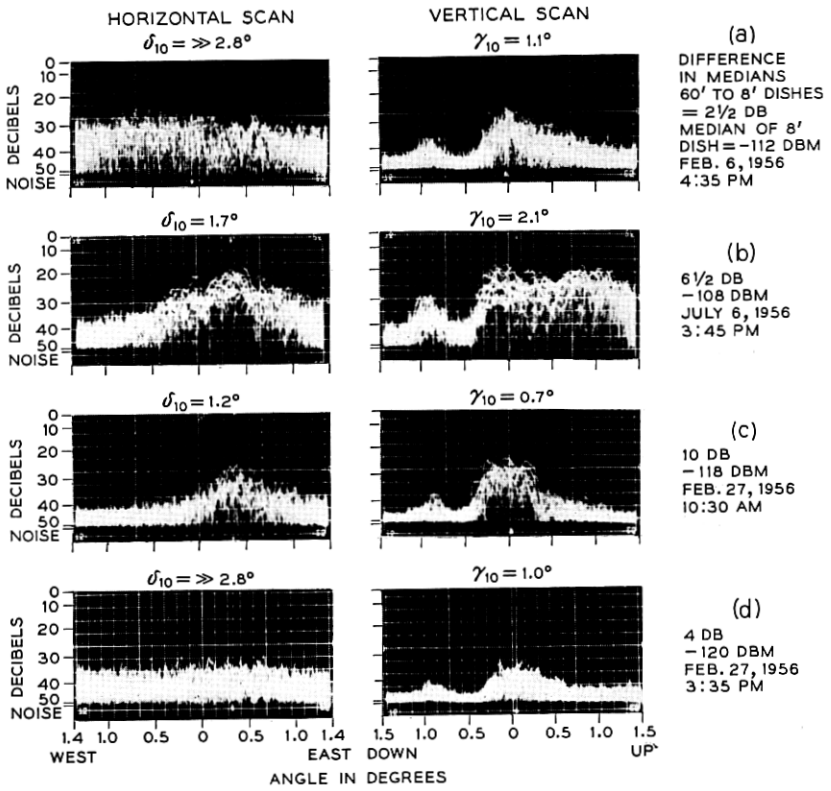

Fig. 21 — Additional sample scans of signals received on the 60-foot antenna at 4110 mc.

The vertical scan in Fig. 21(b) indicates the existence of two strongly reflecting regions in the atmosphere at heights corresponding to 3000 and 11,000 feet above the ground at midpath.

The rapidity with which atmospheric conditions can change is illustrated by comparing Figs. 21(c) and 21(d), which were taken on the same day five hours apart. The horizontal beam-broadening in Fig. 21(d) exceeds that in Fig. 21(c) by about three times, yet the median signal level is the same in the two cases. The weather map for that day indicates a front moving perpendicularly to the transmission path from the west.

The range and rate of fading at the edges of the pictures are greater than at the center. This is caused by two factors: the scanning motion of the antenna is sinusoidal, so that the antenna beam spends more time at the edges of the scan than in the middle, hence both the exposure time and the probability of a high signal are increased at the edges; and the fading rate off the great circle route is greater due to longer path delays.

4.1.2 *Average Scanning Patterns — Comparison with Theory*

To find the average beam-broadening, 30 sets of pictures, similar to those in Figs. 20 and 21 were taken over a period of several months; the envelopes of these were normalized and then averaged. In other words, the average envelope of received power versus angle was obtained. Fig. 22 shows the results of this analysis. The free-space patterns are shown for comparison.

The composite horizontal scan [Fig. 22(a)] shows that, on the average, most of the power directed toward the receiver is contained within an angle of one degree (measured at the 3-db points) in the horizontal plane. Thus the free-space pattern is broadened by a factor of three. There is definite asymmetry in this composite pattern; this is due to the fact that some of the horizontal scan patterns peaked between 0 and 0.5° west rather than at the dead-reckoning position (0.35° east). The cause of this anomalous condition is unknown at present. Large horizontal beam-broadening and rapid fading were present when the shift was evident [see Fig. 21(a)]. When the anomaly was present, a check on the orientation of the antenna was made using the Murray Hill transmitter, and it was determined that the shift was not due to deformation of the antenna itself.

Fig. 22(a) shows the measured azimuth position of Murray Hill with respect to the horizontal scan. Calculation of the initial course angles (dead reckoning) between Crawford Hill and Murray Hill and between

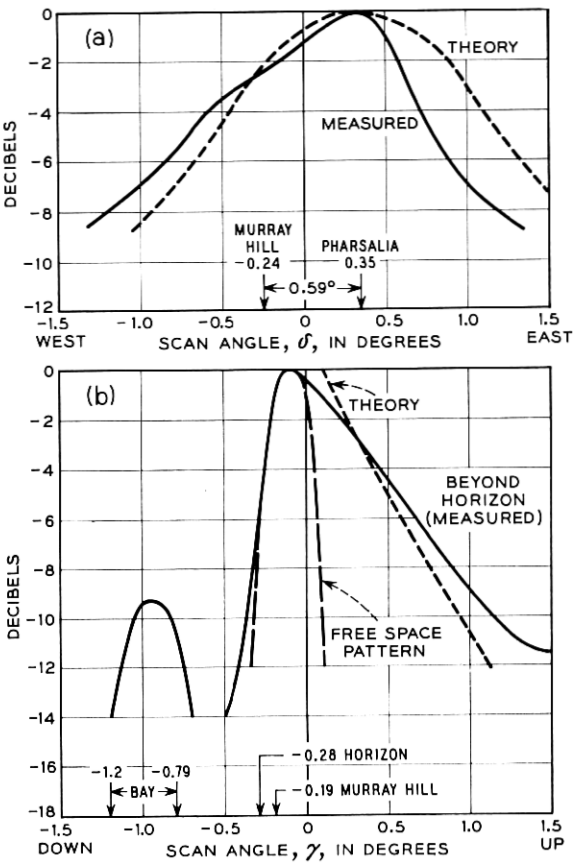

Fig. 22 — Average (a) horizontal and (b) vertical scanning patterns. The experimental curves represent a composite of 30 scans. The theoretical curves are calculated from the theory, using intermediate-size layers.

Crawford Hill and Pharsalia gives a difference in azimuth of 0.59°. This angle also is laid out on the figure; it will be noted that peak signal on the composite scan coincides with the calculated position of Pharsalia.

The composite vertical scan is shown in Fig. 22(b). Reflection from Raritan Bay (shown on the foreground profile in Fig. 3) accounts for the strong lobe which appears when the antenna beam is pointed below the horizon. Using this profile, the position of the bay and other information were calculated and superimposed on the angular scale. It is interesting to note that the drop-off in power as the antenna scans below Murray Hill closely follows the free-space pattern. The power directed

toward the receiver is contained within an angle of 0.6° (measured at the 3-db points) in the vertical plane. A comparison with the free space pattern shows that a three-to-one broadening occurs.* The average curve shows that the received power (in db) falls off rather linearly as the angle of elevation of the antenna is increased from the horizon to higher elevations. If one converts elevation angle to height at the center of the path, one finds that the power fall-off between 3500 feet above sea level (−0.1° on the scale) and 13,500 feet (+1.1°) is 10 db; thus the average rate of fall-off of received power with height is about 1 db per thousand feet.

Using Fig. 78 in the Appendix, one can calculate the beam-broadening of an antenna of given beamwidth. The free-space antenna pattern used in the theory is wedge-shaped, so that the theoretical curve for the vertical beam-broadened pattern rises very steeply for angles near the horizon. The theoretical patterns are shown in Fig. 22; the vertical pattern is normalized with the experimental one at the 3-db point.

The theoretical curves plotted are those for the intermediate size layers (theory, case 3). If one considers the atmosphere to be composed of several large horizontal layers, then one would expect the beamwidth at the receiver to approximate that of free space; this is consistent with the result shown in Fig. 20(b). On the other hand, if one considers several large layers which may be tilted with respect to the horizontal plane (theory, case 1) then a broadened pattern similar to that of Fig. 21(c) is obtained. Furthermore, if small layers (theory, case 2) which are uniformly distributed throughout the atmosphere are considered, a pattern broader than that of Fig. 22(a) is obtained. However, the theory in its present state does not account adequately for very broad patterns,† such as Fig. 21(b).

4.1.3 *Beam-Broadening and the Ratio of the Power Received on the 60-Foot and 8-Foot Antennas*

Since the beam-broadening of the 60-foot antenna varied so much from day to day, as shown by the data just discussed, it seemed desirable to try to obtain a quantitative relation between the beam-broadening and some other parameter such as median signal level. The following experimental procedure was adopted: the horizontal and vertical scans were taken and the 10-db widths of the patterns (δ_{10} and γ_{10}) were

* The beamwidth measured from the peak to the half-power point above the horizon is about 0.4°.

† The very broad patterns might be explained with the assumption of numerous isotropic reradiators.

measured from the photographs. Both before and after the scans, the median signal levels on the 60-foot antenna and on the 8-foot antenna were obtained from the Esterline-Angus recorders. From theoretical considerations, it was believed that the product of the 10-db widths in the two planes and the ratio of the power levels on the large and small antennas were the significant parameters.

In Fig. 23 observed values of the ratio of power on the two antennas are plotted versus measured inverse products of the 10-db pattern widths. The points fit the curve that is discussed in the next paragraph.

Consider antennas as used in a line-of-sight path with plane waves incident upon them. Then the ratio of the power received in free space by a paraboloid of a certain aperture relative to that received by an 8-foot paraboloid can be plotted as a function of the inverse product of the free-space horizontal and vertical beamwidths of that paraboloid as its aperture size is increased, as shown by the curve of Fig. 23. The end points of the curve correspond to the measured gain and beamwidth of the 60-foot and 8-foot antennas; the curve is normalized to give a gain of 0 db for the 8-foot antenna. The ratio of the gains of the 60-foot and the 8-foot is 16.5 db; the 10-db beamwidths are 0.5° and 2.8° respectively.

Consider now two antennas, a 60-foot and an 8-foot paraboloid, used

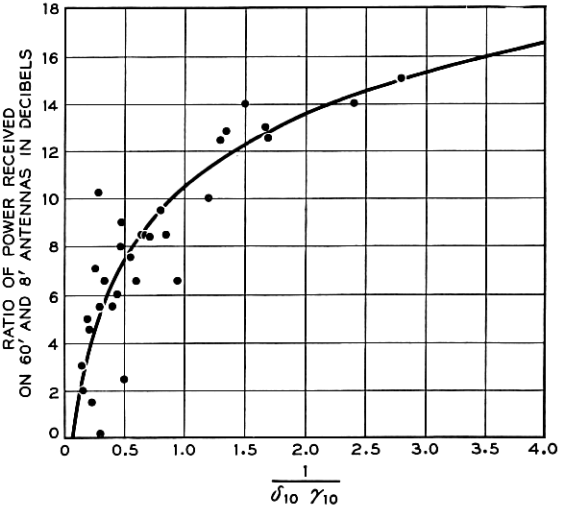

Fig. 23 — Ratio of median signal levels received simultaneously on 60-foot and 8-foot antennas as a function of the inverse product of the 10-db beamwidths; δ_{10} and γ_{10} are the beamwidths in degrees for the horizontal and vertical scans, respectively. Points are experimental; curve is theoretical.

in a beyond-the-horizon propagation test. This experiment is a duplicate of the one on the line of sight, except that antenna size is not a variable. The ratio of the power received on the two antennas is measured simultaneously with the horizontal and vertical beam patterns of the 60-foot antenna, and this ratio is plotted against the inverse product of the 10-db widths of the measured patterns as discussed previously.

Since the experimental points in Fig. 23 lie close to the theoretical curve, it is concluded that the beam pattern and received power of the 60-foot antenna in a beyond-the-horizon circuit change from day to day in a manner corresponding to an antenna of changing size in line-of-sight propagation. The ratio of the power received on the 60-foot and 8-foot antennas in the beyond-the-horizon path is less than that in free space, because the incident energy over the face of the 60-foot antenna has components which are not of equal amplitude nor of equal phase. It is believed that the smaller ratio results from an atmosphere which is made up of layers of small dimension. The 8-foot antenna was used as a reference in this experiment, since it is believed that the received field is correlated over its aperture most of the time.

There is some scatter of the experimental points in Fig. 23 because of the difficulty of measuring the angular widths of the beam patterns, especially if the width is large. If it is greater than 3°, an extrapolation has to be made.

From a year's recording of the power received on the 60-foot and 8-foot antennas (Section 3.1.2) we have found that the average difference in medians is 5.7 db. This corresponds to an average pattern width of 1.8° at the 10-db points compared with the free-space pattern of 0.5°.

4.2 *Antenna Aiming*

As can be seen from the previous section, a problem arises as to how to aim a high-gain antenna (3-db beamwidth $<1°$) in a beyond-the-horizon circuit. The previous section showed that, on the average, the maximum signal level is received when the antennas are aimed along the great circle between transmitter and receiver location, with each being aimed just above the horizon. However, local atmospheric refraction can exert considerable influence on the signals received on narrow beam antennas.

An example of what is believed to be the effect of local meteorological conditions is shown in Fig. 24 for June 8, 1956. In the early part of the evening the atmospheric conditions at the receiving site were quite stable. During the evening the humidity rose slowly, as plotted in the figure, and at about 11:00 p.m. the winds increased considerably. As

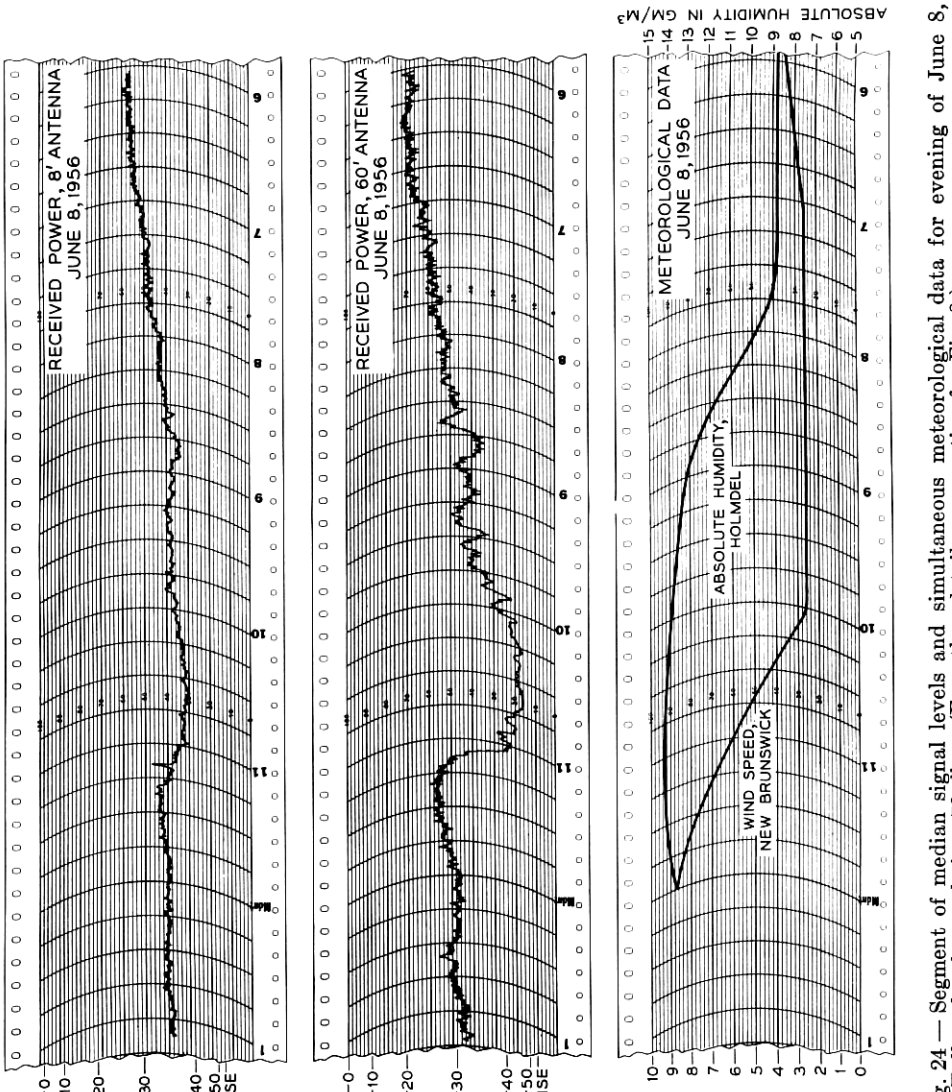

Fig. 24 — Segment of median signal levels and simultaneous meteorological data for evening of June 8, 1956. Full scale of records is −76 dbm. (For other details see caption for Fig. 8.)

observed between the hours of 6:00 p.m. and 11:00 p.m., the power level of the signal received on the 60-foot antenna at 4 kmc slowly decreased some 20 db, whereas the signal on the 8-foot antenna decreased only about 9 db; and then the signal levels of both antennas suddenly returned to their normal levels at 11:00 p.m. This effect is believed to have been caused by increased local bending of the radio waves during the period from 6:00 p.m. to 11:00 p.m. followed by a break-up in this stable condition by the winds at 11:00 p.m.

Fig. 7 illustrates the local refraction which is believed to have taken place. The narrow beam of the 60-foot antenna, as indicated by the broken lines in the figure, is bent some 0.3 degrees into Murray Hill in the foreground of the receiving site; thus the signal level on this antenna decreases considerably. On the other hand, the beam of the 8-foot antenna, although bent, is not completely shadowed and the decrease in signal level is not so pronounced.

Bending of this order of magnitude was frequently observed on the line-of-sight path between Crawford Hill and Murray Hill during the course of angle-of-arrival measurements. Similarly, in these measurements it was observed that the angle of arrival would return to its normal value when winds broke up a stable atmosphere.

This local bending may affect the median signal level over extended periods, as is shown by the data on March 9–12, 1956, and April 6–9, 1956 (Fig. 11). During these weekends the 60-foot antenna was oriented to receive the maximum signal level at the beginning of the period of recording. However, during the run the direction of the received energy changed, thus reducing the median signal level on the narrow beam antenna. The weekend median signal level received on the 60-foot antenna was about the same as that on the 8-foot antenna. The cumulative effect of the local bending undoubtedly decreases the ratio of the power received by the 60-foot and 8-foot antennas, hence the measured 5.7 db yearly difference includes both loss of gain and local bending effects of the 60-foot antenna.

The orientation of the antenna will depend on the beamwidth as well as on the foreground. If one assumes a flat foreground with unity reflection coefficient, then aiming at the horizon will be best for maximum median signal level. If the foreground is not flat, or does not have unity reflection coefficient, an aim slightly above the horizon is preferable. (We are considering a very narrow beamwidth antenna situated at ground level.) For large beamwidth antennas ($>2°$) the aim is not as critical; an aim toward the horizon is satisfactory.*

* Throughout the paper we have used the conventional common volume dia-

V. RATE OF FADING OF RECEIVED SIGNALS

Part of the program of study has been the observation and interpretation of the short-term fading of the received signal. In the first experiment to be described, a 4-kmc cw signal is transmitted; the received power is found to vary in noise-like fashion at a rate of a few cycles per second. The rate of fading varies considerably from day to day and, at times, from hour to hour, due to changes in the atmosphere. The rate is found to depend upon the beamwidths of the transmitting and receiving antennas. Data taken at various times throughout the year have been analyzed and a quantitative relation for fading rate has been developed which is consistent with the experimental results.

A further study is described using simultaneous transmission of two frequencies, 460 and 4110 mc. Here the wavelength dependence of the fading and its relation to the characteristics of the atmosphere is discussed. Antennas of comparable beamwidth are used.

5.1 *Rate of Fading at 4 kmc — Relation to Antenna Beamwidth*

The basic measuring circuit consists of a 10-foot paraboloid transmitting at 4110 mc and two receiving antennas — a 60-foot paraboloid and an 8-foot paraboloid. The outputs of the antennas are recorded separately and the simultaneous short-term fading is examined on a percentage-of-time basis to obtain cumulative probability distributions. Also, the median signal levels are drawn on the records and the fading rates (the number of one-way crossings of the median levels per second) are determined.

From these data one can obtain significant ratios in addition to the absolute fading rate: for instance, the ratio of the fading rate of the signal received on an 8-foot antenna from a 10-foot transmitting antenna, $N_{m(10\text{-}8)}$, to the fading rate observed simultaneously on a 60-foot antenna, $N_{m(10\text{-}60)}$. This ratio $K = N_{m(10\text{-}8)}/N_{m(10\text{-}60)}$ has turned out to be sensibly independent of the absolute fading rates.

On the assumption that propagation beyond the horizon is due to reflections from randomly positioned layers which drift through the atmosphere, a simple formula which predicts the fading ratio, K, for any given combination of antennas is developed. Values of K obtained experimentally by using several combinations of transmitting and receiving antennas check well with the formula.

grams which show idealized antenna beams with the lower *edge* of the beam along the horizon. It is clear from our vertical beam-swinging experiments that for an actual antenna pattern an aim along the horizon results in maximum received power.

From these investigations it has been possible to estimate the effective horizontal scattering angle of the atmosphere for the 171-mile path at 4 kmc. The scattering angle is a measure of the directional properties of the reflections from the layers in the atmosphere. From the data, this angle has turned out to be 0.8 degree, which is in good agreement with the average horizontal beam-broadening of 1 degree discussed in Section IV.

The absolute value of the fading rate for given transmitting and receiving antennas can be estimated with fair accuracy if the winds in the upper atmosphere are known in the region near the center of the path of propagation. Fading rates calculated from known wind data compare favorably with measured fading rates.

5.1.1 *Instantaneous Signal Level Recordings — Analysis*

The horizontal and vertical half-power beamwidths of the antennas used in the basic measuring circuit are shown in Fig. 25. The approximate volume of the atmosphere common to the beams of the 10-foot–8-foot antenna combination is shown by the shaded areas in the figure. The cross-hatched areas show the smaller volume utilized by the 10-foot–60-foot antenna combination. Approximate dimensions are scaled on the left of the sketch.

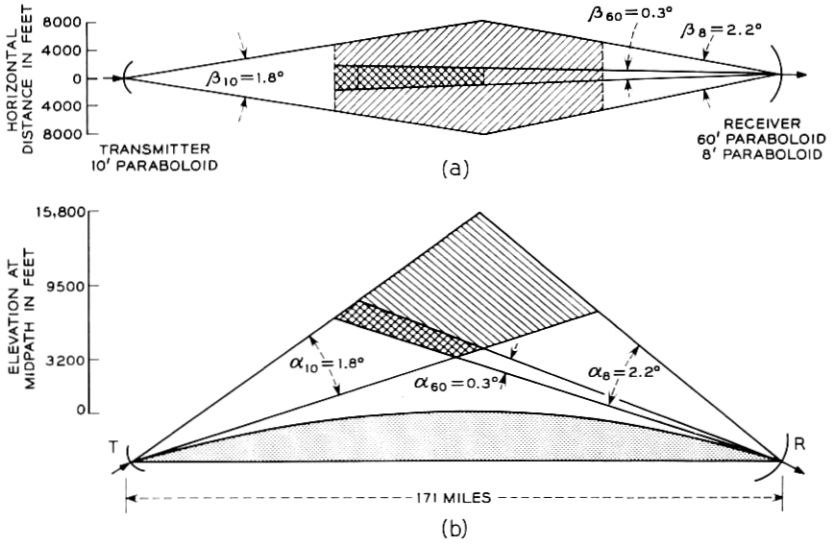

Fig. 25 — Antenna beamwidths and common volumes for fading rate studies at 4110 mc: (a) horizontal; (b) vertical.

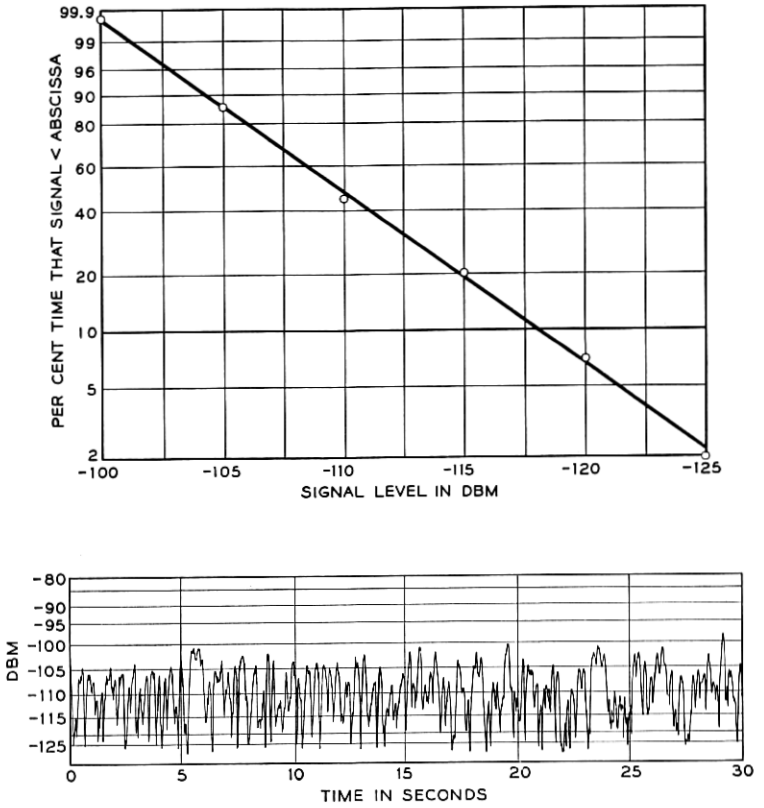

Fig. 26 — Sample and distribution of instantaneous signal levels — very rapid fading at 4110 mc.

The fluctuations in the received signal are recorded on a Sanborn recorder with a time constant of 0.015 second. It is believed that no fluctuations in the received signal were too rapid to be followed by this instrument and, therefore, that the records are a true representation of the received signal.

Sample records of the signal received on the 60-foot antenna, chosen to show the variety of fading rates encountered, are shown in Figs. 26 and 27, with the distribution for each record plotted above the sample. Analysis of Fig. 26, a sample of very rapid fading, indicates a Rayleigh distribution of the signal. Fairly slow fading is shown in Fig. 27 with its distribution curve; within the accuracy of measurement, the Rayleigh distribution is obtained. The Rayleigh distribution indicates that the

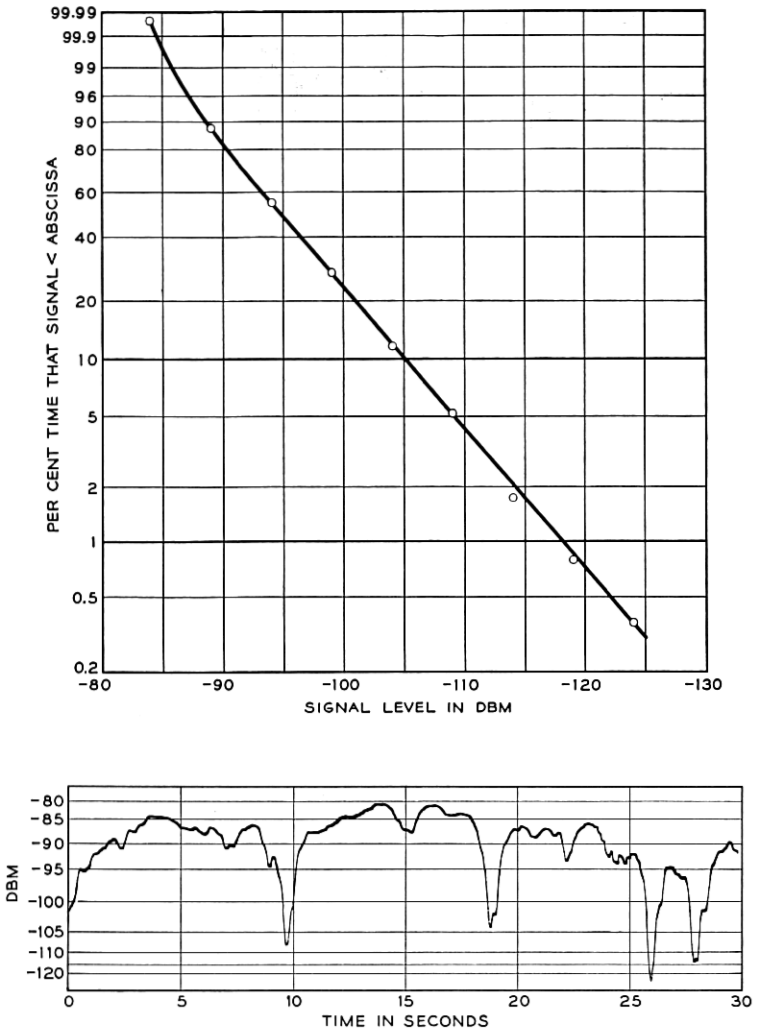

Fig. 27 — Sample and distribution of instantaneous signal levels — slow fading at 4110 mc.

received signal is due to propagation through the atmosphere via many paths of random relative phase.

As previously stated, the rate of fading varies considerably from day to day, and often within the hour. Samples of very rapid, rapid and slow fading signals recorded during one day are shown on Fig. 28. The output

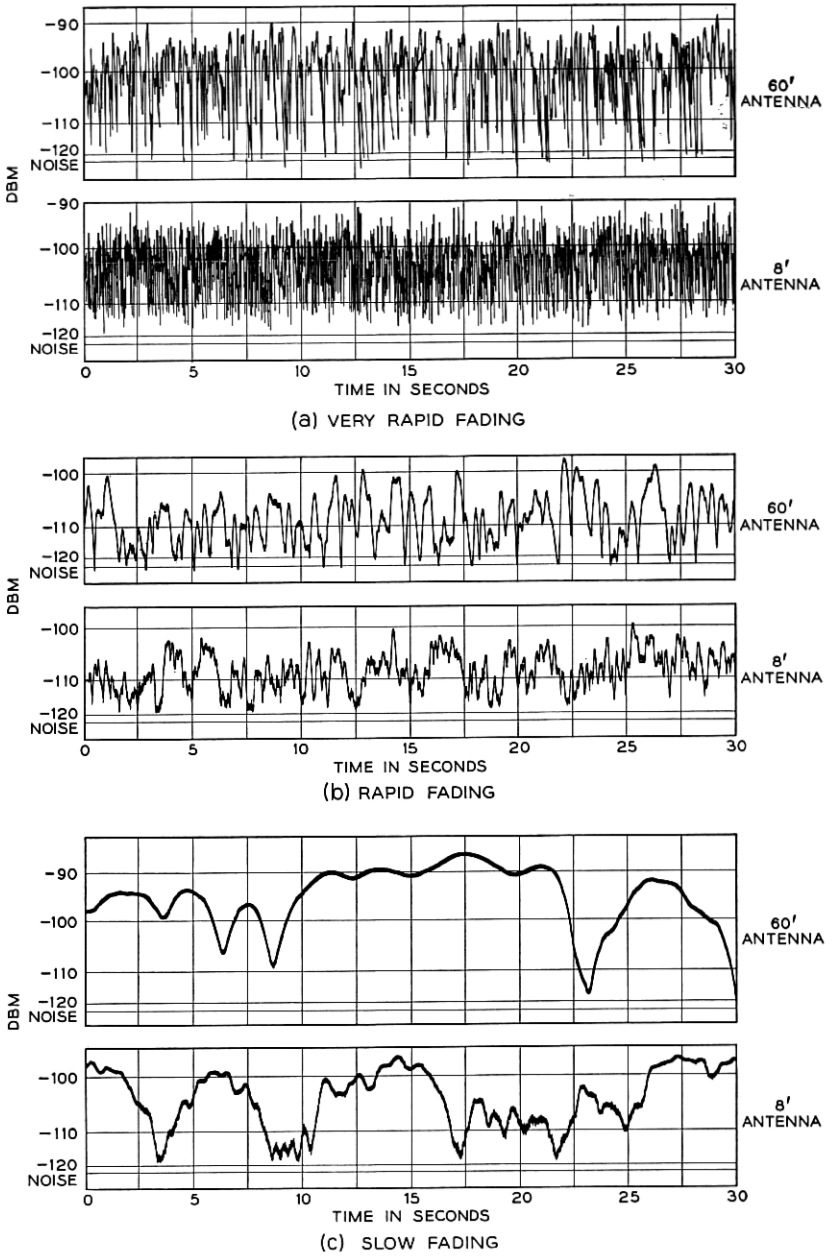

Fig. 28 — Samples of simultaneous recordings of instantaneous signal levels on the 60-foot and 8-foot antennas at 4110 mc.

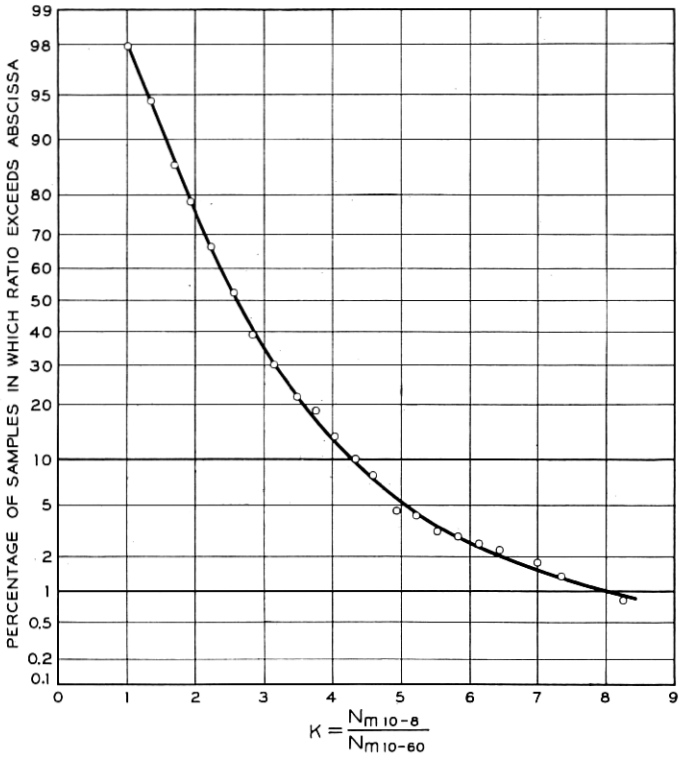

Fig. 29 — Statistical distribution of the ratio of fading rates of the 10-foot–8-foot antenna combination to the 10-foot–60-foot combination at 4110 mc, using 392 samples of 33 seconds in length. Periods: October 1955 through April 1956 and September through November 1957.

of the 60-foot antenna is shown on the top trace of each sample, the output of the 8-foot antenna on the bottom trace. In analyzing the data, the estimated median signal level is drawn on the record and the number of one-way crossings of the median levels is counted; from these, the fading rate and the ratio of the fading rates are derived.

The range of values over which the ratio of the fading rates varies may be seen on the plot of Fig. 29. These data were obtained from a study of 392 sample records taken during the period October 1955 to April 1956 and September to November 1957. The median of the ratios of the fading rate of the signal received on the 8-foot antenna to the fading rate of the signal received on the 60-foot antenna is 2.60. The ratio is well-defined, the spread of values being small.

Table III lists all the antenna combinations used during the measure-

TABLE III — MEASURED AND CALCULATED FADING RATE RATIOS FOR VARIOUS ANTENNA COMBINATIONS — 4 KMC

Transmitting Antenna, feet	Receiving Antennas, feet	K	Number of Samples	K = Ratio of Fading Rates	
				Measured	Calculated
10	8 60	$\frac{N_{m(10\text{-}8)}}{N_{m(10\text{-}60)}}$	392	2.60	—
10	8 28	$\frac{N_{m(10\text{-}8)}}{N_{m(10\text{-}28)}}$	98	1.61	1.47
10	28 60	$\frac{N_{m(10\text{-}28)}}{N_{m(10\text{-}60)}}$	181	1.62	1.67
28	8 60	$\frac{N_{m(28\text{-}8)}}{N_{m(28\text{-}60)}}$	61	1.85	1.86
28	8 28	$\frac{N_{m(28\text{-}8)}}{N_{m(28\text{-}28)}}$	36	1.18*	1.26
28	28 60	$\frac{N_{m(28\text{-}28)}}{N_{m(28\text{-}60)}}$	37	1.65*	1.47

* Limited data, not necessarily typical.

ments, the ratio of fading rates obtained using the various combinations and the number of sample records analyzed.

5.1.2 *Rate of Fading — Theory*

On the assumption that the short-term fading is due mainly to horizontal drift of many randomly positioned layers in the atmosphere which reflect the radio waves, several simple conclusions can be drawn regarding the relation of antenna size and winds to fading rate. The purpose here is to try to obtain a method for calculating the fading rate from known wind data and known antenna beamwidths.

Fig. 30(a) shows a horizontal plan view of a tropospheric circuit in which three rays have been drawn from the transmitting antenna T to reflecting layers A, B and C and thence to the receiving antenna R. The layers are assumed to drift with velocity V at angle δ to the line T-R; the wind component normal to the great circle route is therefore $V \sin \delta$. The length of the path via layer B in excess of the great circle route, TAR, is TBR − TAR = $2x^2/2a$, where x is the distance from layer A to layer B and $2a$ is the distance from T to R.* The phase difference between

* Disposition of the layers in the vertical plane causes path differences larger than this, but, since horizontal winds are much stronger than vertical winds, fading due to vertical motion is not considered here (see Section 6.1).

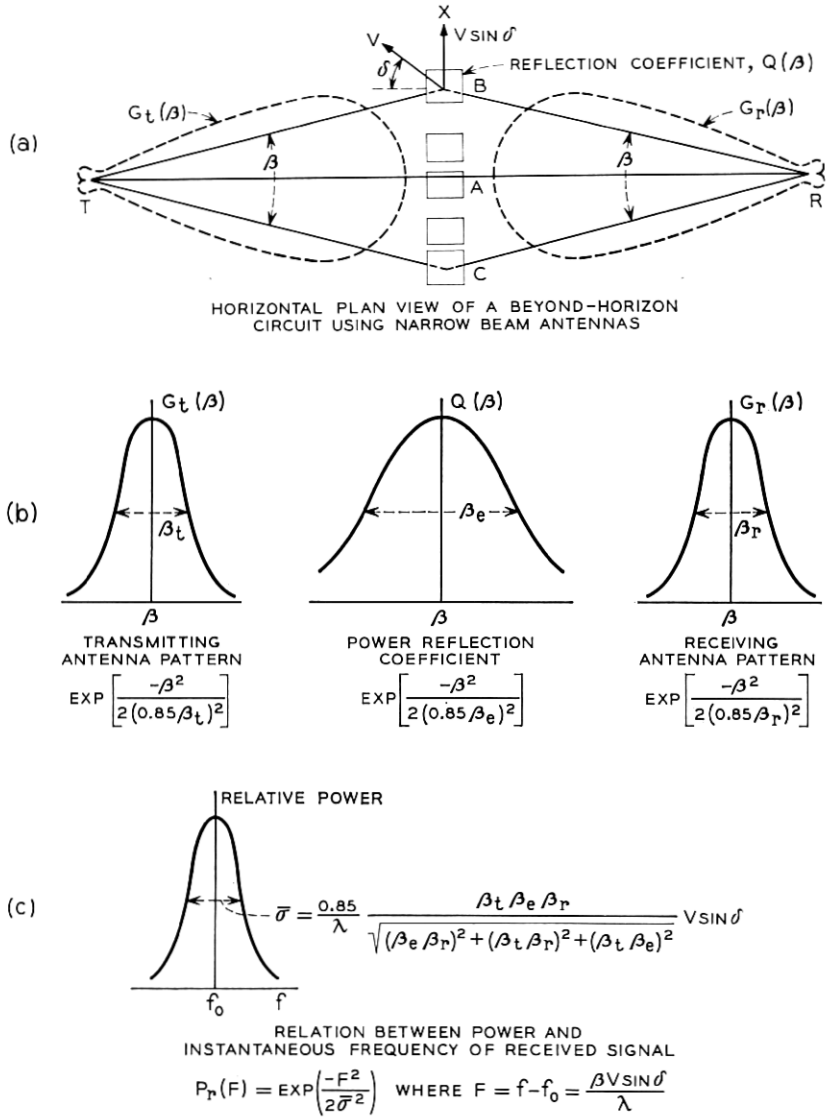

Fig. 30 — Factors affecting the instantaneous frequency of the received signal.

the two paths is $\varphi = [(2\pi/\lambda)\ (x^2/a)]$ and the frequency of fading is

$$F = f - f_0 = \frac{1}{2\pi}\frac{d\varphi}{dt} = \frac{2x}{\lambda a}\frac{dx}{dt} = \frac{\beta}{\lambda} V \sin\delta,$$

where

f_0 = transmitted frequency,
λ = transmitted wavelength,
f = instantaneous frequency, and
$\beta/2 = x/a$ = angle in the horizontal plane between great circle plane and the ray to a layer.

Thus the frequency of fading F is due to the Doppler shift caused by drift of B at velocity $V\sin\delta$ normal to the path. The rate of change of path length due to the wind component along the path is relatively small and is neglected.

The amount of power that reaches the receiver via layer B [Fig. 30(a)] depends on three factors. First, the radiation pattern of the transmitting antenna $G_t(\beta)$ controls the power transmitted in direction β, and therefore the amount of power incident on layer B. Similarly, the radiation pattern of the receiving antenna $G_r(\beta)$ determines the power received from direction β, and therefore influences the amount of power reflected by layer B that enters the receiver. Finally, the power reflection coefficient Q of the layer depends on the angle of incidence of the ray, and therefore on angle β; both experiment and theory* indicate that Q decreases as β increases. Since all three factors tend to decrease the power received from angle β as β increases, and since the frequency of fading, F, is related to β by $F = (\beta/\lambda)\ V\sin\delta$, one would expect the high-fading-frequency components to contribute only small amounts of power to the received signal. In fact, both the atmosphere and the antenna radiation patterns are low-pass filters as far as the frequencies of fading are concerned.

Consider first the effect of the reflection coefficient, Q, on the fading of the received signal. Fig. 30(a) shows numerous layers positioned at random along the x-axis; these are assumed to drift in the x-direction with velocity $V \sin \delta$. At first the transmitting and receiving antenna patterns will be assumed to be omnidirectional; thus, the only factor affecting the power received from a layer at a given angle β is the reflection coefficient Q. Since Q is assumed to be related to β in a gaussian manner, as shown in Fig. 30(b), the power reflection coefficient is

$$Q(\beta) = \exp\left[\frac{-\beta^2}{2(0.85\beta_e)^2}\right], \qquad Q(\beta = 0) = 1,$$

* See Section 4.1.

where β_e is the angle at which $Q = \frac{1}{2}$. β_e is of the order one degree for a 171-mile path at 4 kmc; a detailed discussion is given in Section 4.1.

The received signal is the sum of reflections from all of the randomly positioned layers and, since the reflections are randomly phased, the envelope of the received signal (the rectified signal) is Rayleigh-distributed. For the case of omnidirectional antennas, the distribution of received power versus frequency (the power spectrum) is directly related to the power reflection coefficient, Q. Thus the received power is distributed according to

$$P_r(F) = \exp\left(\frac{-F}{2\sigma_e^2}\right),$$

where $\sigma_e = (0.85\ \beta_e/\lambda)V\sin\delta$ is the standard deviation.* Note that $P_r(F)$ can be obtained directly from $Q(\beta)$ by substituting $F = (\beta/\lambda)V\sin\delta$ for β.

The antenna patterns are taken to be gaussian; that is,

$$G_t(\beta) = \exp\left[\frac{-\beta^2}{2(0.85\beta_t)^2}\right]$$

and

$$G_r(\beta) = \exp\left[\frac{-\beta^2}{2(0.85\beta_r)^2}\right];$$

β_t and β_r are the half-power beamwidths of the radiation patterns [Fig. 30(b)]. The power spectrum of the received signal now depends on $G_t(\beta)$ and $G_r(\beta)$ as well as on $Q(\beta)$. The power received from a layer at angle β is

$$P_r(\beta) = G_t(\beta)Q(\beta)G_r(\beta) = \exp\left[\frac{-F^2}{2}\left(\frac{1}{\sigma_t^2} + \frac{1}{\sigma_e^2} + \frac{1}{\sigma_r^2}\right)\right], \quad (5)$$

where

$$\sigma_{t,e,r} = \frac{0.85\beta_{t,e,r}}{\lambda} V\sin\delta. \quad (6)$$

If we let

$$\frac{1}{\bar{\sigma}^2} = \frac{1}{\sigma_t^2} + \frac{1}{\sigma_e^2} + \frac{1}{\sigma_r^2}, \quad (7)$$

* A formula similar to this was given by Rice[13] (see also Ref. 14). His discussion is based on the assumption of small scattering discontinuities which move in random fashion similar to the thermal motion of the molecules of a gas, and it involves angles in the vertical plane of the propagation path. In the present discussion, horizontal drift of relatively large discontinuities and angles in the horizontal plane are considered to be of major importance.

then

$$P_r(\beta) = \exp\left(\frac{-F^2}{2\bar{\sigma}^2}\right). \tag{8}$$

Substituting (6) in (7), one obtains

$$\bar{\sigma} = \frac{0.85}{\lambda}(V\sin\delta)\frac{\beta_t\beta_e\beta_r}{\sqrt{\beta_e^2\beta_r^2 + \beta_t^2\beta_r^2 + \beta_t^2\beta_e^2}}, \tag{9}$$

where $\bar{\sigma}$ is the standard deviation of the power spectrum that one would expect for the received signal in the circuit of Fig. 30(a). The antenna patterns and reflection coefficient shown in Fig. 30(b) result in the power spectrum of Fig. 30(c).

S. O. Rice has pointed out that fading in beyond-the-horizon circuits behaves like thermal noise that is passed through a filter. In both cases, the rectified signal is Rayleigh-distributed. Similarly, the width of the power spectrum of the signal (the standard deviation, $\bar{\sigma}$) in both cases is related to the fading rate of the envelope. If fading rate, N_m, of the envelope is defined as the number of one-way crossings of the median level per second (this is the definition used in analyzing the experimental data), then the theory of random noise gives $N_m = 1.5\ \bar{\sigma}$. Using the value in (9) for $\bar{\sigma}$, one obtains

$$\begin{aligned} N_m &= \frac{1.27}{\lambda}(V\sin\delta)\frac{\beta_t\beta_e\beta_r}{\sqrt{\beta_e^2\beta_r^2 + \beta_t^2\beta_r^2 + \beta_t^2\beta_e^2}} \\ &= \frac{1.27}{\lambda}(V\sin\delta)g(\beta_t, \beta_e, \beta_r) \end{aligned} \tag{10}$$

for the calculated fading rate, where

$$g(\beta_t, \beta_e, \beta_r) = \frac{\beta_t\beta_e\beta_r}{\sqrt{\beta_e^2\beta_r^2 + \beta_t^2\beta_r^2 + \beta_t^2\beta_e^2}}.$$

We are now able to compare fading rates and ratios of fading rates as calculated by means of (10) with the measured data. First consider the ratio $K = N_{m(10\text{-}8)}/N_{m(10\text{-}60)}$ of the fading rates of the 8-foot and 60-foot receiving antennas with a 10-foot transmitting antenna. Using (10), one obtains after simple reduction

$$\begin{aligned} K &= \frac{N_{m(10\text{-}8)}}{N_{m(10\text{-}60)}} = \frac{g(\beta_{10}, \beta_e, \beta_8)}{g(\beta_{10}, \beta_e, \beta_{60})} \\ &= \frac{\beta_8}{\beta_{60}}\sqrt{\frac{1 + (\beta_{60}/\beta_e)^2 + (\beta_{60}/\beta_{10})^2}{1 + (\beta_8/\beta_e)^2 + (\beta_8/\beta_{10})^2}}. \end{aligned} \tag{11}$$

Substituting the known antenna beamwidths, and the measured value of $K = 2.60$, one can solve for β_e, which turns out to be 0.8°. This value is in good agreement with the 1° obtained for β_e in the beam-swinging experiment. In Table III measured values of K for various antenna combinations are compared with values calculated, using (10) and $\beta_e = 0.8°$.

The good agreement between the measured and calculated values indicates that the term $g(\beta_t, \beta_e, \beta_r)$ in (10) is essentially correct. Therefore, the relationship between fading rate (at 4 kmc) and antenna beamwidth is essentially correct.

5.2 *Rate of Fading at 4 kmc — Relation to Wind*

So far, the discussion has been limited to drift of layers in a horizontal plane in the atmosphere. However, there are two effects with altitude which should be taken into account. First, the contributions to the received power by reflections from layers at high altitudes are less than those from low altitudes (it was shown in Section 4.1.2 that the received power decreases about 1 db per thousand feet of altitude). Also, the drift winds vary in both speed and direction with altitude. Both of these effects, in their relation to fading rate, can be taken into account approximately in the following manner.

The volume, V, common to the transmitting and receiving antenna beams is divided into horizontal segments 1000 feet thick, as shown in Fig. 31(a). Each segment is assumed to contain many randomly positioned layers of finite dimension. The power received from segment 1 is weighted by the factor unity, and the standard deviation of the power spectrum for signals reflected from segment 1 is

$$\sigma_1 = \frac{0.85}{\lambda} g(\beta_t, \beta_e, \beta_r) V_1 \sin \delta_1,$$

where V_1 and δ_1 are the speed and direction of the wind in segment 1 (as obtained from meteorological data). The power spectrum due to segment 1 is therefore

$$\exp\left(\frac{-F^2}{2\sigma_1^2}\right).$$

The power from segment 2 is down (on the average) 1 db from the power from segment 1; the power spectrum for segment 2 is therefore

$$0.8 \exp\left(\frac{-F^2}{2\sigma_2^2}\right),$$

where

$$\sigma_2 = \frac{0.85}{\lambda} g(\beta_t, \beta_e, \beta_r) V_2 \sin \delta_2 ,$$

with V_2 and δ_2 being the speed and direction of the wind in segment 2; and so on to the nth segment. The resultant power spectrum of the received signal is obtained by summing the power spectra for the individual segments as shown in Fig. 31(b). This sum, or resultant, is considered gaussian-shaped for our purposes, although, strictly speaking, this is true only when the winds have the same speed and direction in

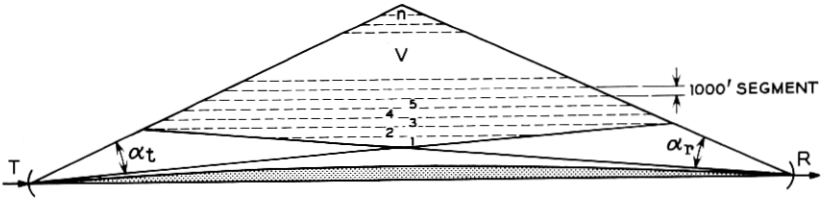

(a) VERTICAL PLAN VIEW OF A BEYOND-HORIZON CIRCUIT

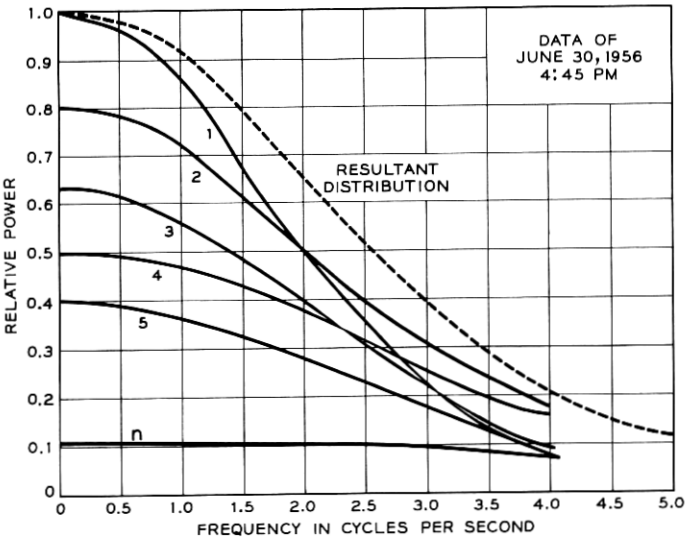

(b) EXAMPLE OF A RESULTANT DISTRIBUTION. DISTRIBUTIONS 1,2---n ARE PLOTTED FROM WIND DATA FOR THE CORRESPONDING SEGMENTS IN (a)

Fig. 31 — Distribution of winds in the common volume region: (a) vertical plan view of a beyond-horizon circuit; (b) example of a resultant distribution, with distributions 1, 2, $\cdots$, n being plotted from wind data for the corresponding segments above.

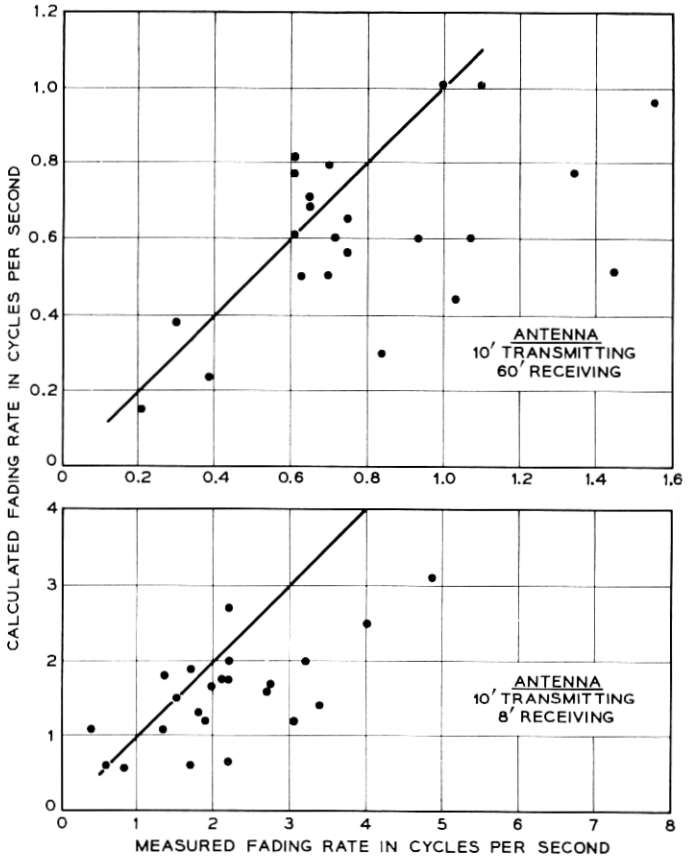

Fig. 32 — Comparison of measured and calculated fading rates. Samples were chosen from data at 4110 mc on 13 different days in the period January through August 1956.

all segments. The estimated fading rate is obtained from the width of the resultant curve. This estimated rate can be compared with fading rates measured from actual records of the received signal.*

In Fig. 32 measured fading rates are compared with fading rates calculated by the method just discussed. The speed and direction of the winds used in the calculations were obtained from the U. S. Weather Station at Binghamton, New York (see Fig. 1). The wind data and the

* If the wind speeds normal to the path are almost the same at all altitudes, the fading rate is given approximately by (10): $N_m = (1.27/\lambda)\ g(\beta_t\ ,\ \beta_e\ ,\ \beta_r)\ \overline{V \sin \delta}$, where $\overline{V \sin \delta}$ is the average normal wind speed.

signal records from which the fading rates were measured were taken at approximately the same time for each point shown.

It is apparent from Fig. 32 that the measured fading rate usually exceeds the calculated rate; this may be due to vertical winds or to turbulent winds, neither of which have been considered here. However, it is significant that no constants need to be adjusted in (10) to calculate fading rate of the correct order of magnitude. The rate of fading at 4 kmc is a strong function of horizontal drift wind.

5.3 *Wavelength Dependence of Fading Rates*

This section is concerned with a comparison of fading rates of signals received simultaneously at 4110 and 460 mc. Since it is known that the beamwidths of the antennas affect the fading rate, the present experiment employs two pairs of antennas, the beamwidths of the 4110-mc pair being of the same order as the beamwidths of the 460-mc pair. Furthermore, we have shown that antennas with very narrow beamwidths (less than about 1° at 4110 mc) reduce the rate of fading. Therefore, antennas with relatively large beamwidths were used to minimize such effects.

5.3.1 *Instantaneous Signal Level Recordings — Analysis*

In this study, the 10-foot transmitting and 8-foot receiving antennas are used at 4110 mc and the 28-foot (transmitting) and 60-foot (receiving) antennas are used at 460 mc. The setup is the same as that used in Section 3.2.

The rate of fading at both frequencies varies considerably from day to day and sometimes within the hour. Portions of samples of rapid, slow and very slow fading at 460 mc, and the corresponding 4110-mc signal, are shown on Fig. 33. The 460-mc signal is shown on the top trace of each sample, the 4110-mc signal on the bottom trace. The samples are normally two to three minutes long and are taken each half-hour during the recording period. It may be noted in Fig. 33 that the fading rate of the 460-mc signal, N_{m460}, changes considerably from sample to sample, whereas the fading rate of the 4110-mc signal, N_{m4110}, remains fairly constant; therefore, changes in the *ratio* of the rates of fading at the two frequencies are due predominantly to changes in the 460-mc fading rate.

The ratio, k, of the fading rates of the signals received simultaneously at the two frequencies ($k = N_{m4110}/N_{m460}$) varies widely, as shown in

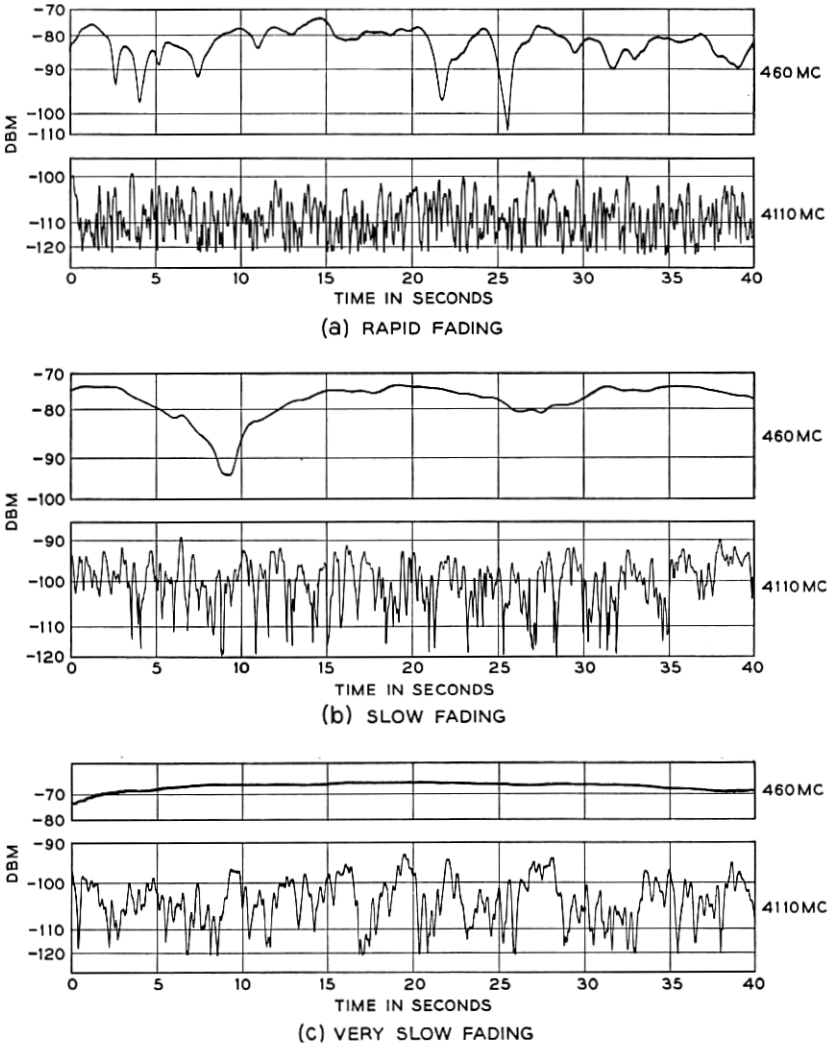

Fig. 33 — Segments of samples of simultaneous recordings of instantaneous signal levels at 460 and 4110 mc.

Fig. 34. The data are taken from a study of 387 samples and show that the median value of the ratio of the fading rate of the signals received at 4110 mc to the 460-mc rate is 12.7. It is believed that this ratio is significantly higher than the ratio of the radio frequencies due to the effect of layer size, as discussed in the following section.

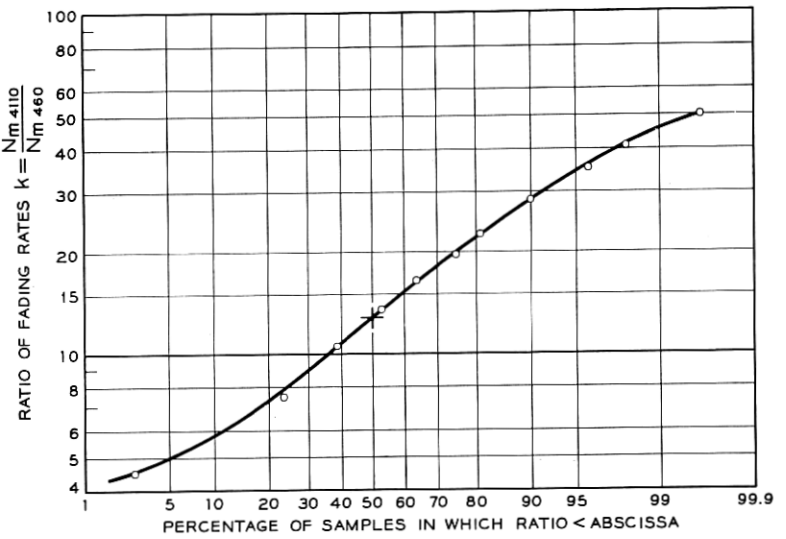

Fig. 34 — Statistical distribution of the ratio of fading rates recorded simultaneously at 4110 and 460 mc — 387 samples of 2 minutes duration. Period: March through December 1956.

5.3.2 *Ratio of Fading Rates and Layer Size*

A discussion of fading of 4-kmc signals was given in Section 5.1. There it was assumed that short-term fading was caused by drift of numerous randomly positioned layers formed by changes in the gradient of the dielectric constant of the atmosphere.

Consider now the effect of the size of the reflecting layers on the fading rates. It will be shown that small layers result in a ratio of fading rates equal to the ratio of the radio frequencies, whereas large periodic layers must be assumed to explain higher ratios of the fading rates.

Small Layers — The diagram in Fig. 30(a) is applicable if the horizontal dimensions of the reflecting layers are small compared to the horizontal dimension of the antenna beam at the operating wavelength. If this condition is fulfilled at wavelengths λ_1 and λ_2, (10) applies to both wavelengths, and for k one obtains the ratio of fading rates measured simultaneously at wavelengths λ_1 and λ_2 with antenna beamwidths β_{t_1}, β_{r_1} and β_{t_2}, β_{r_2}:

$$k = \frac{N_{m1}}{N_{m2}} = \frac{\lambda_2}{\lambda_1} \frac{g_1(\beta_{t_1}, \beta_{e_1}, \beta_{r_1})}{g_2(\beta_{t_2}, \beta_{e_2}, \beta_{r_2})}. \tag{12}$$

The factors g_1 and g_2 are very nearly equal if the beamwidths of the

antennas used are equal and if the reflecting layers are small compared to the Fresnel zone at both wavelengths ($\beta_{e_1} = \beta_{e_2}$). For this case, the ratio of fading rates is just proportional to the ratio of the operating wavelengths. Letting subscripts 1 and 2 refer to 4110 and 460 mc respectively, one obtains

$$k = \frac{N_{m4110}}{N_{m460}} = \frac{\lambda_2}{\lambda_1} = \frac{0.65m}{0.073m} = 9. \tag{13}$$

The experimental data of Fig. 33(a) are an example of the condition where the layers apparently are smaller than a Fresnel zone at both wavelengths, resulting in a value of $k \cong 9$.

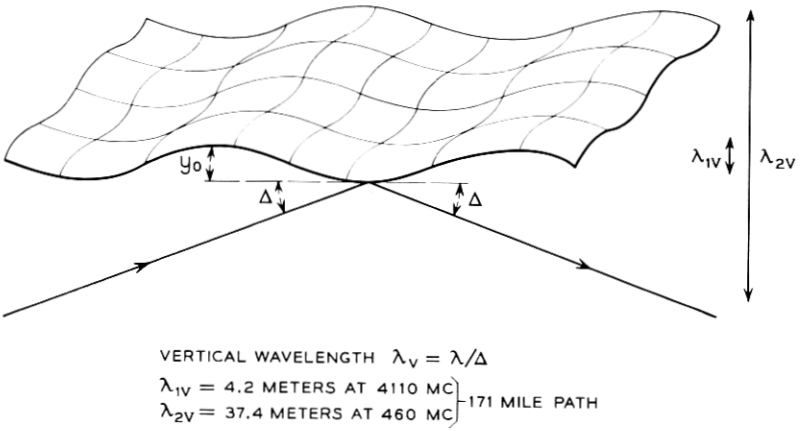

Fig. 35 — Idealized structure representing a single layer at 460 mc and several layers at 4110 mc.

Large Layers — Analysis of many samples makes it clear that the ratio of the fading rates, N_{m4110}/N_{m460}, often far exceeds the value given by (13); the ratio may reach values in excess of 50. This condition is due to a very low fading rate at 460 mc rather than a very high 4110-mc fading rate. When these high ratios exist, the atmosphere apparently acts much differently at 460 mc than at 4110 mc.

A layer such as that shown in Fig. 35 will act as a smooth reflecting surface at the lower frequency, and simultaneously will represent many reflecting surfaces at the higher frequency.* The layer is considered to be a smooth reflecting surface if the roughness as indicated by the spatial amplitude, y_0, in Fig. 35 is less than one-eighth of a vertical wavelength (Rayleigh's criterion). The vertical wavelengths $\lambda_v = \lambda/\Delta$ for a 171-

* A similar argument is used by Anderson and Smyth.[15]

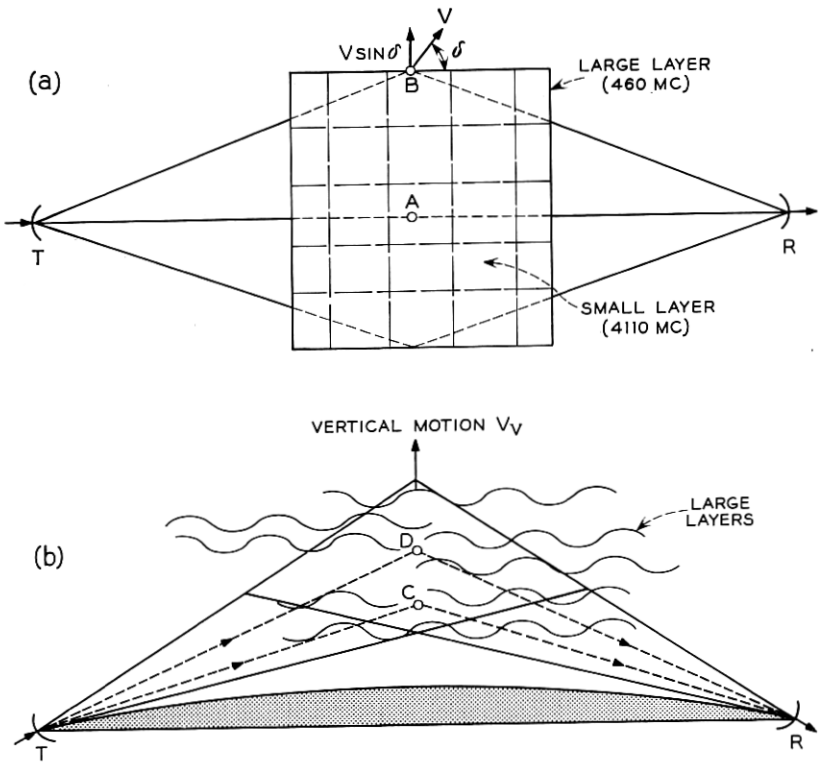

Fig. 36 — Large idealized periodic layers in the propagation path: (a) horizontal; (b) vertical.

mile path and frequencies 4110 and 460 mc are shown in the figure, Δ being the grazing angle.

Thus, if $y_0 < \lambda_{2v}/8 = 4.6$ meters, the layer appears large and smooth at 460 mc. On the other hand, this value for the roughness amplitude, y_0, exceeds an entire vertical wavelength at 4110 mc ($\lambda_{1v} = 4.2$ meters). Therefore, the loops and nodes of the idealized periodic layer will appear as individual layers at 4110 mc.*

The idealized layers which are assumed to exist in the propagation path are shown in Fig. 36. In the vertical plan view, several of the periodic layers are drawn in the volume common to the antenna beams, and in the horizontal plan view, Fig. 36(a), one of these is shown sub-

* Periodic layers such as these probably can be produced by changes in magnitude and direction of winds with height in the atmosphere; no doubt actual layers are more irregular and less systematic than the one shown in Fig. 35

divided by dotted lines to illustrate the periodic structure. Since the layers at 4110 mc are the loops and the nodes of the periodic structure, the situation at 4110 mc is much the same as that already discussed in connection with Fig. 30(a), and the fading rate at 4110 mc will have fairly high values depending on the horizontal wind, as given by (10). However, at 460 mc the horizontal drift wind has little effect on the fading rate if the layers are large and smooth at that frequency, since most of the power is propagated to the receiver along the great circle route TAR and very little along delayed paths such as TBR. Nevertheless, relative delays at 460 mc do exist in the vertical plane as shown by rays TCR and TDR in Fig. 36(b), and some fading will occur due to interference of reflections from the several periodic layers. But the fading rate at 460 mc will be relatively low, since the vertical motion of the layers V_v is usually very much less than the horizontal drift V. Large periodic layers therefore can give rise to high ratios N_{m4110}/N_{m460}.

5.3.3 *Fading Rate Ratios and Ratios of Median Received Powers — Diurnal Effects*

It has been observed that the ratio of the fading rates N_{m4110}/N_{m460} may change considerably during the course of a day, as shown in Fig. 37. Moreover, the relative median received power at the two frequencies, P_{4110}/P_{460}, is found to change simultaneously with the fading ratio; the out-of-phase relationship between fading ratio and received power ratio is evident in Fig. 37. The median received powers P_{4110} and P_{460} used in Fig. 37 both have the free-space transmission loss factored out; the ratio P_{4110}/P_{460} therefore is a measure of the relative transmission coefficient of the atmosphere at the two frequencies. When the fading ratio is low ($k \cong 9$) the ratio of received powers P_{4110}/P_{460} is between 0 and -5 db, whereas a high ratio of fading rates ($k \geqq 20$) occurs when the power ratio is between -10 and -15 db. The relationship between fading ratio and power ratio can be discussed qualitatively by means of the theory, as follows:

In Section 3.2.2 the median received power is discussed for three cases depending on the horizontal dimensions of the reflecting layers. The received power, relative to the free-space value, at two wavelengths λ_1 and λ_2 is:

Case 1. Large Layers (Dimension > Fresnel Zone):

$$\frac{P_R(\lambda_1)}{P_R(\lambda_2)} = \left(\frac{\lambda_1}{\lambda_2}\right)^2.$$

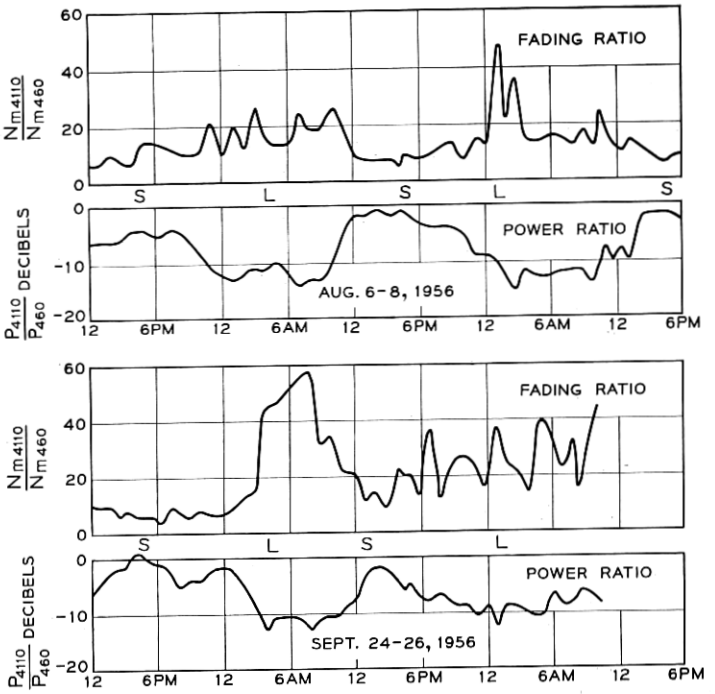

Fig. 37 — Correlation between ratio of median fading rates and ratio of median received powers (relative to free space) at 4110 and 460 mc.

Case 2. Small Layers (Dimension < Fresnel Zone):

$$\frac{P_R(\lambda_1)}{P_R(\lambda_2)} = \left(\frac{\lambda_1}{\lambda_2}\right)^0.$$

Case 3. Layers of Intermediate Size (Dimension ≈ Fresnel Zone):

$$\frac{P_R(\lambda_1)}{P_R(\lambda_2)} = \left(\frac{\lambda_1}{\lambda_2}\right)^1.$$

Consider Case 2. This formula indicates that both wavelengths, λ_1 and λ_2, are propagated equally well when the atmosphere contains small reflecting layers. In terms of Fig. 37, it means that small layers are present when $P_{4110}/P_{460} \approx 0$ db (various portions where $P_{4110}/P_{460} \approx 0$ are labeled s). During the same periods the ratio of fading rates is low ($k \approx 9$), as discussed previously. Thus, the observed ratio of received powers and the observed ratio of the fading rates are both consistent with the existence of small layers during the period labeled s.

If the formulas for Cases 3 and 1 are applied to the 4110- and 460-mc circuits, one obtains

Case 3: $\frac{P_{4110}}{P_{460}} = -9.5$ db for layers of intermediate size

Case 1: $\frac{P_{4110}}{P_{460}} = -19$ db for large layers.

Thus, the propagation at the lower frequency is favored more and more as the layer dimensions increase. It is believed that the observed power ratios of between -10 and -15 db, shown in the portions of Fig. 37 labeled L, are due to large layers at 460 mc and small layers at 4110 mc (Fig. 35). However, this case cannot be calculated with confidence by theory, since our knowledge of the sizes and refractive index gradients of the layers is insufficient. Nevertheless, the observed power ratios during periods L (Fig. 37) are consistent with the concept of large layers at 460 mc and with high ratios of fading rate as discussed previously.

Additional data have been plotted in the manner of Fig. 37; all of these show the out-of-phase relationship between N_{m4110}/N_{m460} and P_{4110}/P_{460}. The two plots shown in Fig. 37 were chosen to illustrate the diurnal effect; it will be noted that large layers exist in the early morning hours when the atmosphere is believed to be more stable.

Diurnal Variation. An analysis was made of the fading rate at 460 mc as a function of time of day; Fig. 38(a) shows these results. It indicates that the atmosphere is stable at night and during the morning hours.

The fading rate is low between the hours of 9:00 p.m. and 9:00 a.m. As heating by the sun occurs, the fading rate increases rapidly between 9:00 a.m. and 11:00 a.m., staying relatively high until 7:00 p.m. It drops rapidly between 7:00 p.m. and 9:00 p.m., as radiation cooling occurs.

The diurnal effect is not strong so far as the median signal level is concerned, particularly in the winter months; however, there is a trend which follows the fading rate variations; i.e., at higher fading rates the median signal level decreases. Fig. 38(b) shows this relation.

5.3.4 *Fading Ratio and Fading Rate*

An interesting relationship shows up if the measured ratios of fading rates $k = N_{m4110}/N_{m460}$ are plotted versus the rates themselves. Fig. 39 shows plots of 387 ratios obtained from fading rates measured on the 4110- and 460-mc circuits. It is evident that there is a sharp break in the data of Fig. 39(a), in which the ratios are plotted against the 460-mc fading rate. The ratio varies only slightly ($k \leqq 9$) as the fading rate

decreases from 1.4 cps to 0.2 cps, at which point the ratio begins to increase rapidly. This plot emphasizes that the high ratios N_{m4110}/N_{m460} are caused by very low values of N_{m460}. A similar effect is seen in Fig. 39(b), where the same measured data are plotted versus the fading rate at 4110 mc.

Consistent with all previous discussion, these data show that two rather well-defined ranges of 460-mc fading rate exist. One concludes that, when the periodic layers illustrated in Fig. 36 are present, the 460-mc fading rate is less than 0.2 cps [Fig. 39(a)] and the 4110-mc rate is less than about 2 cps [Fig. 39(b)], and the rates are higher than these values when the layers are broken up.

The rate of fading of 4110-mc signals, N_{m4110}, is related to the horizontal drift winds in the atmosphere. The fading rates calculated by

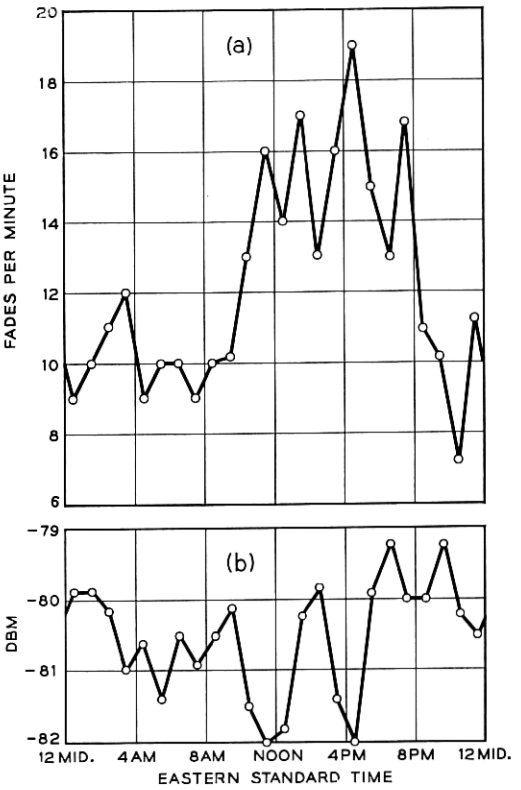

Fig. 38 — Diurnal variation in (a) median fading rate and (b) median signal level at 460 mc — 1680 samples. Period: September 1956 through April 1957.

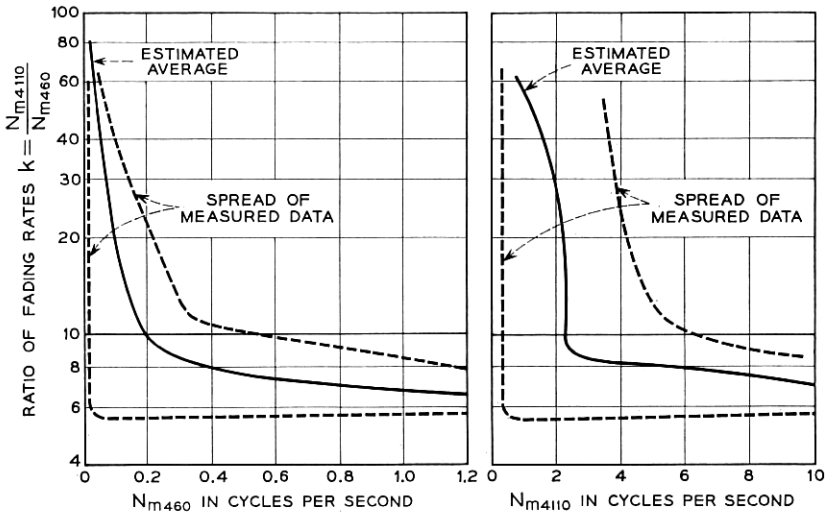

Fig. 39 — Ratio of median fading rates at 460 and 4110 mc as a function of absolute median fading rate — 387 samples.

(10), that is, $N_m = (1.27/\lambda)g(\beta_t, \beta_e, \beta_r)\ V\sin\delta$, using measured wind velocities (V,δ), were shown to agree fairly well with the actual fading rates of the received signal. Therefore, since $N_{m4110} = 2$ cps is the value at which the curve of Fig. 39(b) suddenly changes slope, one can write the equation

$$\frac{1.27}{\lambda}\, g(\beta_t, \beta_e, \beta_r)\ V\sin\delta = 2 \text{ cps},$$

and solve for the wind velocity corresponding to the breaking point of the curve. This results in $V \approx 15$ meters per second (30 knots) for the "critical" velocity below which large layers can exist. One concludes that formation of the large layers depends not only on the stability of the atmosphere as related to time of day but also on the wind conditions in the volume of the atmosphere that is common to the beams of the transmitting and receiving antennas.

VI. TWIN-FEED DIVERSITY STUDIES

In propagation beyond the horizon there are two principal types of fading, defined somewhat arbitrarily as "long-term" and "short-term" fading. The long-term fading is caused by changes in the refractive properties of the atmosphere over periods of from several hours to days

(Section III); short-term fading is due to multipath changes caused by movement of discontinuities (Section V). In short-term fading the received signal level follows, in most instances, a Rayleigh distribution.

A system is designed to operate for a given percentage of the time above a certain signal-to-noise level. To decrease the time the signal spends at low levels for a given system, diversity reception is used to obtain two or more uncorrelated signals at the receiver. The usual type is space diversity: two or more receiving antennas are spaced about 100 wavelengths perpendicular to the great circle between transmitter and receiver. The output from each antenna is amplified and combined with the outputs of the other antennas.[16] If the signals are uncorrelated, the percentage of time the combined output stays below a certain level will be less than the time the signal from either channel stays below that level.

The diversity systems to be described use one receiving antenna with two feeds.* Uncorrelated signals should be obtained from the two feeds because they are oriented to illuminate different parts of the atmosphere. Two types of feed positions are described: horizontal feeds placed side by side and vertical feeds placed one on top of the other.

In order to check the experimental results with theory, we first must determine whether or not the envelope of the signals is Rayleigh-distributed, since the subsequent calculations on the diversity systems are based on a Rayleigh distribution. The following few paragraphs discuss this aspect.

6.1 *Types of Distributions of Instantaneous Signal — Non-Rayleigh*

The distribution of the envelope of the instantaneous signal level usually follows a Rayleigh distribution. A sample is shown in Fig. 40. Other examples of the distributions may be found in Section 5.1.1.

An analysis of numerous short-term fading samples has shown that the envelope of the signals is Rayleigh-distributed when the fading rate is greater than about 8 fades per minute at 460 mc and 12 fades per minute at 4 kmc. In Fig. 41, distributions of fading rates taken over a considerable period of time are shown for both 4110 and 460 mc. From these data one concludes that the signals are not Rayleigh-distributed for 35 per cent of the time at 460 mc and 3 per cent of the time at 4 kmc.

The distributions which are not Rayleigh-distributed usually occur when the median fading rate is very slow. While the very slow fading rates occur at both 460 mc and 4.11 kmc, they occur more often at 460

* Suggested by H. T. Friis.

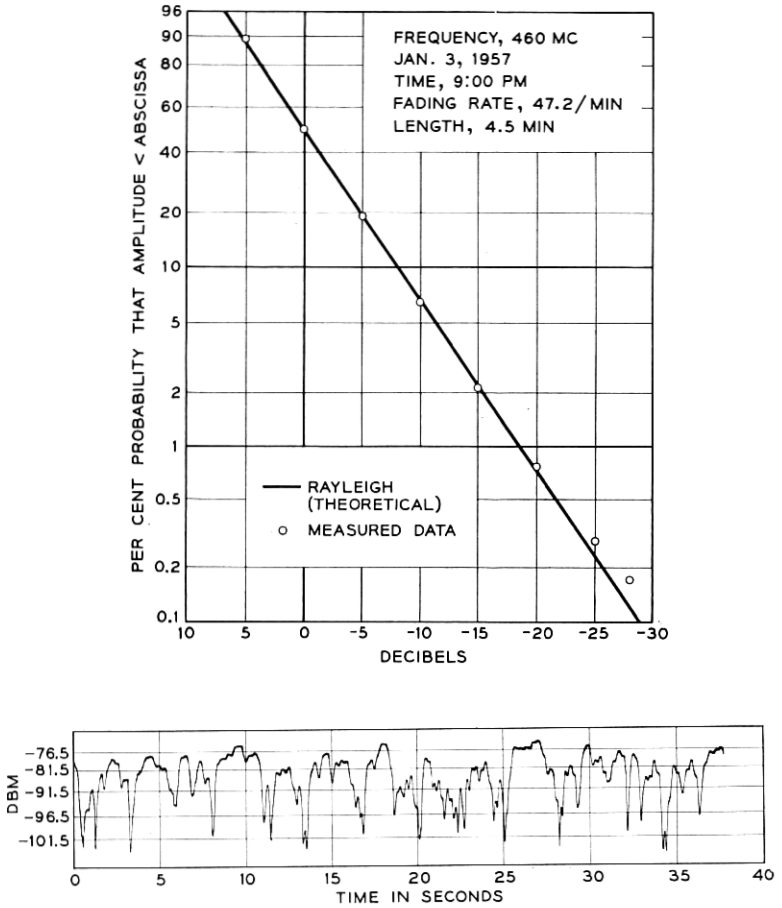

Fig. 40 — Segment of recording and distribution of instantaneous signal levels of Rayleigh-distributed signal.

mc; hence the examples cited are for 460 mc. During these periods of very slow fading the number of layers or discontinuities in the common volume is reduced to a few, and also the drift of these layers is slow. It is possible to fit these distributions to some theoretical models. Fig. 42 shows the distribution for the model of a constant vector and a Rayleigh-distributed vector;[17] the points are experimental. Figs. 43, 44 and 45 show the model for two, three and four equal-amplitude but randomly phased vectors, respectively. Some of the distributions obtained from other samples do not fit any simple theoretical model. One

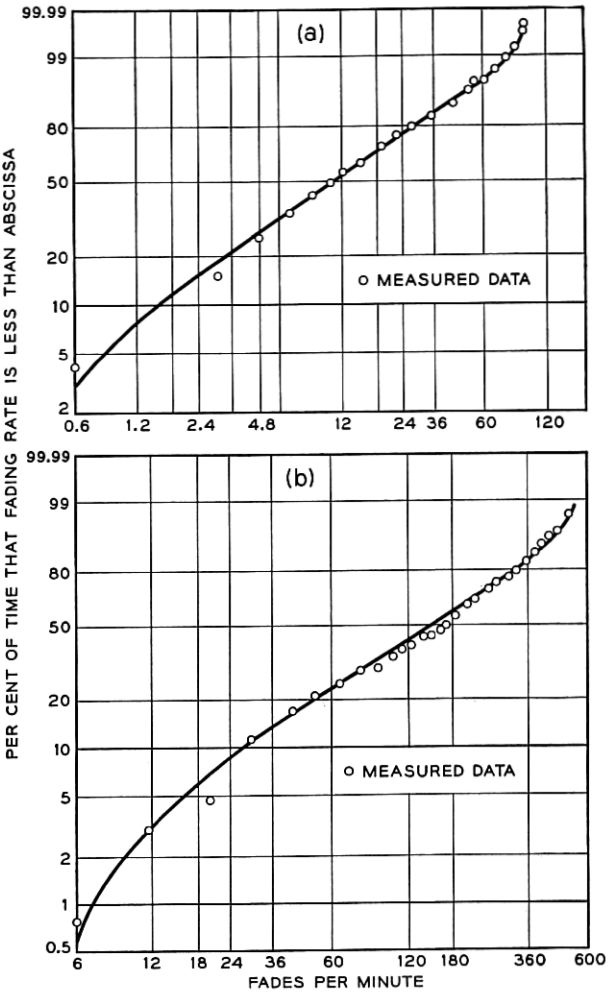

Fig. 41 — (a) Distribution of median fading rates at 460 mc — 1680 samples each 2 minutes long; 28-foot transmitting antenna, 60-foot receiving antenna. Period: September 1956 through April 1957. (b) Distribution of median fading rates at 4110 mc — 780 samples each 2 minutes long; 10-foot transmitting antenna, 8-foot receiving antenna. Period: October 1955 through April 1956.

would expect the lower fading rates to be due to a stable atmosphere composed of a few large layers. That there is a relationship between fading rate and horizontal wind speed has been shown in Section 5.2. These results do not indicate the correlation between vertical winds and fading rate, since the vertical component usually produces only a secondary effect.

During the periods of very slow fading it is sometimes possible to infer that the fading is caused by the vertical component of the wind. The 60-foot paraboloid is scanned in order to find the angular dependence of the scattered energy. (The rate of scan is four per minute; the transmitter frequency is 4.11 kmc.) Consider Fig. 46, which shows these scans. The horizontal patterns in Figs. 46(b) and 46(c), while changing in amplitude, do not move in position; the vertical scans have a tendency to change in position as well as in amplitude. If large layers tend to move vertically, one would expect the signals from two adjacent parts of the atmosphere to be correlated in the horizontal plane but not necessarily in the vertical plane. Fig. 46(d) shows an instance of some-

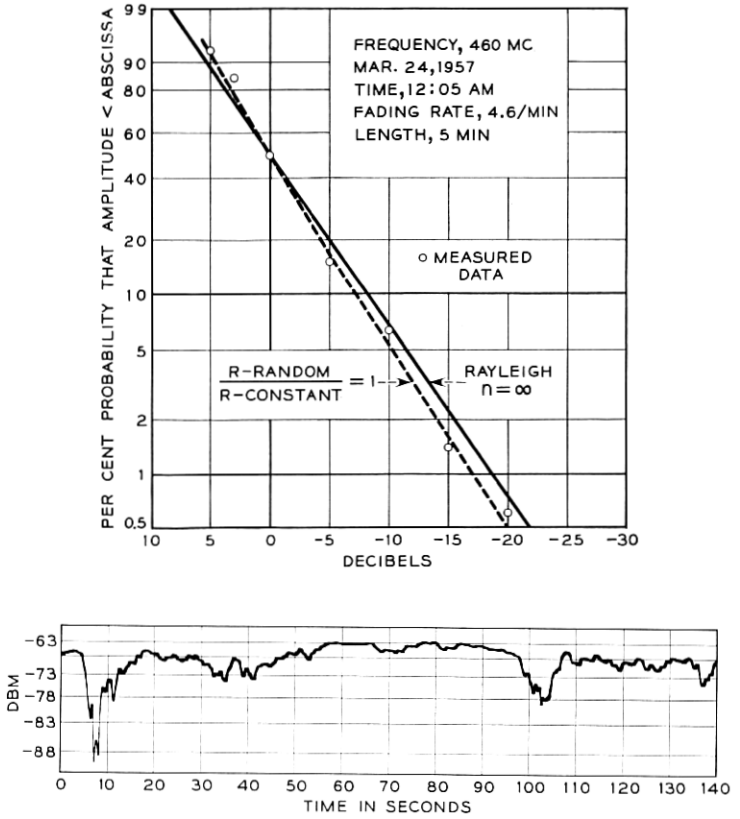

Fig. 42 — Segment of recording and distribution of instantaneous signal levels of the resultant of a constant vector plus a Rayleigh-distributed vector of equal amplitude. Points are experimental; curves are theoretical.

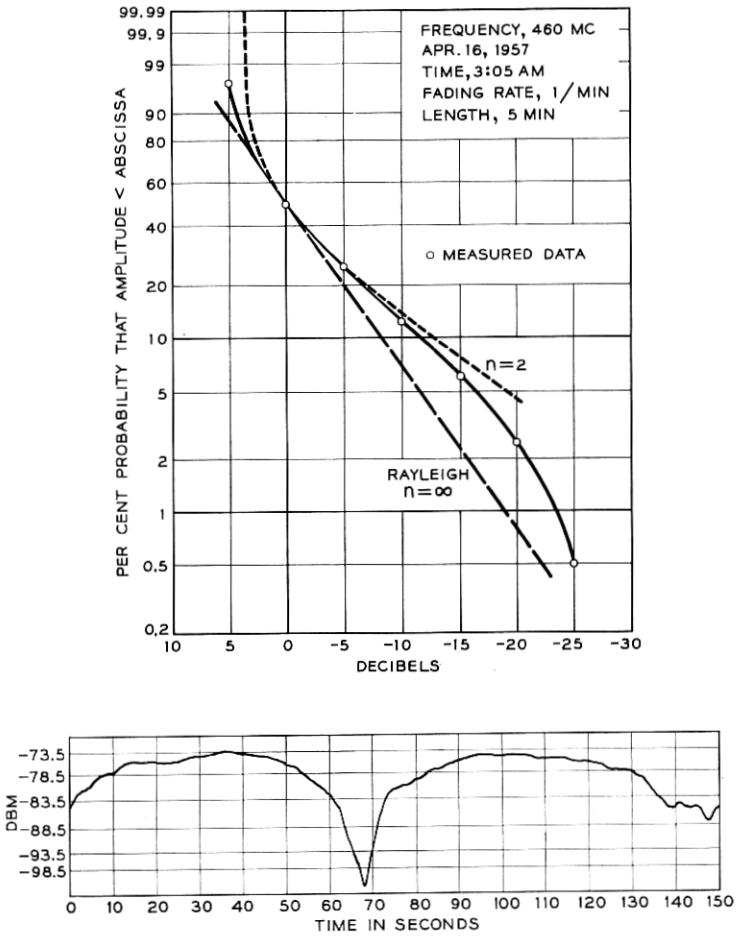

Fig. 43 — Segment of recording and distribution of instantaneous signal levels of the resultant of two unit vectors with random relative phase. Points are experimental.

what the opposite effect. However, here the fading is more rapid, indicating the effect of horizontal winds.

6.2 *Two-Channel Switch-Type Diversity*

We will first analyze the advantages obtainable in diversity systems. In this analysis we assume that the uncorrelated signals of two receivers

are combined by a switch-type combiner, which selects the higher of the instantaneous signals. The signals need not have the same median level.

The envelope of the instantaneous signal level will be Rayleigh-distributed in most cases, as was pointed out in the previous section. This probability distribution results from an addition of an infinite number of components of random phase and amplitude. The probability, P, that

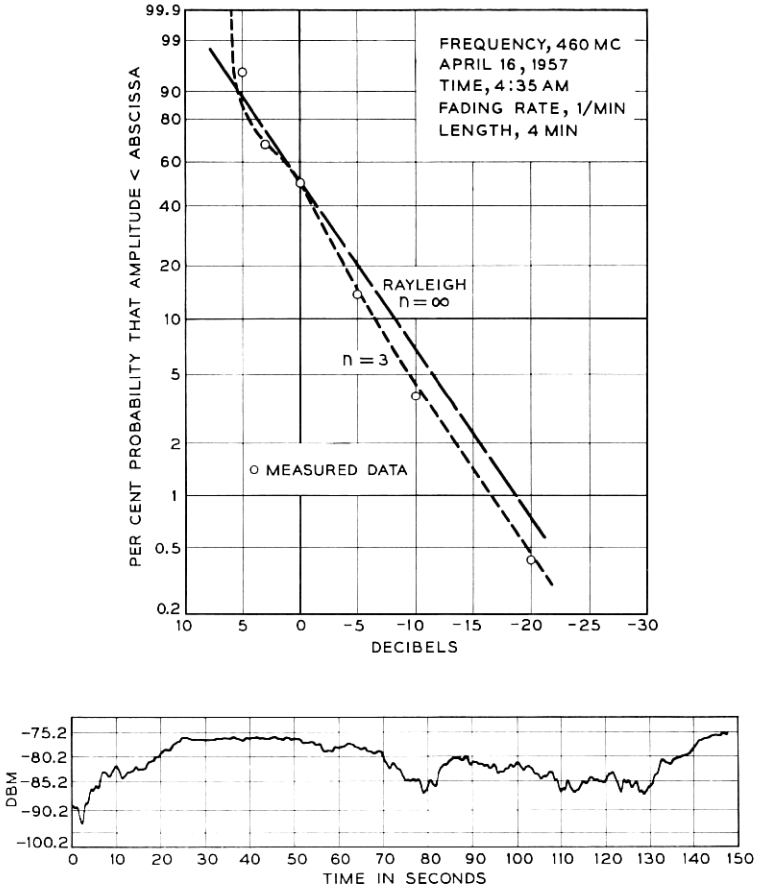

Fig. 44 — Segment of recording and distribution of instantaneous signal levels of the resultant of three unit vectors with random relative phase. Points are experimental; curves are theoretical.

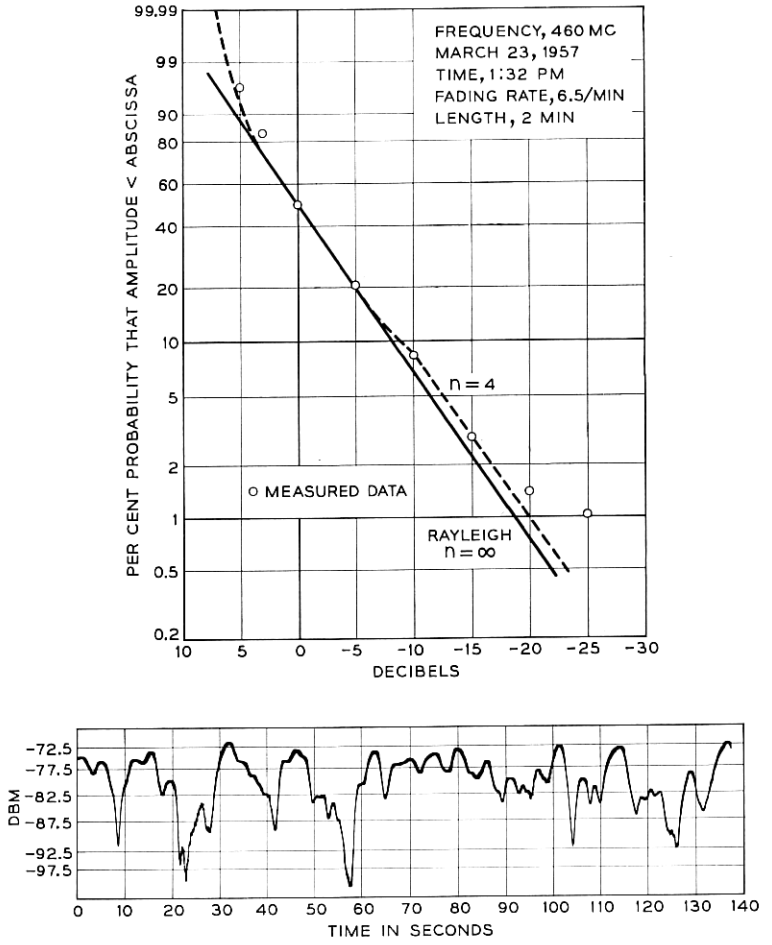

Fig. 45 — Segment of recording and distribution of instantaneous signal levels of the resultant of four unit vectors with random relative phase. Points are experimental; curves are theoretical.

the signal amplitude E_1 is less than a given value E is

$$P(E_1 < E) = 1 - \exp\left[-\left(\frac{E}{E_r}\right)^2\right], \tag{14}$$

where E_r is the rms value. For $P = 0.50$, E is equal to the median value E_m ; hence,

$$E_m^2 = (\ln 2)\, E_r^2; \tag{14a}$$

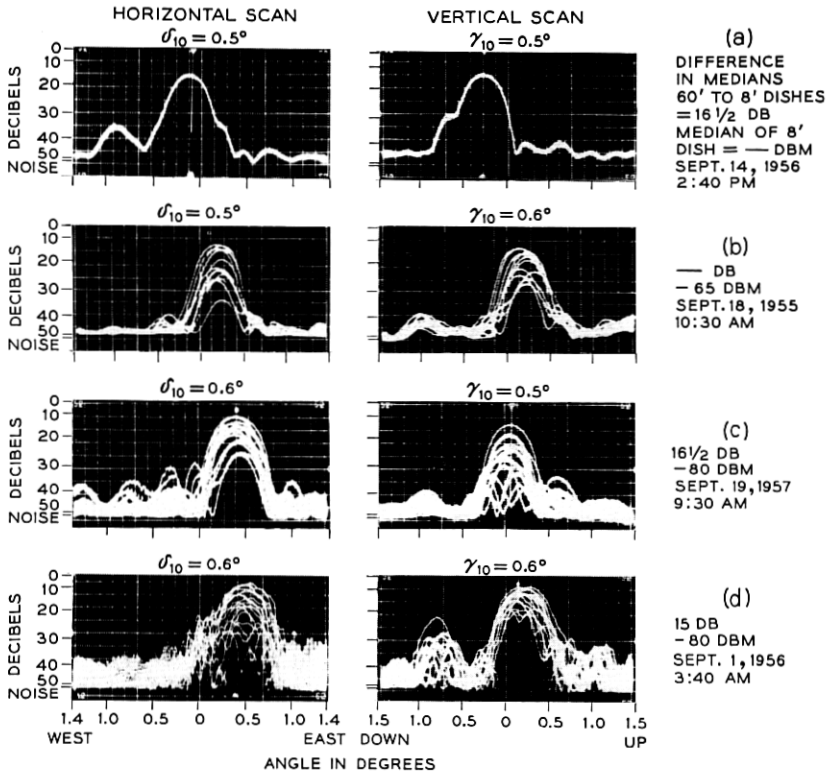

Fig. 46 — Scans of signals received on the 60-foot antenna at 4110 mc.

and

$$P(E_1 < E) = 1 - \exp\left[-\ln 2\left(\frac{E}{E_m}\right)^2\right]. \tag{15}$$

This equation, plotted in Fig. 47, is labeled "single channel." If we have two signals, E_1 and E_2, then

$$\begin{aligned} P(E_1 < E) &= 1 - \exp\left[-\ln 2\left(\frac{E}{E_{m_1}}\right)^2\right], \\ P(E_2 < E) &= 1 - \exp\left[-\ln 2\left(\frac{E}{E_{m_2}}\right)^2\right]. \end{aligned} \tag{16}$$

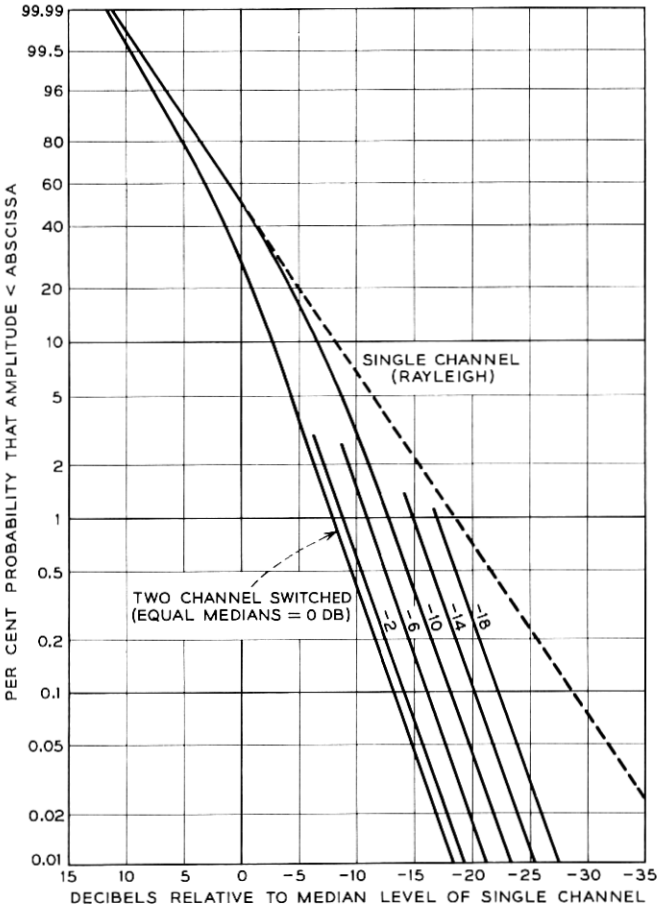

Fig. 47 — Distribution of amplitudes for two-channel switched diversity system with unequal median signal levels for uncorrelated Rayleigh-distributed channels. Curves are referred to the median of the single channel with the higher median.

The probability that both E_1 and E_2 are less than E is

$$\begin{aligned} P(E_1, E_2 < E) &= [P(E_1 < E)][P(E_2 < E)] \\ &= \left\{1 - \exp\left[-\ln 2 \left(\frac{E}{E_{m_1}}\right)^2\right]\right\} \\ &\quad \cdot \left\{1 - \exp\left[-\ln 2 \left(\frac{E}{E_{m_2}}\right)^2\right]\right\}. \end{aligned} \tag{17}$$

For equal medians $E_{m_1} = E_{m_2} = E_m$, (17) reduces to

$$P(E_1, E_2 < E) = \left\{1 - \exp\left[-\ln 2 \left(\frac{E}{E_m}\right)^2\right]\right\}^2. \tag{18}$$

The probability that both signals are below a pre-set level is the square of the probability of one signal channel being below that level.

For very small signal levels (E less than 0.3 E_m) we now compare the various systems — single-channel, equal median diversity and unequal median diversity — at the same percentage of time. We shall use as reference the median of the single-channel E_{m_1}.

i. Single-Channel:

$$P(E_1 < E) \approx \ln 2 \left(\frac{E}{E_{m_1}}\right)^2; \tag{19}$$

ii. Two-Channel, Equal Medians:

$$P(E_1, E_2 < E) \approx \left[\ln 2 \left(\frac{E}{E_{m_1}}\right)^2\right]^2; \tag{20}$$

iii. Two-Channel, Unequal Medians:

$$P'(E_1, E_2 < E') \approx \left[\ln 2 \frac{E'^2}{E'_{m_1} E_{m_2}}\right]^2. \tag{21}$$

For the same probability, $P = P'$, the degradation of the switched signal for an unequal median system over that of an equal median signal is (set $E'_{m_1} = E_{m_1}$):

$$\frac{E'^2}{E_{m_1} E_{m_2}} = \frac{E^2}{E_{m_1}{}^2}; \qquad \text{hence,} \quad \frac{E}{E'} = \sqrt{\frac{E_{m_1}}{E_{m_2}}}. \tag{22}$$

In this comparison we have set the median of the single channel for the equal median case (E_{m_1}) equal to the median of the single channel with the larger median (E'_{m_1}) for the unequal median case. At a given probability, the level for the two-channel switched diversity with unequal medians will be below that of the two-channel switched diversity with equal medians by one-half of the difference in decibels of the two medians. For a difference of 10 db in medians, the level of the switched channel with unequal medians will be 5 db below the level of the switched channel with equal medians. Fig. 47 shows the distributions for various ratios in medians.

6.3 *Twin-Feed Diversity — Horizontally Disposed Feeds*

In this type of diversity, the two horns are mounted side by side on one paraboloidal reflector so that each beam illuminates horizontally adjacent volumes in the common volume region (Fig. 48). The antenna is oriented so that each feed receives the same median signal level.

Successful diversity reception requires that the signals received on the two horns be uncorrelated. If the discontinuities in the common volume are so large that most of the energy is transmitted to the receiver along a great circle route, then the signals received on the separate horns will be correlated. An attempt to correct this condition by separation of horns will lead to degradation in the median signals received.

6.3.1 *Experimental Setup and Analysis of Data*

Fig. 49 shows the free-space antenna patterns at 460 mc using the 60-foot paraboloid. The separation of the beams is 2.33°, which corresponds to 3.5 miles at the midpath. The signal level received is 4.5 db down at the crossover point.

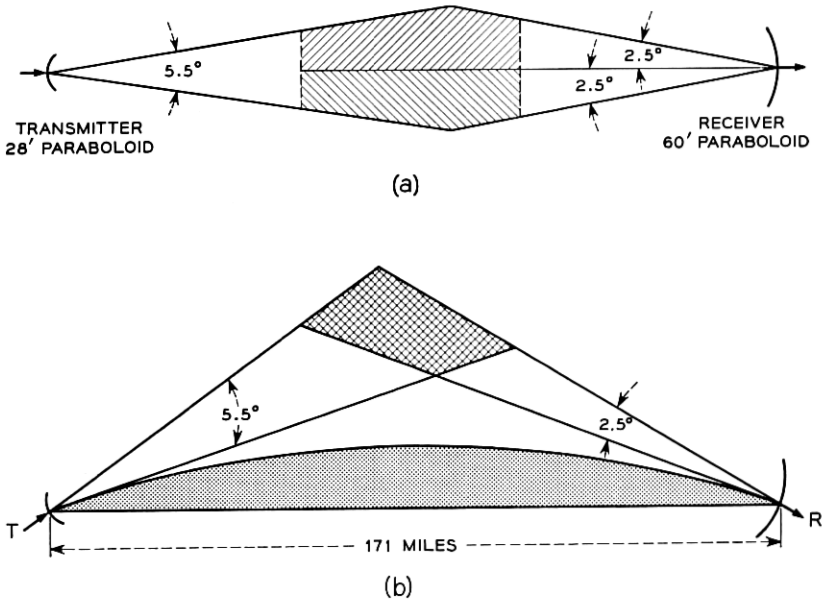

Fig. 48 — Common volume configuration for twin-feed diversity system with horizontally disposed feeds, at 460 mc, using 60-foot antenna: (a) horizontal; (b) vertical.

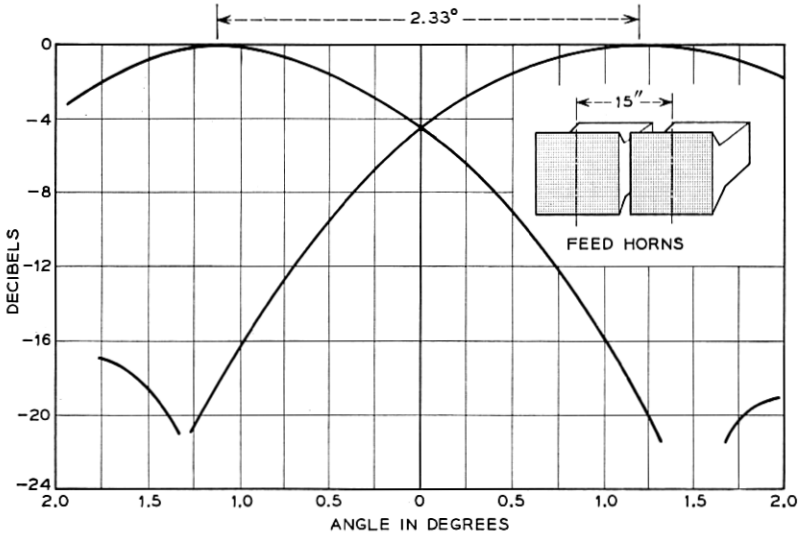

Fig. 49 — Free-space patterns for twin-feed diversity system with horizontally disposed feeds, at 460 mc, using 60-foot antenna.

The purpose of the experiment is to determine whether or not an advantage is obtained when the higher of the two signals is chosen instead of the signal from one channel. The degree of correlation between the two signals determines the diversity improvement of the system. The signal levels below the median value are chiefly of interest, since the low levels determine the operational reliability of the system.

Fig. 50 shows the setup wherein the signals are combined in the diversity combiner; the output of the combiner is put on one channel of the Sanborn recorder. One of the signals is put on the other channel. The median level of each channel is recorded on the E-A recorders. The combiner consists of two vacuum tube diodes whose plates are tied together, each cathode being connected to one of the two channels; the output is taken from the plates. Since the receiver output impedance is low compared to the diode resistance and the voltage into the combiner is high (0 to −100 volts dc), no appreciable error is introduced because of the diode resistance and emission current.

Since the nature of the received signals is such that the signal spends little time at levels well below the median, it becomes difficult to measure, using the Sanborn records, the time that the signal spends at these levels. This problem is especially acute in the diversity studies, since these levels are the ones of interest. More accurate results can be obtained by

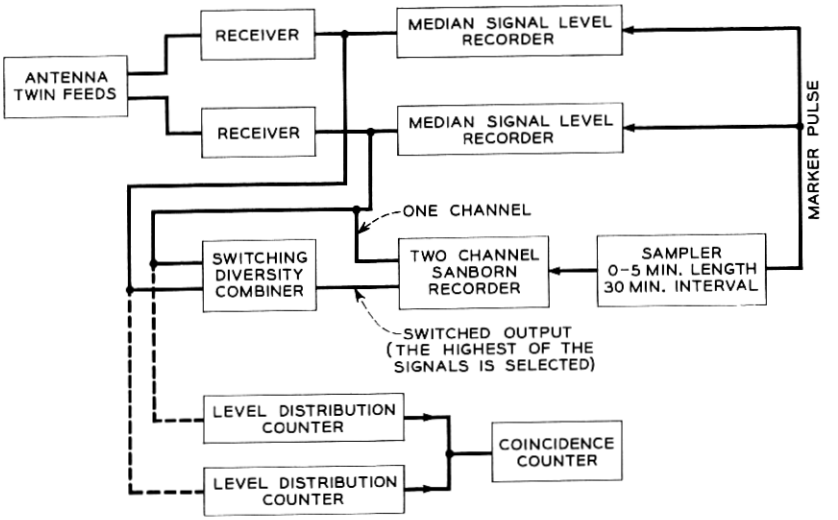

Fig. 50 — Recording setup for measurement of diversity properties of two-channel switched diversity system.

using level distribution counters which totalize the time the signal is below a certain set level. These counters are gated, with the gate opening when the signal drops below the preset level. The counting frequency is 2000 cps. The level can be set to an accuracy of 0.3 volts input for the gate to open or close. A clock is used as a time totalizer.

The counters can be so connected that one counts on one channel, the second counts on the same level on the other channel and the third counts when both channels are below the common preset level; the third counter registers coincidences, and hence gives a direct measure of the properties of the diversity system.

There is an important difference between using the Sanborn recorder with the diversity combiner and the level-distribution counters. The Sanborn recorder gives the diversity action at all levels of signal, while the counters only give information about one level. To get equivalent information a bank of counters would be needed.

For the recordings on the Sanborn to give quantitative results, a further condition is necessary. The combiner does not select the higher of the two signal levels but only the higher of the two receiver outputs, thus for quantitative results the calibration of the two receivers must be identical. By adjusting the gain and AGC level it is possible to get the calibrations to be within ± 1 db over the 50-db range.

For the horizontally spaced twin feeds the instantaneous signal levels are recorded on the Sanborn recorder and the following analysis of the data is made. A probability distribution is plotted for the single channel as well as the switched channel. Fig. 51 shows a sample distribution. Since the experimental points lie close to the theoretical curve, the signals are Rayleigh-distributed and uncorrelated in this case. We define diversity improvement as follows: at 10 db below the median of the single channel the probability is 6.70 per cent for the single channel and 0.45 per cent for the switched channel; hence the diversity improvement is 6.25 per cent. It is possible for the single-channel distribution to be Rayleigh, but for the switched channel not to follow the theoretical curve, due to correlation between the two signals.

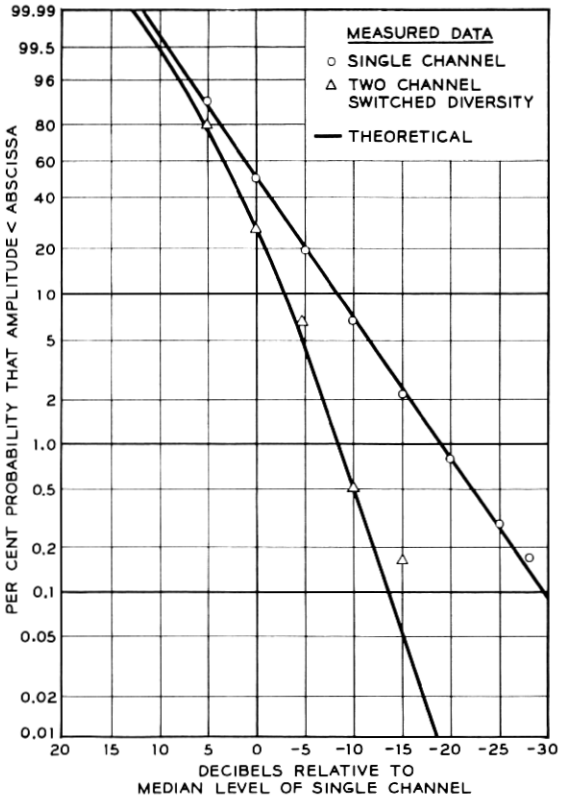

Fig. 51 — Distribution of instantaneous signal levels of a two-channel switched diversity system with equal median signals at 460 mc. Sample length, 4½ minutes; median fading rate of single channel, 47.2 cpm.

6.3.2 *Results of the Experiment*

The experiments at 4 kmc using the twin feeds on the 60-foot antenna as well as the 28-foot antenna show that the theoretical improvement was obtained in nearly all cases. The only time it did not occur was when the fading rate was extremely slow, indicating the presence of very large horizontal layers.

At 460 mc the theoretical diversity improvement was not obtained in many cases. Since the fading rate is an indication of the stability of the atmosphere, one might expect a relation between the fading rate and diversity improvement. To check this hypothesis, 460-mc records for several days during the year were selected. For each sample the probability distribution was plotted. In Fig. 52 the diversity improvement is plotted against the fading rate of a single channel. It shows that, when the fading is relatively fast (40 fades per minute or more) the theoretical improvement of 6.25 per cent is approached. As the fading becomes slower, the diversity improvement becomes less. The data give the same results for the three periods showing no seasonal dependence.

Since the individual signals are Rayleigh-distributed for fading rates greater than 8 per minute, it is possible to calculate a cross-correlation coefficient for two signals from the observed diversity improvement (as

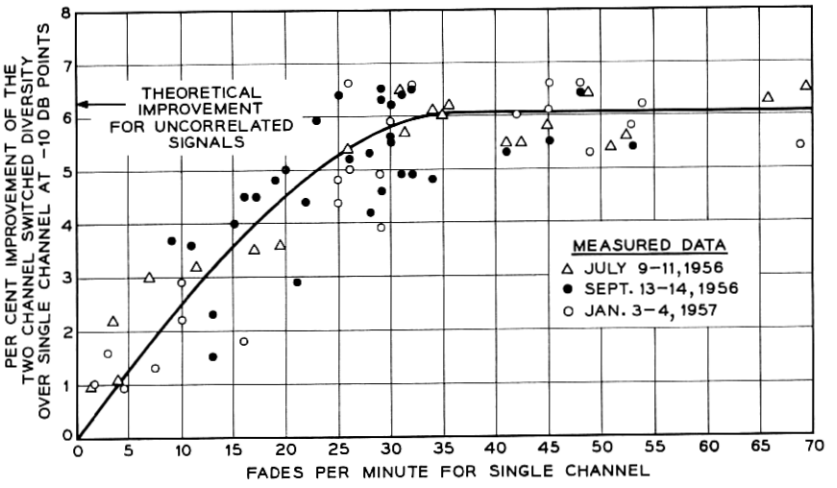

Fig. 52 — Improvement of twin-feed diversity system with horizontally disposed feeds as a function of the median fading rate, at 460 mc.

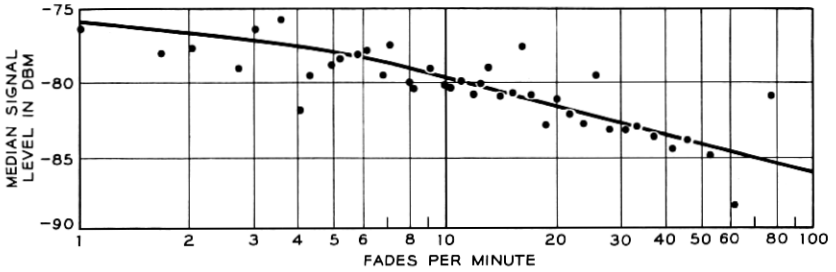

Fig. 53 — Median signal level as a function of the median fading rate. Each point represents the median signal level of 41 samples that had approximately the same fading rate at 460 mc — 1680 samples. Period: September 1956 through April 1957.

shown in Fig. 52) using S. O. Rice's theory.[18,19] The coefficient* of the envelope is indicated in this table:

Fades per Minute, Single Channel	0	20	25	30	35	70
Correlation coefficient, k^2	1.00	0.88	0.77	0.59	0.38	0.00

For two uncorrelated signals of equal median, the combined output is 0.45 per cent of the time below the level which is 10 db below the median of one of the channels. For a correlation coefficient of 0.6, the per cent of time increases to about 1 per cent, indicating that most of the diversity advantage is still obtained. For the system discussed, the correlation coefficient is less than 0.6 for fading greater than 30 cpm.

It has been observed that there is a seasonal dependence in the median signal level. During low-signal periods there is a tendency for the fading rate to be greater than during high-signal periods. If this trend is sufficiently strong, then this system will be as reliable as one which received uncorrelated signals at all signal levels, since a system has to be engineered only for low-signal levels.

An analysis was made to determine this effect. Fig. 53 shows a study of 1680 samples during the period of September 1956 to April 1957. This period was chosen because the median signal level is low during

* The correlation coefficient is calculated from the approximate expression:

$$P_j \leqq [1 - k^2][(1 - e^{-u})^2 + k^2(u^2/2 - u^3/3 + u^4/8 - u^5/30)^2],$$

where

P_j = probability of the switched channel,
p = probability of a single channel,
$k^2 \approx$ correlation coefficient of the envelope,
$u \approx p/(1 - k^2)$.

This equation holds for $0 \leqq k^2 \leqq 0.9$ when $p < 0.1$.

the winter months. Each point represents the *median* signal level of 41 samples that had approximately the same fading rate. From 30 fades per minute (where diversity improvement begins to decrease) to 1 fade per minute, the increase in signal level is about 7 db. A trend is definitely apparent, but it is not significant enough to compensate for the increase in correlation between the signal channels.

One can conclude that the diversity is no longer effective for a fading rate less than 30 cpm. The percentage of time that the diversity is not fully effective can be obtained from Fig. 41(a); 80 per cent of the time the fading rate is less than 30 cpm. Horizontally spaced feed diversity at 460 mc is not useful from a systems viewpoint.

6.4 *Twin-Feed Diversity — Vertically Disposed Feeds*

In this section we discuss an experiment in which separate signals are obtained from two horns stacked vertically at the focus of the receiving paraboloid. The two feeds are placed one above the other; they are so aimed that the upper feed (in-line) receives the maximum signal level. Under these conditions, the lower feed (off-axis) receives a median signal level which is 10 db or so lower (Fig. 54). The diversity results from the fact that each receiving beam subtends a different volume in the atmosphere. The median signal level from the off-axis feed normally

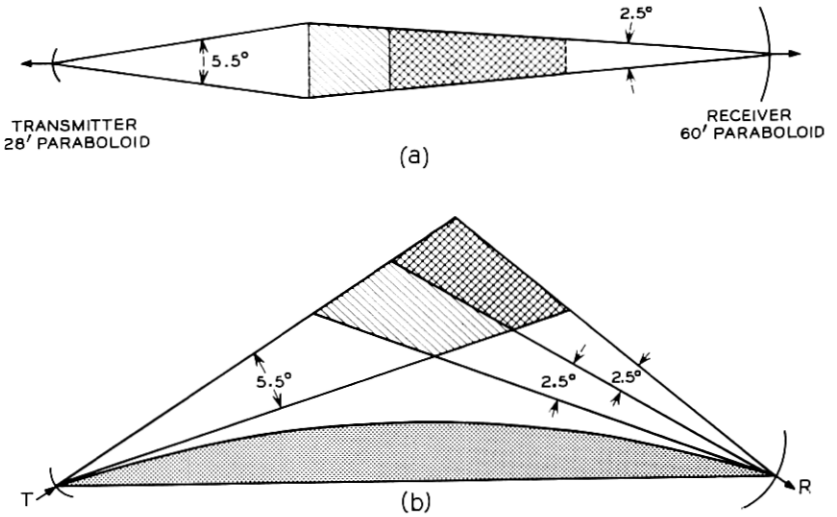

Fig. 54 — Common volume configuration for twin-feed diversity system with vertically disposed feeds, at 460 mc: (a) horizontal; (b) vertical.

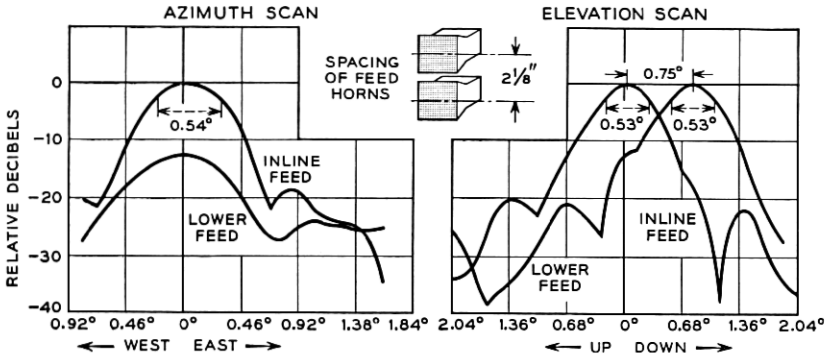

Fig. 55 — Free-space patterns for twin-feed diversity system with vertically disposed feeds using 28-foot antenna, at 4110 mc.

will be lower than that from the in-line feed because the power received from discontinuities at higher elevations is less (Section 4.1.2). The median signal level will vary between feeds depending on the strength of the atmospheric discontinuities.

6.4.1 *Experimental Setup and Analysis of Data*

Fig. 55 shows the antenna patterns taken on a line-of-sight path for twin feeds on the 28-foot antenna at 4 kmc. The signal is down 5.6 db at the crossover point. The level distribution counters are used to find the time that the signal spends below a preset level. The time when both channels are below the same level simultaneously is also measured on a coincidence counter. To check the theory the following is done:

i. The median signal level from each feed is recorded.
ii. The level at which the counters are set is recorded.
iii. The time the amplitude of the switched channel should spend below the level where the counter is set (if the signals are uncorrelated and Rayleigh-distributed) is computed using the curves of Fig. 47.
iv. The time the switched channel actually spends below the setting is read off the coincidence counter.

The percentage of time for the switched channel is computed with the aid of Fig. 47, using the medians of the two signals and the switched-channel level distribution counter setting; it is called "theoretical per cent of time." The percentage of time read off the coincidence counter is called "measured per cent of time." For uncorrelated signals, a plot of the measured versus the theoretical per cent of time should result in a 45° straight line.

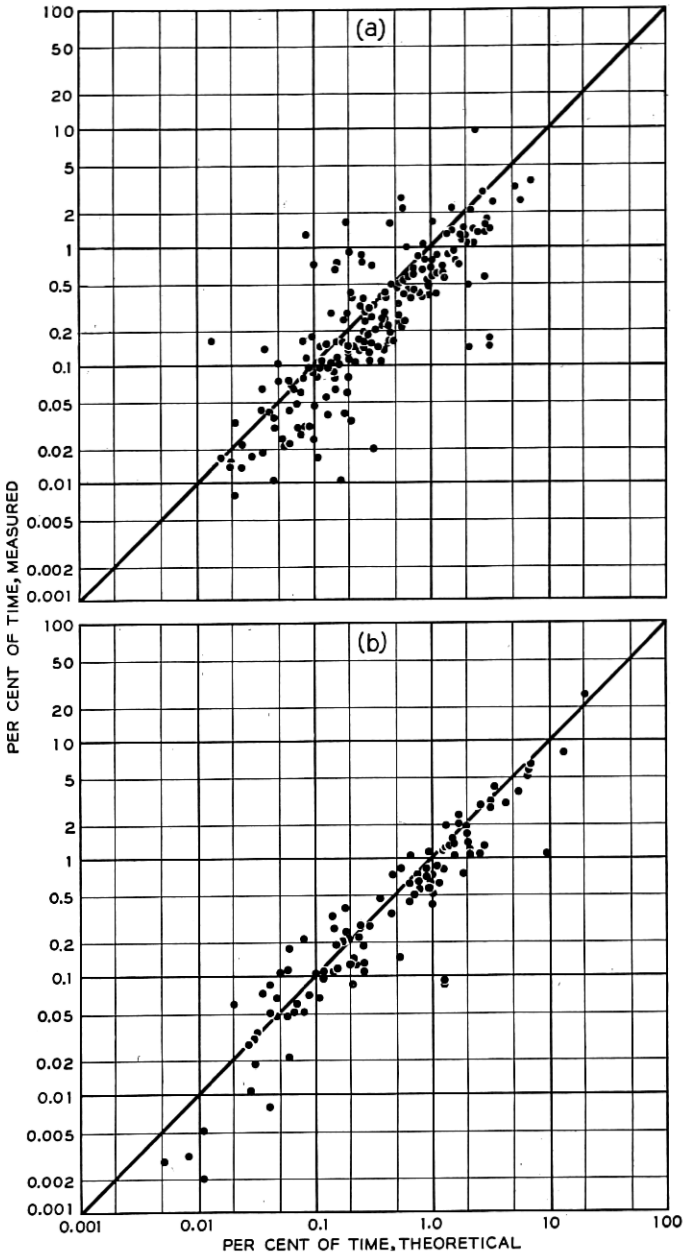

Fig. 56 — Effectiveness of twin-feed switch-diversity system with vertically disposed feeds, showing theoretical vs. measured percentage of time switched channel is below coincidence counter setting (counter set relative to median signal level of in-line single channel). Curves are theoretical for uncorrelated signals; points are experimental: (a) 460 mc; 28-foot–60-foot antennas; period: June through September 1957; (b) 4110 mc; 10-foot–28-foot antennas; period: April through June 1957.

6.4.2 *Results.*

Fig. 56 shows the results of a study of several months' data for both 460 and 4110 mc. The experimental points fall on both sides of the theoretical curve due to experimental inaccuracies. Several errors are introduced in recording the data, the most pronounced being that of estimating the median signal level.

The curves indicate that the predicted theoretical diversity improvement is realized in all cases; thus, the signals from the two vertically spaced feeds are not correlated.

It should be noted that the difference between the medians of the two feeds changes continuously as the structure of the atmosphere varies. Fig. 57 shows an extreme case. At 1:00 p.m. the difference between the medians on the feeds of the 28-foot antenna was about 8 db, with the in-line feed at the higher median signal level. By 4:00 p.m. the median of the off-axis feed had increased by 5 db, while the in-line feed

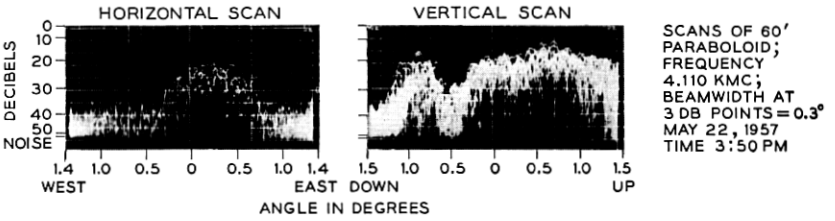

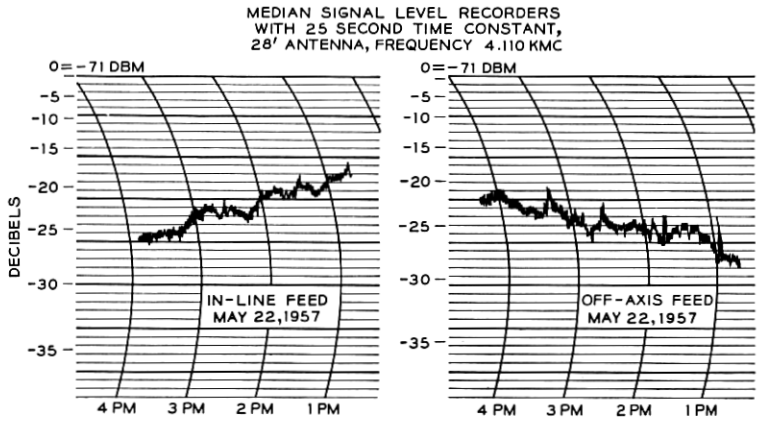

Fig. 57 — Segment of median signal recordings for twin-feed diversity system with vertically disposed feeds on the 28-foot antenna. Also shown are scans on the 60-foot antenna (at 4110 mc) taken at the same time.

median had dropped by 7 db, giving a difference of 4 db in favor of the off-axis feed. The lower part of Fig. 57 shows a scanning sequence using the 60-foot dish taken at 4:00 p.m. The vertical scan indicates that the maximum energy was coming from 0.6° up. The positioning of the feeds on the 28-foot antenna was such that the beam of the in-line feed was pointed 0.15° down and the off-axis feed was at 0.60° up. (The zero on the angle scale is arbitrary.*) This demonstrates why the off-axis feed was receiving the higher median signal in this case.

6.5 *Summary*

The twin-feed diversity studies give more evidence that the region in the common volume of two antenna beams used in a beyond-the-horizon system is composed of horizontal striations. Since the striations are essentially horizontal, uncorrelated signals will be received with the vertically placed feeds at both 460 mc and 4110 mc. These discontinuities are in the form of layers whose undulations are of such length and shape that they affect the propagation frequencies in different ways. Most of the time the layer size is large for 460 mc and small for 4 kmc. Under these conditions, diversity systems using horizontally disposed feed horns are effective at 4 kmc but not at 460 mc.

VII. CHARACTERISTICS OF SHORT-TERM FADING

In a beyond-the-horizon system using data transmission the length of fade at various levels is of importance in relation to the number of allowable errors.

Since rapid fluctuations in the level of received signal are always present, a problem exists in choosing the pulse width required for reliable transmission in systems using pulse-type modulation. For example, the simultaneous occurrence of a fade and the transmission of a pulse with a width less than the duration of the fade may result in the complete loss of that particular pulse. Accordingly, then, the choice of pulse width in these situations concerns the length of time the signal fades below a given level. If the length of fade is such that a sequence of pulses is lost, then knowledge of the length of fade will enable the system designer to devise the appropriate error-correcting code.

We will first outline the derivation for the number of crossings of the envelope of the instantaneous signal at any signal level. The results are given for the single channel, two-channel switch-type diversity and two- and four-channel combiner diversity — all for uncorrelated Rayleigh-

* See Section 4.1.1.

distributed signals with equal median signal levels. Results are also given for the average length of fade for these systems. A comparison is made between theory and experiment for the single channel and for the two-channel switch-type diversity. Finally, the system reliability is considered from the point of view of the length of fade.

7.1 *Number of One-Way Crossings and Average Length of Fade*

From the theory of random noise it is possible to find the number of crossings of the signal at a given level when the probability distribution of the signal is known. In our derivation, a Rayleigh distribution will be assumed for the envelope of the received signal. If we define $N(E)$ as the number of one-way crossings at a level E, then[20,21]

$$N(E) = (\sqrt{2\pi}\,\sigma E_r)(\text{probability density of } E). \tag{23}$$

This relation holds if the power spectrum is of gaussian form (σ is the standard deviation). With the aid of (14), we obtain for the single channel

$$\frac{dP_1}{dE} = \frac{2E}{E_r^2} \exp\left[-\left(\frac{E}{E_r}\right)^2\right]. \tag{24}$$

Let us write the number of one-way crossings $N(E)$ in terms of the median signal level E_m. Using (23), (24) and (14a), we obtain

$$N(E) = (8\pi \ln 2)^{1/2}\sigma \left(\frac{E}{E_m}\right) \exp\left[-\ln 2 \left(\frac{E}{E_m}\right)^2\right]. \tag{25}$$

At the median signal level, the number of one-way crossings will be

$$N(E_m) = (8\pi \ln 2)^{1/2}\sigma e^{-\ln 2} = \sqrt{2\pi \ln 2}\,\sigma. \tag{26}$$

Hence the number of one-way crossings at any level E with respect to the number of crossings at the median E_m is

$$n_1 = \frac{N(E)}{N(E_m)} = 2\left(\frac{E}{E_m}\right) \exp\left[-\ln 2 \left(\frac{E}{E_m}\right)^2\right]. \tag{27}$$

The average length of fade is the ratio of the probability distribution and the number of crossings.* For the single channel we have (14) divided by (27) [also using (14a)]:

$$\bar{t}_1 = \frac{1 - e^{-(E/E_r)^2}}{\dfrac{2}{\sqrt{\ln 2}}\left(\dfrac{E}{E_r}\right) e^{-(E/E_r)^2}}. \tag{28}$$

* Rice[22] has studied in detail the question of the distribution of the duration of fades.

TABLE IV — EQUATIONS FOR THE INSTANTANEOUS SIGNAL-LEVEL DISTRIBUTIONS, NUMBER OF ONE-WAY CROSSINGS AND AVERAGE LENGTH OF FADE FOR VARIOUS DIVERSITY SYSTEMS

Equations are based on uncorrelated Rayleigh-distributed channels with the same median. The equations are normalized to the variable at the median of the single channel. $E_m = \sqrt{\ln 2} E_r$, where E_m is median amplitude and E_r is rms amplitude.

Type of Combiner	Probability Distribution for Combined Channel	Number of One-Way Crossings	Average Length of Fade for $E/E_r < 0.3$
Single Channel	$1 - e^{-(E/E_r)^2}$	$\frac{2}{\sqrt{\ln 2}} \left(\frac{E}{E_r}\right) e^{-(E/E_r)^2}$	$\approx \frac{1}{2} \sqrt{\ln 2} \left(\frac{E}{E_r}\right)$
Two-Channel Switched	$[1 - e^{-(E/E_r)^2}]^2$	$\frac{4}{\sqrt{\ln 2}} \left(\frac{E}{E_r}\right) [e^{-(E/E_r)^2}][1 - e^{-(E/E_r)^2}]$	$\approx \frac{1}{4} \sqrt{\ln 2} \left(\frac{E}{E_r}\right)$
Two-Channel Combiner	$1 - e^{-(E/E_r)^2} \left[1 + \left(\frac{E}{E_r}\right)^2\right]$	$\frac{2}{\sqrt{\ln 2}} \left(\frac{E}{E_r}\right)^3 e^{-(E/E_r)^2}$	$\approx \frac{1}{4} \sqrt{\ln 2} \left(\frac{E}{E_r}\right)$
Four-Channel Combiner	$1 - e^{-(E/E_r)^2} \left[1 + \left(\frac{E}{E_r}\right)^2 + \frac{1}{2}\left(\frac{E}{E_r}\right)^4 + \frac{1}{6}\left(\frac{E}{E_r}\right)^6\right]$	$\frac{1}{3\sqrt{\ln 2}} \left(\frac{E}{E_r}\right)^7 e^{-(E/E_r)^2}$	$\approx \frac{1}{8} \sqrt{\ln 2} \left(\frac{E}{E_r}\right)$

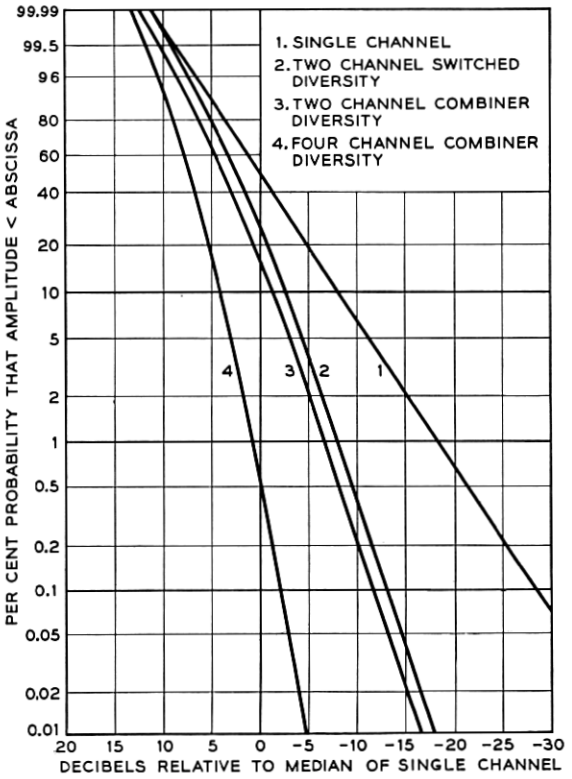

Fig. 58 — Rayleigh distributions of uncorrelated signals for various diversity systems. Curves are normalized to the median of a single channel. Results are for signal channels with the same median.

For small values of E/E_r ($E/E_r < 0.3$), (28) reduces to

$$\bar{l}_1 \approx \frac{1}{2}\sqrt{\ln 2}\left(\frac{E}{E_r}\right).$$

The equations for the probability distributions, number of crossings and average length of fade for the single channel, two-channel switch-type, two-channel and four-channel combiner diversity are listed in Table IV. The equations are plotted in Figs. 58, 59 and 60. The equations and curves are all for the combination of individual channels which have the same median signal level. (The case of unequal medians for the switch-type diversity was treated in Section VI.) In looking at the curves it must be remembered that the median level increases (as compared to a single channel) by 2.49 db for switched diversity, by 3.89 db for the

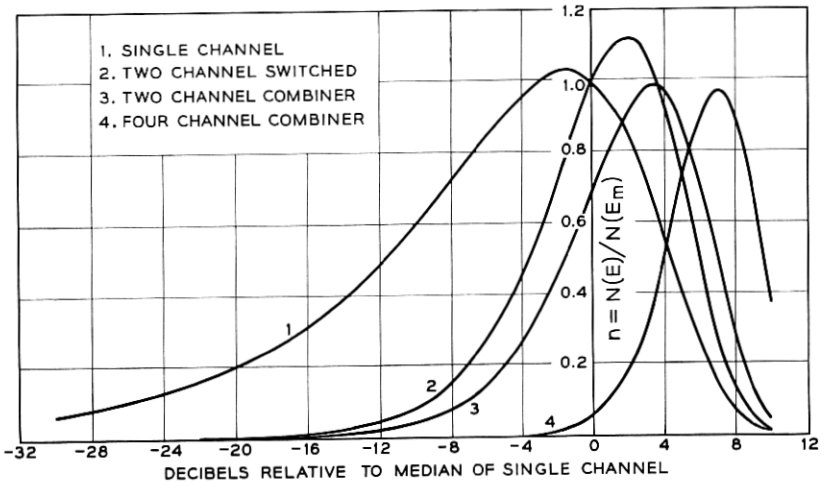

Fig. 59 — Number of one-way crossings, $N(E)$, of the instantaneous signal level for various diversity systems. Curves are for uncorrelated Rayleigh-distributed signal channels with the same median; curves are normalized to the number of crossings at the median of a single channel, $N(E_m)$.

two-channel diversity combiner and by 7.24 db for the quadruple diversity combiner.

This analysis applies for cw transmission. If FM or AM modulation gives a frequency diversity effect, then the results shown here should be modified to include it.

7.2 *Analysis of Experimental Results*

The measured number of crossings at various signal levels will now be compared with the theoretical values of a Rayleigh-distributed signal, given by (27).

Fig. 61 is a detailed analysis of a two-minute sample of the 460 mc signal with a fading rate of 1.2 cps; there is good agreement between the measured data and (27). The signal level as shown in Fig. 62 is, in fact, Rayleigh-distributed. Fig. 63 shows another comparison between data and theory. The agreement between the theoretical curve of (27) and the data points for the number of crossings is not good; a look at the corresponding signal-level distribution, Fig. 64, shows that the signal is not Rayleigh-distributed. In this sample the median fading rate is quite slow, hence a deviation from a Rayleigh distribution occurs, as discussed in Section 6.1. From the experimental signal-level distribution of Fig. 64 it is possible to calculate the corresponding distribution

of the number of crossings.[23] The results of this calculation are shown by the solid curve of Fig. 63; the agreement between the curve and the experimental points is good. It might be noted that the distribution of the number of crossings is very sensitive to a deviation from the Rayleigh distribution and offers a means of obtaining the distribution without the need for measuring the percentage of time the signals spends at various levels.

7.3 *Computed Average Duration of Fades*

The average length of time that the signal remains below a fixed threshold level in a system depends on two factors: the long-term

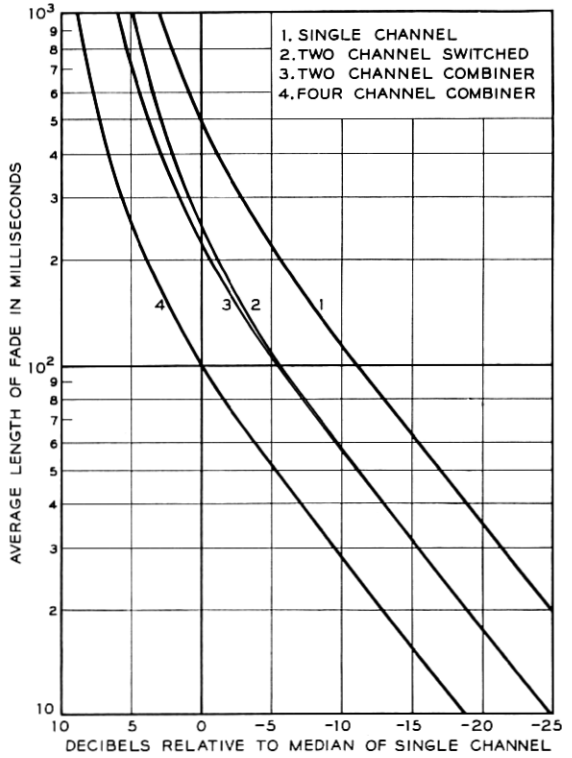

Fig. 60 — Average length of fade at a given level for various diversity systems. Curves are for uncorrelated Rayleigh-distributed signal channels with the same median; the curves are normalized for one crossing per second at the median of a single channel.

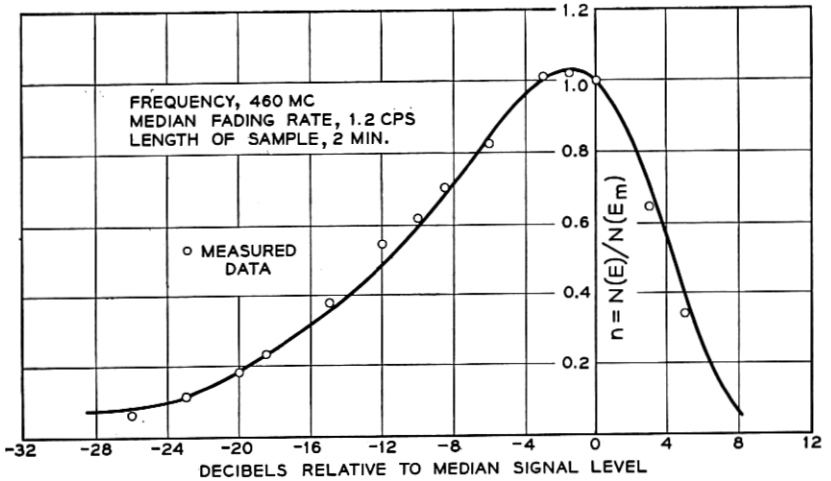

Fig. 61 — Number of one-way crossings of the instantaneous signal level for a single channel. The number of crossings is normalized to the number of crossings at the median level. Curve is theoretical [from (27)]; points are experimental.

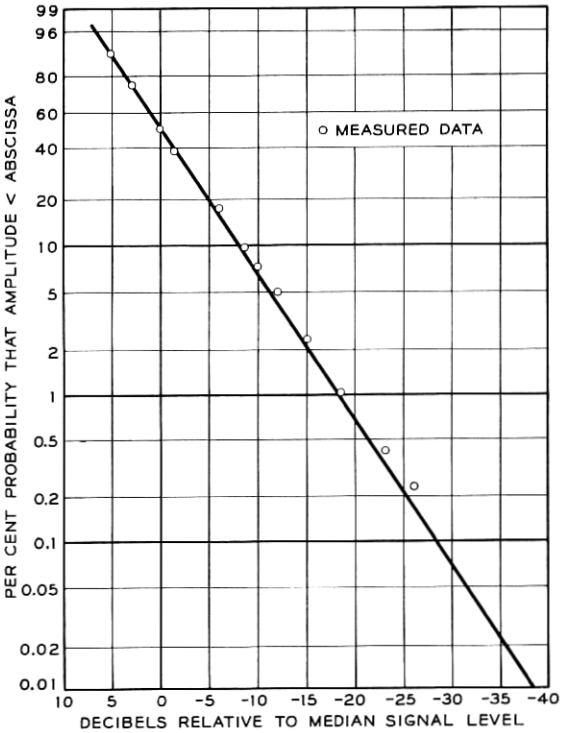

Fig. 62 — Distribution of instantaneous signal levels for the same sample analyzed in Fig. 61. Curve is Rayleigh distribution; points are experimental.

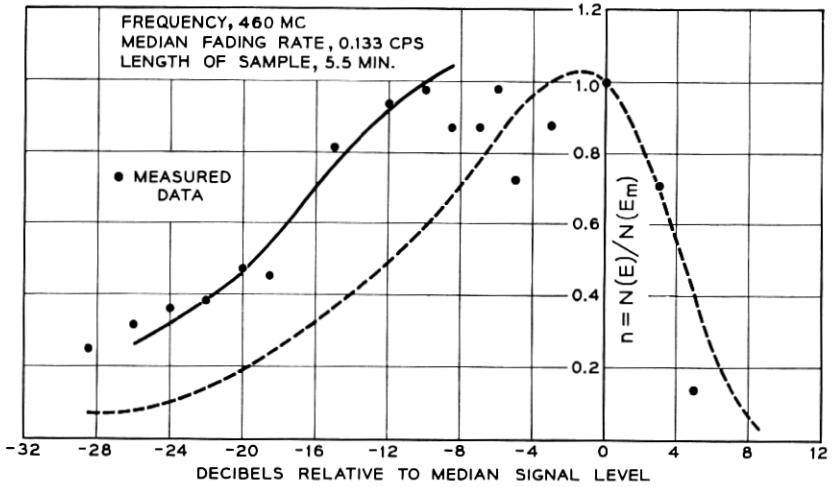

Fig. 63 — Number of one-way crossings of the instantaneous signal level for a single channel. The number of crossings is normalized to the number of crossings at the median level. Dashed curve gives the number of one-way crossings based on the Rayleigh distribution (27); solid curve is a calculation, for the number of crossings based on the measured distribution of Fig. 64. Frequency, 460 mc; median fading rate, 0.133 cps; length of sample, 5½ minutes.

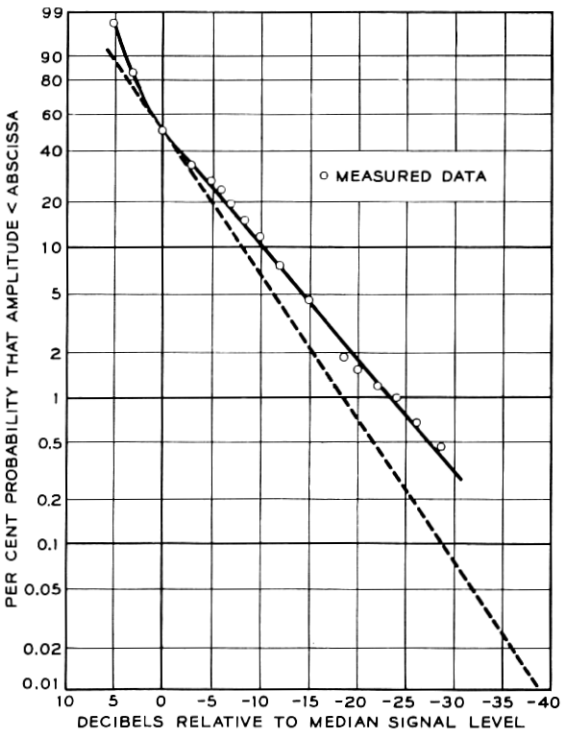

Fig. 64 — Distribution of instantaneous signal levels for the sample analyzed in Fig. 63. Dashed curve is Rayleigh distribution.

changes in the median level of the signal with respect to the fixed level and the rate of fading of the signal, assuming the median signal level to be fixed.

The following will show how the average length of fade at a given signal level can be computed using the distribution of fading rates (Fig. 41), the signal-level distribution (usually a Rayleigh distribution) and the number of times the signal crosses the particular level [from (27)].

In the following example it is arbitrarily assumed that, for a given system, the signal threshold during the worst period of transmission is at a level 18.5 db below the median (the 1 per cent point on the distribution curve). From the distribution of fading rates at 4 kmc (Fig. 41), the median fading rate of 150 cpm is obtained. The ratio of the number of crossings $N(E)$ at the threshold level (in this case -18.5 db) to the fading rate at the median $N(E_m)$ is obtained from Fig. 59. This value is 0.239; therefore

$$\frac{N(E)}{N(E_m)} = 0.239 \quad \text{and} \quad N(E) = 0.239\left(\frac{150}{60}\right) = 0.6 \text{ cps}$$

is the average number of crossings at the -18.5 db level.

The average length of fade is equal to the percentage of time the signal is below a given level, divided by the number of one-way crossings at this level. Since the time spent below the -18.5 db level is 1 per cent, $\bar{t} = 0.01/0.6 = 16.7$ milliseconds. Hence, 16.7 milliseconds is the average length of fade that will be exceeded 50 per cent of the time at the assumed threshold level of -18.5 db. A tabulation of the spread of average fade lengths to be expected using the 10 and 90 per cent values from the distributions of fading rate (Fig. 41) is given in Table V for both the 4110 and 460 mc signals.

From Table V, the average length of fade for a 4-kmc signal at the assumed threshold level of -18.5 db will be between 6.2 and 92 milli-

TABLE V — AVERAGE LENGTH OF FADE AT THE ASSUMED LEVEL OF 18.5 DB BELOW THE MEDIAN SIGNAL LEVEL (RAYLEIGH-DISTRIBUTED SIGNALS ARE ASSUMED)

Percentage of Time That Length of Fade Exceeds $\bar{t}$	4110 mc, $\bar{t}$ in Milliseconds	460 mc, $\bar{t}$ in Milliseconds
10	92	1590
50	16.7	233
90	6.2	61.2

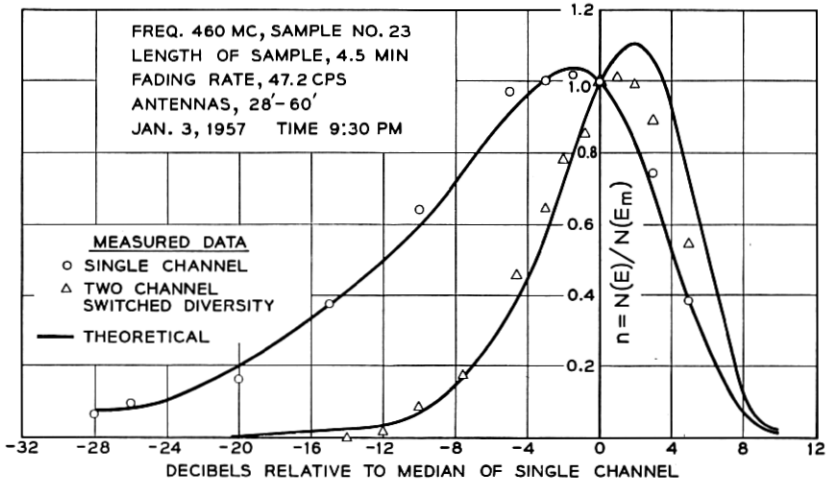

Fig. 65 — Number of one-way crossings at a given signal level for a two-channel switched diversity system. The number of crossings is normalized to the number at the median of the single channel. Curves are theoretical; points are experimental.

seconds for 80 per cent of the time. Similarly, a Rayleigh-distributed 460-mc signal at the same threshold level has average fade lengths between 61.2 and 1590 milliseconds for 80 per cent of the time.

7.4 *Twin-Feed Diversity — Average Length of Fade*

Fig. 65 shows the analysis of the number of crossings for a simultaneous recording of a switched channel and the single channel. (Fig. 51 gives the analysis of the probability distribution for this sample.) The agreement is very good between theory and experiment below the median level but does depart somewhat for the levels above the median. This is probably due to inaccuracies in receiver and recorder calibrations, since we depend on equal receiver calibration for quantitative data.

It is interesting to note that, while the number of crossings decreases very rapidly when more diversity channels are used, the average length of a fade stays fairly constant; this results from the fact that the time spent at low levels is also very small. This point is worth noting in the design of digital systems, since diversity will not reduce the average length of a drop-out as much as one might expect at first glance. We will discuss this aspect in the next section.

TABLE VI — CHARACTERISTICS OF DIVERSITY SYSTEMS FOR GIVEN VALUES OF POWER RELIABILITY

Diversity	Crossings*	Average Length of Fade, milliseconds†	Level Below Median, db‡	Reduction in Transmitter Power, db§
Power Reliability¶ 99.0 per cent				
None	0.23	42	18.5	0
Two-Channel Switched	0.148	73	8.0	10.5
Two-Channel Combiner	0.126	86	6.7	11.8
Four-Channel Combiner	0.028	116	−0.6	19.1
Power Reliability¶ 99.9 per cent				
None	0.0751	13	28.5	0
Two-Channel Switched	0.025	38	13.3	15.2
Two-Channel Combiner	0.023	44	11.8	16.7
Four-Channel Combiner	0.014	75	2.0	26.5

* Normalized to number of crossings at median of single channel.
† Normalized to one one-way crossing per second at median of single channel.
‡ With respect to median of single channel.
§ At the stated reliability.
¶ Defined as percentage of time the received power level stays above a given absolute power level.

7.5 *Reliability*

The usual definition of "reliability" is concerned with the percentage of time the received power stays above a given absolute level. Table VI illustrates the power reliability of a transmission system which employs diversity reception to reduce the power requirement on the transmitter. The received power at the output of the combined channel is maintained at the same absolute level as the order of diversity is changed. For example, for the 99 per cent reliability, the amount of transmitter power needed is 19 db less for quadruple combiner diversity than for a single channel. If we now look at the average length of fade, we note that it has increased about threefold. To keep the average length of fade constant when going from a single channel to the quadruple diversity combiner, a decrease of only 11.8 db in transmitter power could be realized (see Fig. 60). Table VI also shows the reliability factors when a 99.9 per cent power reliability is the design criterion.

VIII. BANDWIDTH IN TROPOSPHERIC PROPAGATION

In previous sections we have discussed the various characteristics of the received signals when cw signals are transmitted. In this section we consider the bandwidth characteristics of the propagating medium. To

make this study a frequency-sweep experiment* was performed using a 4.11-kmc transmitter sawtooth-modulated at a 1000 cps rate over a 20-mc band. The receiver was swept nonsynchronously over the same band at a 30-cps rate. The resultant pulses were displayed on an oscillograph and photographed at the rate of one frame every two seconds. The experiment used a 28-foot transmitting antenna and 8-, 28- and 60-foot receiving antennas.

Samples of sweep-frequency pictures are shown for various antenna combinations and transmission conditions. The bandwidths deduced from the experimental data are compared with a calculation based on the geometry of the common volumes.

An analysis of the sequences of frequency sweep photographs is made and the frequency auto-correlation function and distribution of bandwidths are computed. Photographs of signals received simultaneously from a twin-feed horizontal diversity system are also shown and discussed.

8.1 *Experimental Setup*

The transmitter consists of a klystron oscillator frequency-modulated by a 1000-cps sawtooth voltage applied to the repeller. This signal is amplified by a stagger-tuned klystron-amplifier. The output power is about 10 watts with a bandwidth of 10 mc at the 1-db points and 15 mc at the 3-db points. No ripples occur across the band.

The receiver consists of a triple detection set with two IF amplifiers whose center frequencies are 66 mc and 3 mc. The output of the second IF amplifier (150-kc bandwidth) is connected to the Y-axis of an oscilloscope (Fig. 66). The first beating oscillator is frequency-modulated at a 30- or 60-cps rate in a manner similar to the transmitter. These rates were chosen to be an order of magnitude higher than the fading rates usually encountered on this circuit.

With the aid of Fig. 67 we see that, whenever the difference between the transmitter frequency and the beating oscillator frequency is 66 mc, a pulse will appear on the oscilloscope connected to the last IF amplifier. The oscilloscope presentation is therefore amplitude versus frequency.

8.2 *Sweep-Frequency Photographs*

Samples of sweep-frequency photographs selected from runs taken on different days are shown in Fig. 68. Each run consisted of a series of 150

* It is possible to obtain equivalent information using pulse techniques but the interpretation of overlapping and distorted pulses is often difficult.[24]

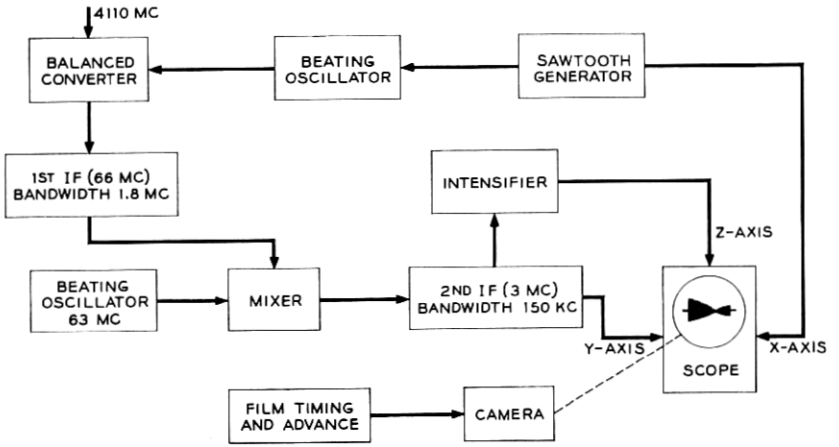

Fig. 66 — Block diagram of sweep-frequency receiver.

frames taken at $2\frac{1}{2}$ second intervals with a $\frac{1}{10}$ second exposure. In the first three sets, Fig. 68(a), (b) and (c), the antenna sizes (28-foot to 60-foot) remain fixed; these sets were taken on different days to show the variability of transmission conditions.

Fig. 68(a) shows the photographs for the 28-foot–60-foot combinations

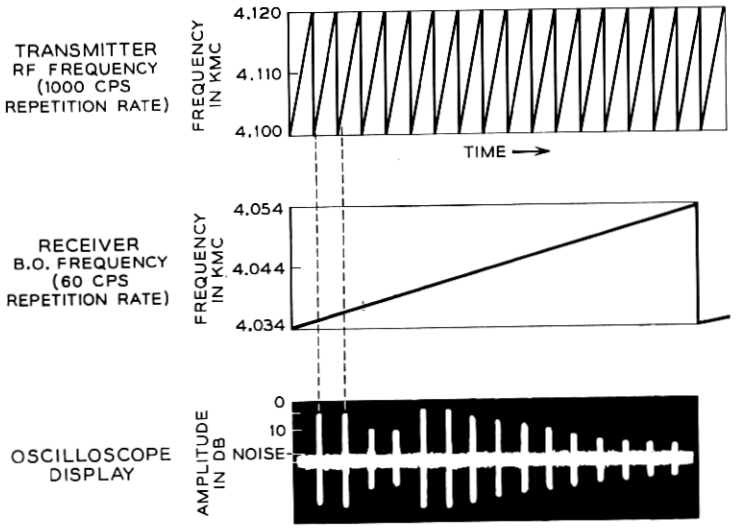

Fig. 67 — Combination of transmitter and receiver sweep-frequency waveforms.

on a day when the median signal level was high with a very slow fading rate (for a 4-kmc cw signal). Since the fading rate is slow, the sequence appears continuous. The signal goes to one deep fade for the samples shown. It should be noted that the amplitude fall-off at the extremities of the photographs is due to the limited bandwidth of the transmitter. In this case, the usable bandwidth of the medium exceeds 15 mc. The wide bandwidth suggests that rather large layers are primarily responsible for the propagation and that they are contained in a rather small height interval. In Fig. 68(b) we observe at times a narrower bandwidth (Photograph c) as well as a very wide one (D). The characteristic which is most noticeable is the variability from sample to sample. Had a continuous record been taken, continuous changes would have been noted. Fig. 68(c) shows, on the average, a broader bandwidth than the previous one. However, the narrowest bandwidth (A) is about 6 mc wide. (For the qualitative discussion we define the bandwidth as the frequency difference between two adjacent amplitude minima.)

Fig. 68(c) is for the 28-foot–60-foot antenna combination, as were all the preceding ones. This and the following figures were taken on the same day, with the receiving antenna as the variable. Fig. 68(d) shows the received signal using the 28-foot–28-foot antennas; these photographs were taken 7 minutes after those of Fig. 68(c). Here the narrowest bandwidth is about 3 mc (c). Fig. 68(e) shows the received signal on an 8-foot antenna a few minutes later. Due to the lower gain of the 8-foot antenna, the signal level is closer to the noise level of the system. However, one notes the narrowest bandwidth to be about 3 mc (c).

The photographs show that the medium introduces selective fading which bears a remarkable similarity to the fading which occurs on a line-of-sight path during anomalous propagation conditions.[25] This raises the question as to how many layer-like discontinuities are present at one time. The hypothesis that there are a limited number of regions of discontinuities does not necessarily contradict the fact that the received signal is Rayleigh-distributed as a function of time. In each region several layers can be present; these can change both in amplitude and position with time, therefore giving a Rayleigh distribution.

8.3 *Calculation of Bandwidth*

The bandwidth can be estimated by calculating the relative delay produced by the two limiting paths obtained from the common volume geometry. From the common volume concept it is apparent that the delays will be greatest in the vertical plane. Assuming the 3-db points of the antenna patterns to define the boundaries limiting the transmis-

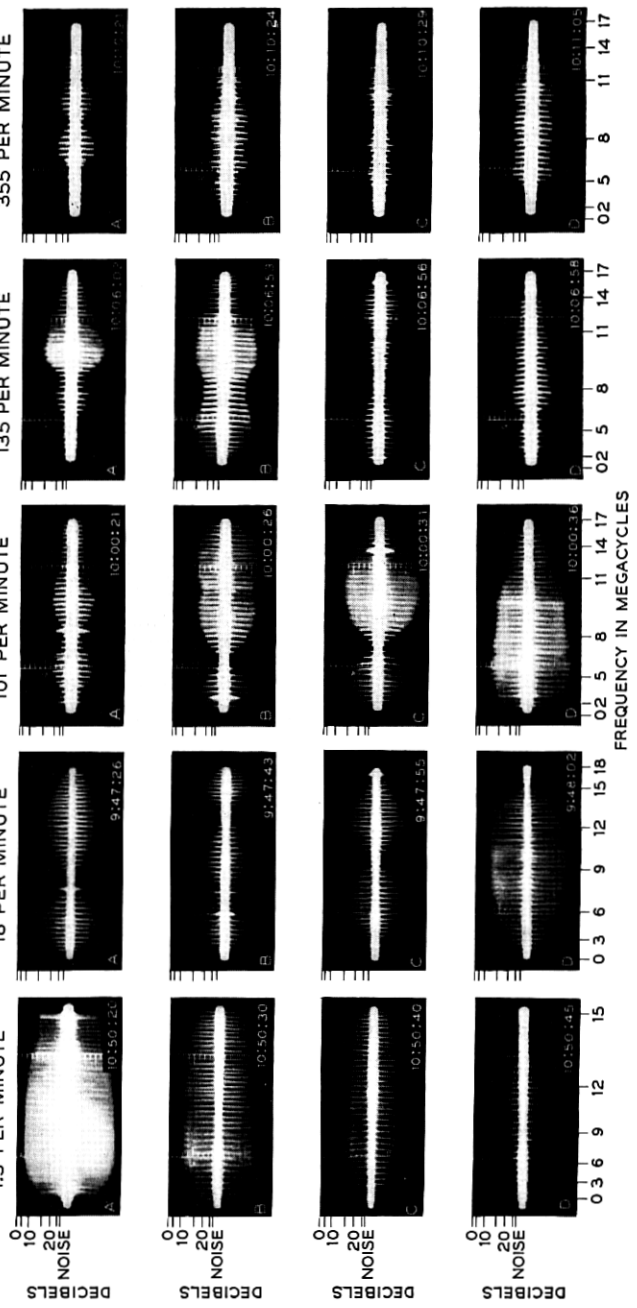

Fig. 68 — Sweep-frequency photographs: (a) September 30, 1957; 28-foot–60-foot antennas; cw median fading rate, 1.5 per minute. (b) October 15, 1957; 28-foot–60-foot antennas; cw median fading rate, 18 per minute. (c) November 8, 1957; 28-foot–60-foot antennas; cw median fading rate, 101 per minute. (d) November 8, 1957; 28-foot–28-foot antennas; cw median fading rate, 135 per minute. (e) November 8, 1957; 28-foot-8-foot antennas; cw median fading rate, 355 per minute.

sion, we calculate the maximum path difference, δ. With the aid of Fig. 13, we see that the path length difference δ will be

$$\delta = a\theta^2\left[\left(1 + \frac{\alpha_T}{\theta}\right)\left(1 + \frac{\alpha_R}{\theta}\right) - 1\right], \tag{29}$$

where α_T and α_R are the 3-db beamwidths in radians of the transmitting and receiving antennas and θ is the angle in radians between the lower edge of the beam at the horizon and the straight line joining the terminals. For our path, $2a = 171$ miles and $\theta = 0.9°$ (4/3 earth).

For the 28-foot–60-foot antenna combination $\alpha_T = 0.6°$ and $\alpha_R = 0.33°$. Using (29), we get $\delta = 142$ feet, which gives a corresponding bandwidth of 7.0 mc between adjacent amplitude minima. For the 28-foot–28-foot and 28-foot–8-foot, antenna combinations we note that the limiting factor in transmission is the atmosphere. From our beam-swinging experiment (Section 4.1.2), we found that the received power was contained on the average within an angle of 0.6° (half-power points) in the vertical plane. Hence, using $\alpha_T = \alpha_R = 0.6$, we obtain a maximum path difference of $\delta = 198$ feet; the corresponding bandwidth is 5.1 mc.

Depending on the structure of the atmosphere, these bandwidths will change. The actual bandwidth will be determined by the distribution and strength of the discontinuities in the common volume region. For example, if there were only one discontinuity, then one would expect a fairly large bandwidth. Nevertheless, the prediction of a bandwidth of the order of 5 to 7 mc is consistent with experimental data. In the next section a more quantitative analysis is made of the data.

8.4 *Statistical Distributions of Bandwidth*

While a qualitative presentation of bandwidth gives one a feeling for the capabilities of the propagating medium, a quantitative analysis should yield data which can form a basis for the design of communication systems.

The reduction of the photographic data consisted of the translation of the amplitude-versus-frequency function on each photograph into 30 discrete amplitude values; i.e., an amplitude value was obtained at $\frac{1}{2}$-mc intervals for the 15-mc band. The majority of the data reduction was accomplished using semiautomatic machines, which punched the coordinates for each discrete amplitude into IBM cards for computer processing.

A run of data for any antenna combination consisted of approximately 150 photographs. It should be noted that the median cw fading rate can

be of the order of magnitude of the rate of photographic sampling; hence one must insure that the number of photographs analyzed is sufficient to obtain a valid distribution. A test was therefore made to determine the amount of data needed for analysis. The cw fading rate for the run selected was 85 fades per minute; the rate of photographic sampling was about 25 frames per minute. For this analysis the same frequency was selected on each frame and a signal level distribution was plotted for the first 50, 100 and 160 frames. As the number of frames included in the distribution was increased, the level distribution curve approached the Rayleigh curve. While there was some deviation from the theoretical distribution, no significant change was introduced with the increase in sample length from 100 to 160 frames. One therefore concludes that 100 photographs are sufficient for analyzing the bandwidth. This test is perhaps more stringent than necessary when computing the frequency autocorrelation function, since each photographic frame contains 30 frequency points instead of only one.

There were two main analyses made on the data. One was the frequency autocorrelation function, the other was the amplitude-frequency distribution.

8.4.1 *Frequency Autocorrelation Function*

We define the frequency autocorrelation function of the envelope

$$\tau = \frac{\int_{-\infty}^{\infty} v_m(t)v_n(t)\ dt}{\int_{-\infty}^{\infty} v_m{}^2(t)\ dt}, \tag{30}$$

where v is the amplitude function of the envelope; m and n are different frequencies (see Fig. 69) and τ is a function of the frequency difference $m - n$.

Since the data are quantized in $\frac{1}{2}$-mc intervals and only a limited frequency band is available, the integrals are converted to these summations:

$$\tau = \frac{\sum_{N=1}^{M} v_m(t_N)v_n(t_N)}{\frac{1}{2}\sum_{N=1}^{M} [v_m{}^2(t_N) + v_n{}^2(t_N)]}. \tag{31}$$

The averaging is done in the denominator to smooth out transmitter amplitude fluctuation. This method works best for $m - n$ small. Due to the decrease in power output of the transmitter at the edges of the band,

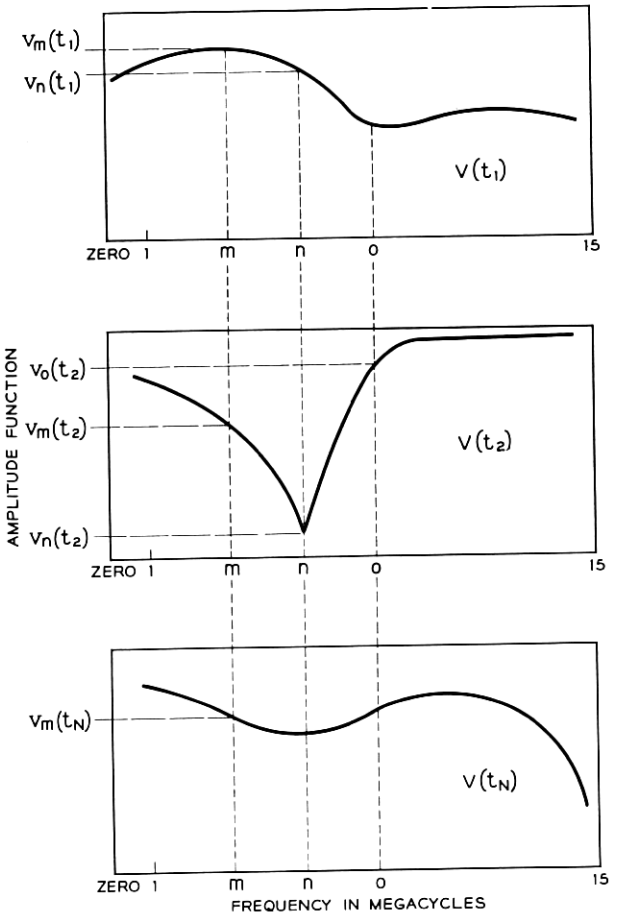

Fig. 69 — Sweep-frequency patterns; $v(t)$ is the amplitude function.

only the center 10 mc are used in the computation. The τ's for the same $m - n$ are calculated and averaged for each run. For $m - n = \frac{1}{2}$ mc (the smallest increment) one obtains 3000 values from a 150-frame sample when the center 10 mc are used in the computation; for $m - n = 10$ mc only 150 values are available.

From the frequency autocorrelation function, τ, of the envelope, we can compute the frequency autocorrelation coefficient, k. The equation relating the two is given[26] by

$$\tau = E(k) - \left(\frac{1 - k^2}{2}\right) K(k), \tag{32}$$

where $E(k)$ and $K(k)$ are the complete elliptic integrals of modulus k. Booker, Radcliffe and Shinn[27] have shown that k^2 is approximately the correlation coefficient of the envelope. It can be shown from (32) that as the frequency interval $m - n$ becomes large, $\tau \to \pi/4$.

In all, 10 runs were analyzed, using different combinations of receiving antennas. The runs were chosen to give a wide range of transmission conditions, and the cw fading rate and the median signal levels were the parameters measured before and after each frequency-sweep run.

Fig. 70 shows the autocorrelation function for the 28-foot–60-foot combination. Except for the data of September 30, 1957, the curves for the autocorrelation function do not change appreciably. The unusual propagation conditions on September 30, 1957, were discussed in Section 8.2 in conjunction with Fig. 68(a). We note that $\tau \to \pi/4$ as $(m - n) \to 10$ mc.

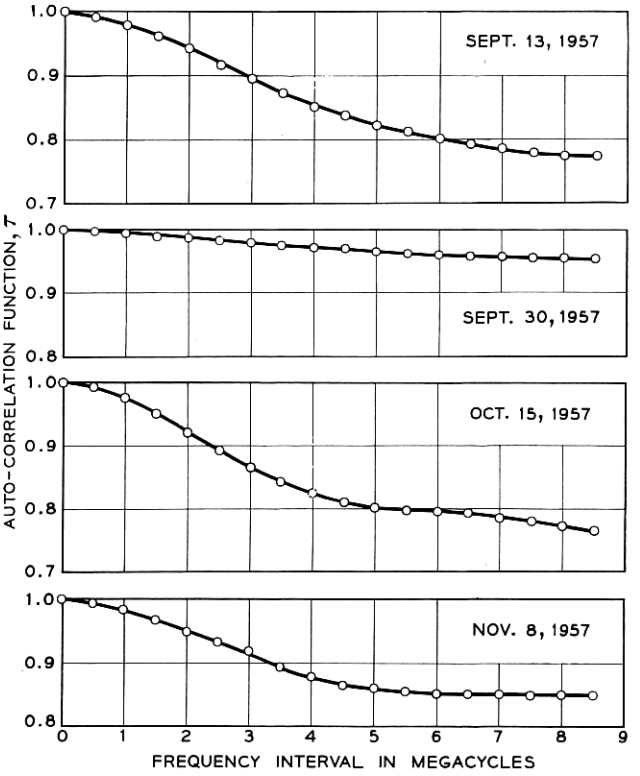

Fig. 70 — Frequency autocorrelation functions, 28-foot–60-foot antennas.

TABLE VII — PARAMETERS IN SWEEP-FREQUENCY RECEIVED DATA

frequency: 4110 mc
cw transmitting power: 43 dbm (10-ft transmitting antenna)
$k^2 \approx$ correlation coefficient of envelope of received signal

Antennas, feet	Date	cw Median Signal (−dbm)		cw Median Fading Rate, per Minute	Bandwidth in mc at Correlation Coefficient; $k^2 = 0.6$
		Before	After		
28–60	9-13-57	97.5	93	85	5.2
	9-30-57	58	65	1.5	≅16.0*
	10-15-57	96	95	18	4.5
	11-8-57	89	89	101	6.3
28–28	9-13-57	92	94	148	7.4
	9-30-57	68.5	62	1.25	≅12.5*
	10-15-57	99.5	102	18	5.6
	11-8-57	92.5	94	135	5.5
28–8	9-30-57	70	73.5	3	≅16.0*
	11-8-57	99	96	355	4.5

* $k^2 = 0.8$

Table VII summarizes the bandwidth for the various runs. A more meaningful definition is used than that employed in our qualitative analysis of bandwidth in Section 8.3. The bandwidth may be defined as the frequency separation for which the correlation coefficient $k^2 = 0.6$ ($\tau = 0.904$). [Since the bandwidth was extremely large on September 30, 1957, we have used the criterion $k^2 = 0.8$ ($\tau = 0.952$).] It is seen that the bandwidth varies from 4.5 to 6.3 mc (omitting the data of September 30, 1957) and does not appear to be correlated with cw median signal level, cw median fading rate or antenna size.

8.4.2 *Amplitude-Frequency Characteristics*

The analysis of the amplitude-frequency characteristics consisted of calculating the maximum ratio of signal amplitudes in a given frequency interval $m - n$. A cumulative distribution is plotted as a function of $m - n$. The distribution of slopes can be obtained by looking at the results for the smallest frequency interval ($\Delta f = \frac{1}{2}$ mc). For larger intervals the results do not give the slopes but only the ratio of amplitudes. [In frame 2 of Fig. 69 for $m - o$ the maximum amplitude ratio is $v_o(t_2)/v_n(t_2)$.]

Fig. 71 shows the amplitude-frequency distributions. These give the frequency separation for various amplitude ratios which are exceeded 10, 50 and 90 per cent of the time. Figs. 72 and 73 give the corresponding

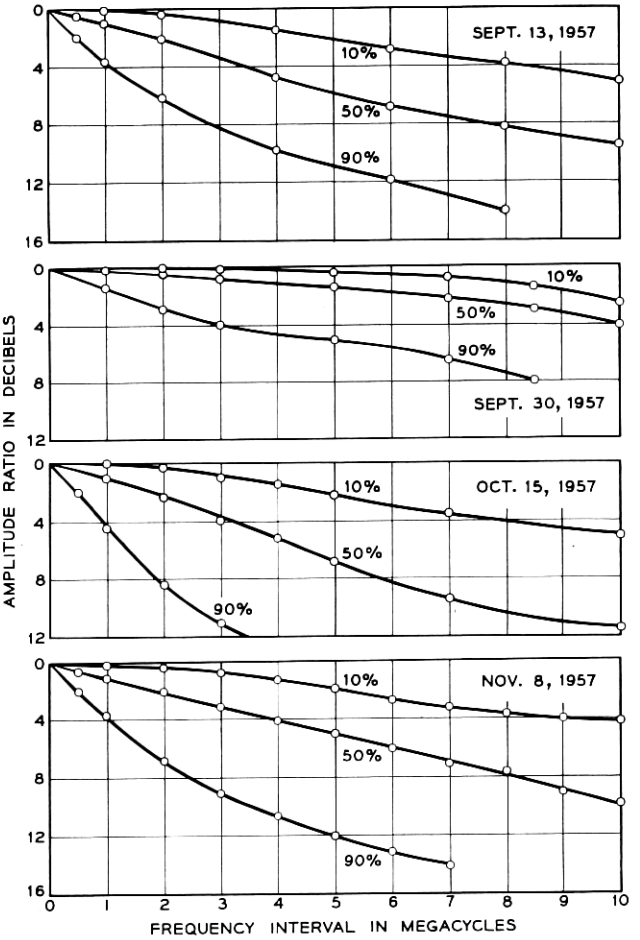

Fig. 71 — Bandwith exceeded 10, 50 and 90 per cent of the time — 28-foot–60-foot antennas.

distributions for the 28-foot–28-foot and 28-foot–8-foot combinations. While the curves differ somewhat, there are no significant differences except for the curve for September 30, 1957.

Fig. 74 gives the amplitude ratio distribution for the 28-foot–60-foot antenna combination on September 13, 1957. This curve gives the distribution for a day when the bandwidth was about average.

Except for the unusual propagation of September 30, 1957, the auto-correlation functions, as well as the bandwidth distributions, are sensibly independent of the median signal level, cw fading rate and antenna

sizes used in these tests. To obtain a wider bandwidth, one must use extremely narrow beam antennas on the order of 0.1°. In that case, one probably would expect a marked increase in bandwidth with antenna size.

8.5 *Synthesis of Sweep-Frequency Photographs*

One of the interesting questions in the analysis of the sweep-frequency records is the number of signal components present in the received signal

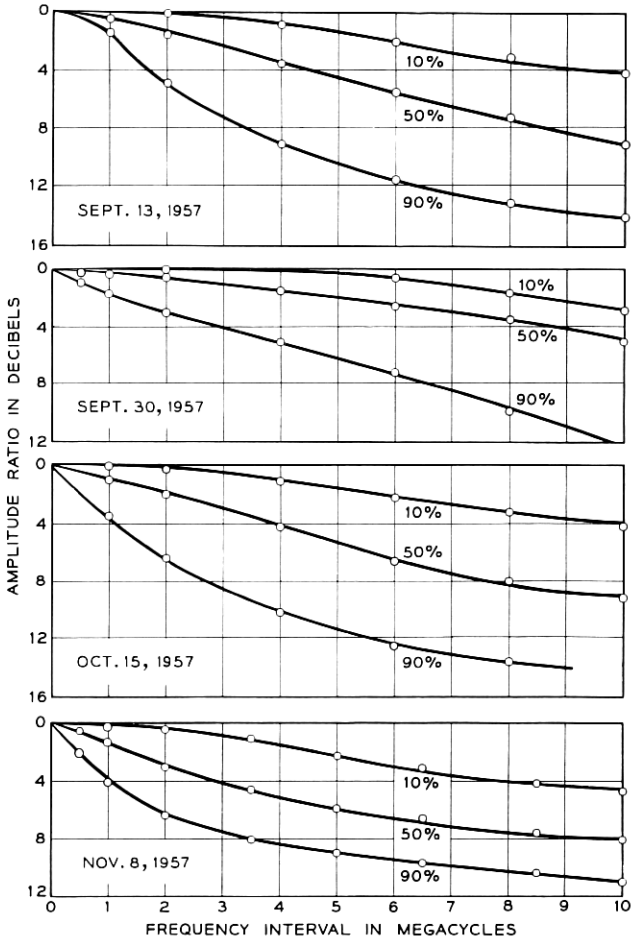

Fig. 72 — Bandwidth exceeded 10, 50 and 90 per cent of the time — 28-foot–28-foot antennas.

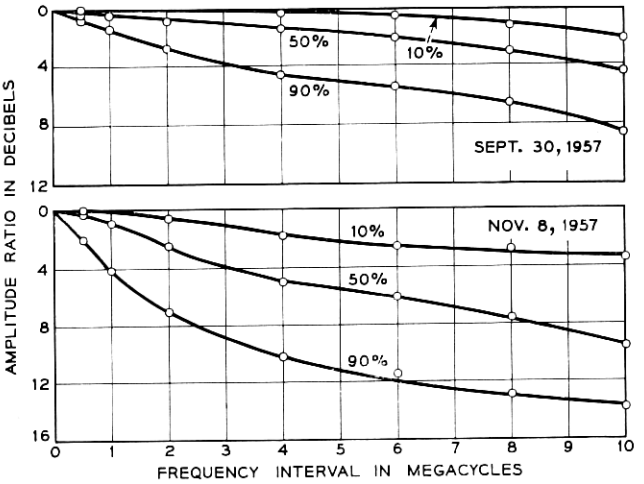

Fig. 73 — Bandwidth exceeded 10, 50 and 90 per cent of the time — 28-foot–8-foot antennas.

at any one instant. We indicated that the photographs bore a striking similarity to those obtained on a line-of-sight circuit under anomalous propagating conditions.[25] We have synthesized a sequence of seven photographs from the run of November 8, 1958. The analog computer was the one used previously by Crawford and Jakes,[25] which combines four components of arbitrary amplitude and phase. Fig. 75 shows the synthesis of one of the samples. It was possible to synthesize all seven photographs approximately with only four components. Due to the limited band of the frequency sweep, it is difficult to tag the components with small delays, but the four components give an adequate representation of those with large amplitudes and relatively short delay.

8.6 *Twin-Feed Diversity*

Twin-feed diversity experiments using cw transmissions have shown that signals from the two received channels are uncorrelated most of the time at 4 kmc. There has been speculation that a frequency effect gives an additional improvement in signal to noise for a single FM channel.[28] If the RF energy spectrum is distributed over several megacycles and if the dropout at low signal levels is only several hundred kilocycles wide, then only a small part of the signal information may be lost. This is in contrast to a cw channel, where the complete channel would be lost.

To examine the frequency correlation between two diversity channels, tests were made using the 28-foot transmitting antenna and the 28-foot receiving antenna with horizontally disposed twin feeds. Simultaneous recordings were made on the two sweep-frequency channels using a dual trace oscilloscope. Photographs were taken with a Polaroid camera, using a $\frac{1}{25}$-second exposure. Fig. 76(a) shows the calibration for the photographs. Several frames have been selected to illustrate the frequency diversity characteristics. Figs. 76(b), (c) and (d) were taken on a day when the bandwidth was rather broad, whereas the remaining ones were

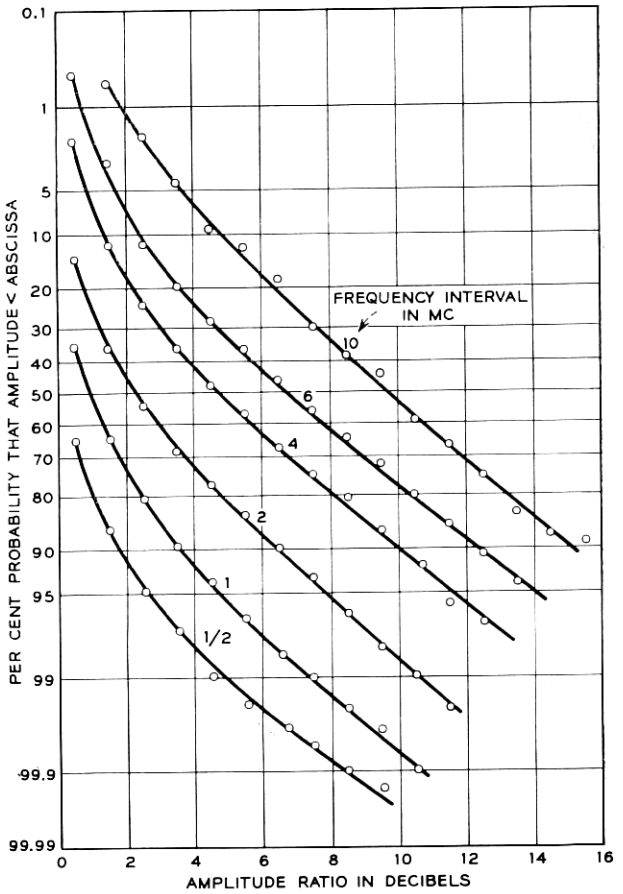

Fig. 74 — Distribution of amplitude ratios for a run where the bandwidth is about average.

recorded on a more representative day. In Figs. 76(b) and (f) the amplitude-frequency characteristics are very similar for the two feeds; on the remaining ones there is little similarity. In all the runs the signals on the two feeds were uncorrelated at any particular frequency. An examination of several hundred frames shows that a frequency effect does occur between the two diversity channels when the frequency separation is of the order of several megacycles at 4 kmc.

If the received channels are combined in a switch-type combiner, the percentage of time that the switched signal (at one frequency) spends below a certain level will decrease and the bandwidth will be broader.

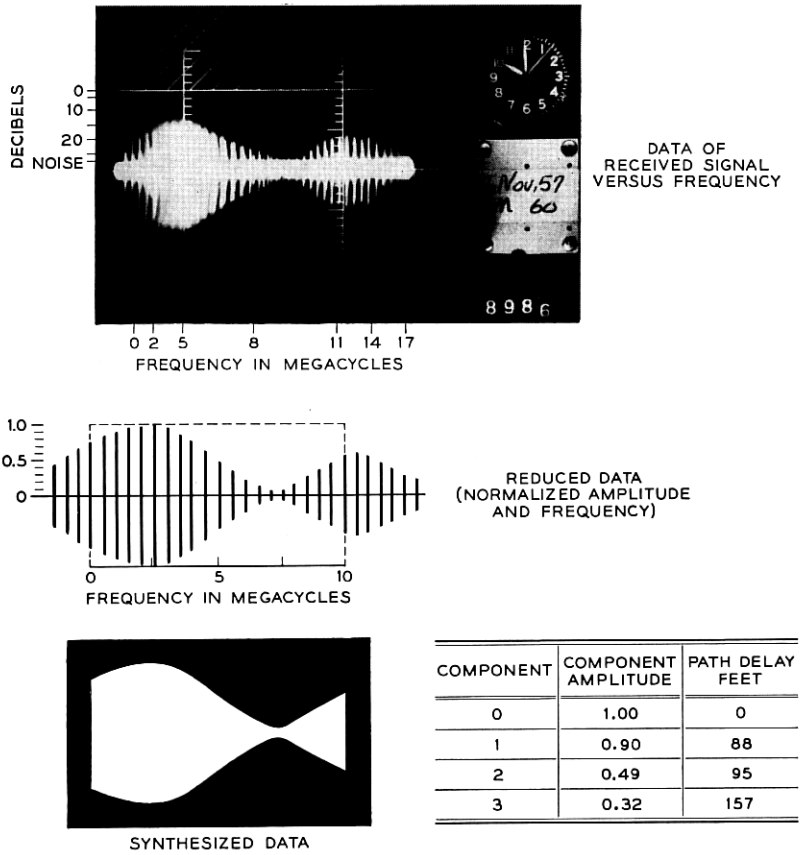

COMPONENT	COMPONENT AMPLITUDE	PATH DELAY FEET
0	1.00	0
1	0.90	88
2	0.49	95
3	0.32	157

Fig. 75 — Synthesis of a sweep-frequency photograph.

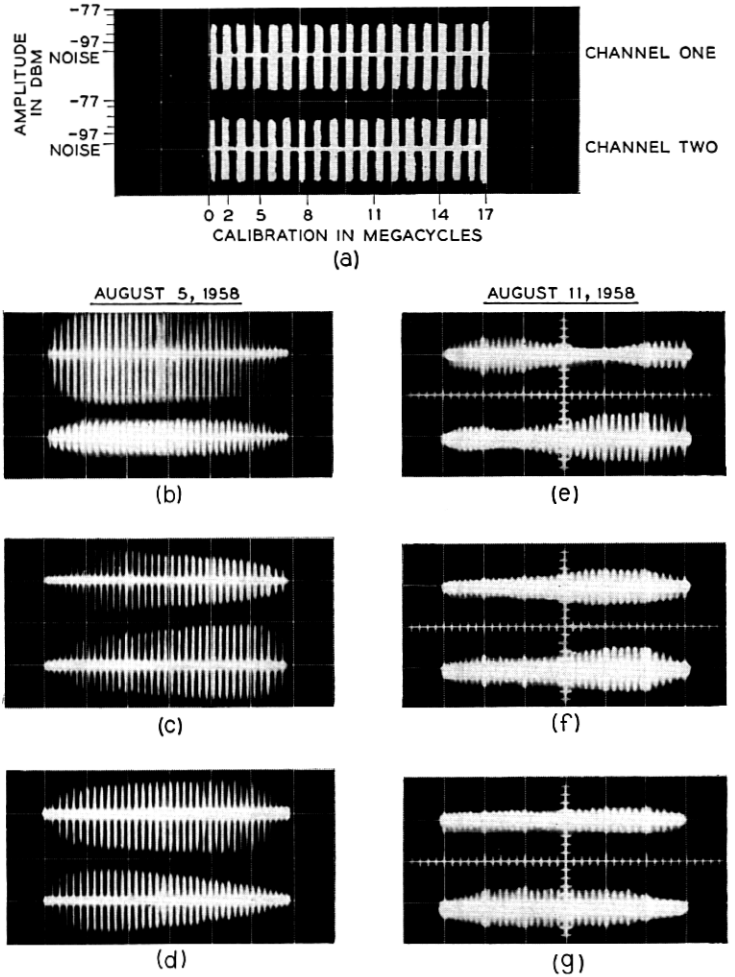

Fig. 76 — Sweep-frequency photographs of single channels in a twin-feed diversity system — horizontally disposed feeds, 4110 mc.

IX. CONCLUDING REMARKS

The results of the several experiments discussed in the foregoing sections are interrelated in various ways, but it is perhaps most significant that the results can be interpreted in terms of reflections from layers in the troposphere. In many cases, such as the dependence of the propagation on wavelength, antenna size and beam orientation, quantitative

agreement is obtained between experiment and the theory of reflection by layers of intermediate size. The 4110-mc data on bandwidth and on fading rate are consistent with the theory. Moreover, one concludes that delays in the vertical plane of propagation are most important in determining the bandwidth, whereas delays in the horizontal plane determine the fading rate. The propagation mechanism itself determines the bandwidth and fading rate unless antennas with extremely narrow beamwidths are employed. The 460-mc experiments on twin-feed diversity and those dealing with the dependence of received power and fading rate on wavelength indicate that the effective horizontal extent of the layers increases significantly as the frequency of propagation is decreased. Where possible, the influence of these concepts on the design of systems has been discussed.

X. ACKNOWLEDGMENTS

We wish to express appreciation to H. T. Friis for his active leadership and encouragement in this work. We also wish to thank R. P. Booth of the Military Systems Engineering Department of Bell Telephone Laboratories for his continued interest and for making available some of the equipment needed for the experiment. Several members of the Radio Research Department assisted in this program. R. A. Semplak, who was a full-time participant, built and maintained much of the apparatus and obtained and analyzed much of the data. L. R. Lowry, R. A. Desmond and J. H. Hammond participated in some phases of the experiment and analyzed some of the data. Others active in the program from time to time were W. E. Legg and H. A. Gorenflo. The cooperation of Orton J. Newton and his family, on whose property the transmitting site was located, was most valuable and greatly appreciated.

APPENDIX

Calculation of Received Power Using Unequal Transmitting and Receiving Antennas

The formula for received power using antennas with equal beamwidths is given by (1) in Section 3.1.3 and in the theory (Ref. 5, p. 635, Equations 5 and 7):

$$P_R = P_T M a A_T A_R \lambda^{-1} \int_V \rho^{-6}\, dV = P_T M a A_T A_R \lambda^{-1} \left[\frac{\beta}{6\theta^4 a^3} f\left(\frac{\alpha}{\theta}\right) \right]. \quad (33)$$

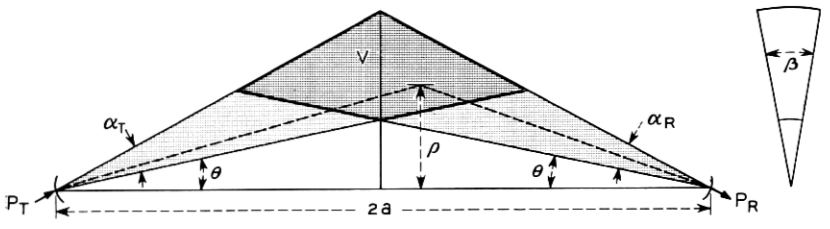

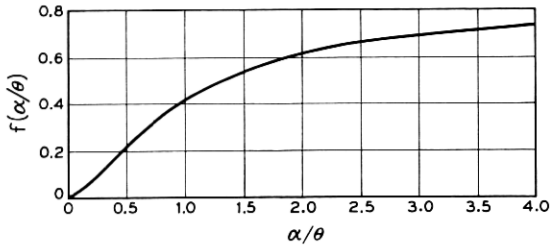

Fig. 77 — Power received beyond the horizon on antennas of equal size, $\alpha_R = \alpha_T$ for symmetrical volume $V = V(\alpha, \theta)$.

The symbols are defined in Section 3.1.3 and in Fig. 77, and A_T and A_R are the effective areas of the antennas. For antennas of equal size with beams of unity aspect ratio (see Ref. 5, pp. 635–636):

$$A_T = A_R = \frac{\lambda^2}{\alpha_T^2} = \frac{\lambda^2}{\alpha_R^2}.$$

The factor

$$\left[\frac{\beta}{6\theta^4 a^3} f\left(\frac{\alpha}{\theta}\right)\right]$$

depends upon the magnitude and location of the symmetrical volume, $V(\alpha,\theta)$; a plot of $f(\alpha/\theta)$ [see (2)] is shown in Fig. 77. For the idealized antenna beams used in the theory, the wedge angle β is given by

$$\beta = \frac{2\alpha}{\alpha + 2\theta}$$

where α is the 3-db beamwidth of the actual antennas.

Consider now the case of unequal transmitting and receiving beams, as shown in Fig. 78. The resulting common volume is asymmetrical about the center line OA, thus one cannot apply (33) directly. However, the asymmetrical volume can be expressed as a sum of symmetrical

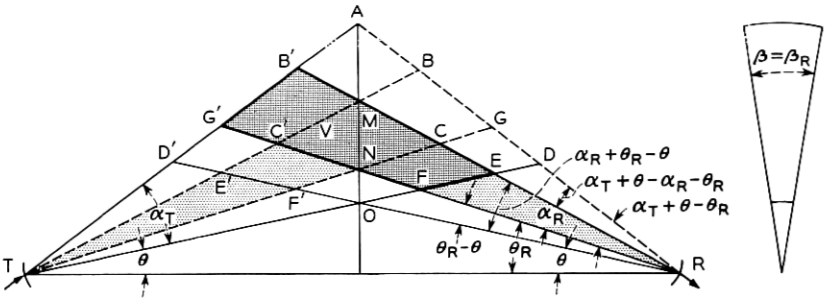

Fig. 78 — The asymmetrical volume B'EFG' expressed in terms of symmetrical volumes, valid when $\theta_R + \alpha_R \leqq \theta + \alpha_T$ and $\beta_R < \beta_T$ (unequal transmitting and receiving antennas). We require V = B'EFG' = ADOD' − ADEB' − G'D'OF. Now, ADEB' = ABMB' + BDEM and ADOD' − MEOE' = B'D'E'M + BDEM + ABMB'. Therefore, ADEB' = ½(ADOD' − MEOE' + ABMB'). Similarly, G'D'OF = ½(ADOD' − AGNG' + NFOF'). Therefore, V = ½(AGNG' + MEOE' − ABMB' − NFOF') = ½[$V_1(\alpha_T + \theta - \theta_R, \theta_R) + V_2(\alpha_R + \theta_R - \theta, \theta) - V_3(\alpha_T + \theta - \alpha_R - \theta_R, \theta_R + \alpha_R) - V_4(\theta_R - \theta, \theta)$].

volumes as shown in the figure. If both beams are oriented along the horizon, $\theta_R = \theta$ and the asymmetrical volume becomes

$$V = \tfrac{1}{2}[V_1(\alpha_T, \theta) + V_2(\alpha_R, \theta) - V_3(\alpha_T - \alpha_R, \theta + \alpha_R)]. \quad (34)$$

The received power is obtained by substituting the appropriate angles from the V_1, V_2, V_3 into the factor in (33) and summing. Thus

$$P_R = P_T M A_T A_R \lambda^{-1} \frac{\beta_R}{12a^2}\left[\frac{1}{\theta^4} f\left(\frac{\alpha_T}{\theta}\right) + \frac{1}{\theta^4} f\left(\frac{\alpha_R}{\theta}\right) - \frac{1}{(\theta + \alpha_R)^4} f\left(\frac{\alpha_T - \alpha_R}{\theta + \alpha_R}\right)\right], \quad (35)$$

which holds for $\beta_R < \beta_T$. For this case the effective areas of the idealized antennas with beams of unity aspect ratio are

$$A_T = \frac{\lambda^2}{\alpha_T^2} \quad \text{and} \quad A_R = \frac{2\lambda^2}{\alpha_R \beta_R (\alpha_R + 2\theta)},$$

which results in

$$P_R = P_T \frac{M}{6a^2} \frac{\lambda^3}{\alpha_T^2} \frac{1}{\alpha_R(\alpha_R + 2\theta)} \left(\frac{1}{\theta^4}\right)\left[f\left(\frac{\alpha_T}{\theta}\right) + f\left(\frac{\alpha_R}{\theta}\right) - \frac{\theta^4}{(\theta + \alpha_R)^4} f\left(\frac{\alpha_T - \alpha_R}{\theta + \alpha_R}\right)\right]. \quad (36)$$

Special treatment is required when the elevation and beam angles

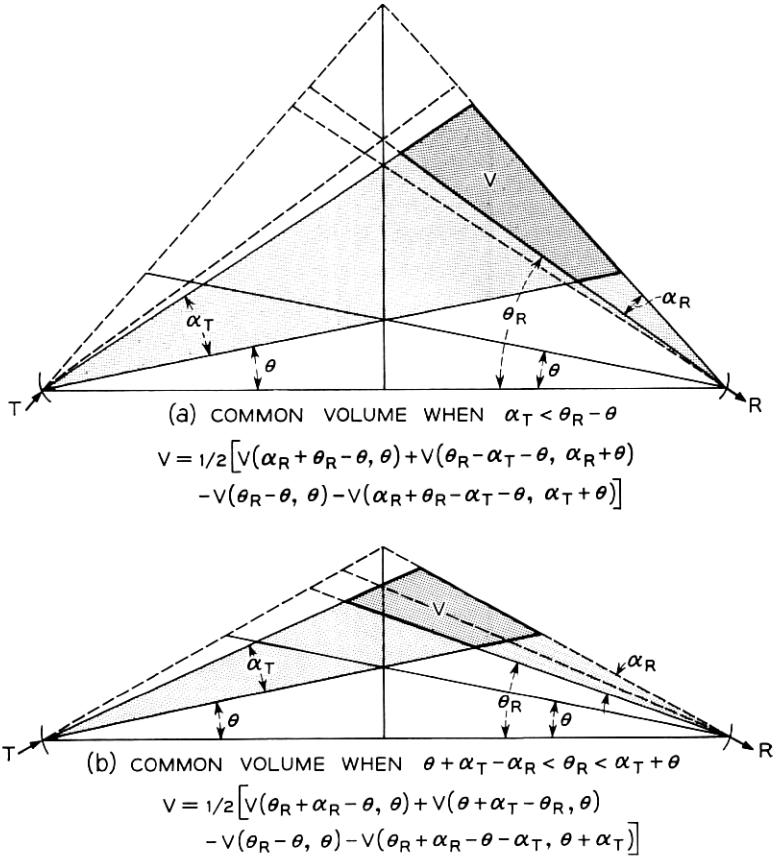

Fig. 79 — Asymmetrical volumes — special cases.

involved are such that the apex of the common volume in Fig. 78 is situated to the right of centerline OA; the resulting common volumes are shown in Fig. 79. Again, one can express these asymmetrical volumes in terms of symmetrical ones. The resulting expressions for the common volume and the range of validity are given in the figure; with these, (33) can be applied to obtain the received power.

REFERENCES

1. Bullington, K., Propagation of UHF and SHF Waves Beyond the Horizon, Proc. I.R.E., **38,** October 1950, p. 1221.
2. Proc. I.R.E., **43,** October 1955 (entire issue).
3. Booker, H. G. and Gordon, W. E., A Theory of Radio Scattering in the Troposphere, Proc. I.R.E., **38,** April 1950, p. 401.

4. Carroll, T. J. and Ring, R. M., Propagation of Short Radio Waves in a Normally Stratified Troposphere, Proc. I.R.E., **43,** October 1955, p. 1384.
5. Friis, H. T., Crawford, A. B. and Hogg, D. C., A Reflection Theory for Propagation Beyond the Horizon, B.S.T.J., **36,** May 1957, p. 627.
6. Crawford, A. B., Friis, H. T. and Jakes, W. C., Jr., A 60-Foot Diameter Parabolic Antenna for Propagation Studies, B.S.T.J., **35,** September 1956, p. 1199.
7. Bullington, K., Radio Transmission Beyond the Horizon in the 40 to 4000 mc Band, Proc. I.R.E., **41,** January 1953, p. 132.
8. Nupen, W. and Thuronyi, G., Checklist of References to Literature on Tropospheric Propagation of UHF, VHF and SHF Radio Waves, Bulletin 6001, National Bureau of Standards, Boulder, Colo., August 1958.
9. Ortwein, N. R., An Annotated Bibliography of Literature Pertinent to Tropospheric Scatter Propagation, 1945–1957, N.E.L. Report 858, August 1958.
10. Bean, B. R. and Meany, F. M., Some Applications of the Monthly Median Refractivity Gradient in Tropospheric Propagation, Proc. I.R.E., **43,** October 1955, p. 1419.
11. Bolgiano, R., Jr., Wavelength Dependence in Transhorizon Propagation, Proc. I.R.E., **47,** February 1959, p. 331.
12. Waterman, A. T., Jr., A Rapid Beam-Swinging Experiment in Transhorizon Propagation, Trans. I.R.E., **AP-6,** October 1958, p. 338.
13. Rice, S. O., Radio Field Strength Statistical Fluctuations Beyond the Horizon, Proc. I.R.E., **41,** February 1953, p. 274.
14. Norton, K. A., Rice, P. L., Janes, H. B. and Barsis, A. P., The Rate of Fading in Propagation Through a Turbulent Atmosphere, Proc. I.R.E., **43,** October 1955, p. 1341.
15. Anderson, L. J. and Smyth, J. B., The Effect of Uniform Layers on the Propagation of Radio Waves, Trans. I.R.E., **PGAP-2,** March 1952, p. 28.
16. Mack, L. C., Diversity Reception in UHF Long-Range Communications, Proc. I.R.E., **43,** October 1955, p. 1281.
17. Norton, K. A., Vogler, L. E., Mansfield, W. V. and Short, P. T., The Probability Distribution of the Amplitude of a Constant Vector Plus a Rayleigh-Distributed Vector, Proc. I.R.E., **43,** October 1955, p. 1354.
18. Rice, S. O., Mathematical Analysis of Random Noise, B.S.T.J., **24,** January 1945, p. 78.
19. Staras, H., Diversity Reception with Correlated Signals, J. Appl. Phys., **77,** January 1956, p. 93.
20. Rice, S. O., Statistical Properties of a Sine Wave Plus Random Noise, B.S.T.J., **27,** January 1948, p. 109.
21. Law, H. B., Lee, F. T., Looser, R. C. and Levett, F. A. W., An Improved Fading Machine, Proc. I.E.E., **104B,** March 1957, p. 117.
22. Rice, S. O., Distribution of the Duration of Fades in Radio Transmission—Gaussian Noise Model, B.S.T.J., **37,** May 1958, p. 581.
23. Rice, S. O., private communication.
24. Chisholm, J. H., Portmann, P. A., DeBettencourt, J. T. and Roche, J. F., Investigations of Angular Scattering and Multipath Properties of Tropospheric Propagation of Short Radio Waves Beyond the Horizon, Proc. I.R.E., **43,** October 1955, p. 1317.
25. Crawford, A. B. and Jakes, W. C., Jr., Selective Fading of Microwaves, B.S.T.J., **31,** January 1952, p. 68.
26. Lawson, J. L. and Uhlenbeck, G. E., *Threshold Signals*, McGraw-Hill Book Co., New York, 1939, pp. 62, 156.
27. Booker, H. G., Ratcliffe, J. A. and Shinn, D. H., The Diffraction from an Irregular Screen, Phil. Trans. Roy. Soc. (London), **242,** 1950, p. 579.
28. Willson, F. E., private communication.